Design of a Motorcycle Mount with Integrated Roll-and-Pitch-Torque Measurement on a Motorcycle Simulator

Master thesis No. 712/18

Editor: Ricardo Delgado Ojeda | 2892957
Supervising tutor: Raphael Pleß, M.Sc.

TECHNISCHE UNIVERSITÄT DARMSTADT

FZD FAHRZEUGTECHNIK TU DARMSTADT

Ricardo Delgado Ojeda
Matriculation number: 2892957
Course of study: Master Mechanical and Process Engineering

Master thesis No. 712/18
Topic: Design of a Motorcycle Mount with Integrated Roll-and-Pitch-Torque Measurement on a Motorcycle Simulator

Handed in: 28th of March 2019

Technische Universität Darmstadt
Fachgebiet Fahrzeugtechnik
Prof. Dr. rer. nat. Hermann Winner
Otto-Berndt-Straße 2
64287 Darmstadt

Abstract

On the new motorcycle simulator developed by the Institute of Automotive Engineering (FZD) of the Technische Universität Darmstadt, a measuring system should be incorporated with the aim of determining the forces generated by the motion of the rider. The objective of this thesis is to design a mount for the future simulator capable of measuring the two main outputs of rider motion: the roll and pitch rider-induced torques. The current simulator of the department located at WIVW measures only the torque around the rolling axis and the used concept does not provide the desired performance nor precision; the solution designed in this thesis should present an improvement in regards to those features as well.

In order to come up with the most suitable design, the standard product development proceeding has been followed. First, by defining the demands of the mount on a request list. Next, following an organized creative process, several concepts have been proposed. All the alternatives have been evaluated in regards to relevant criteria and the most appropriate solution has been chosen. An exhaustive multibody model has been developed using MatLAB/Simulink with Simscape extension in order to analyze the dynamic behavior of the chosen solution under any possible scenario. Finally, a basic CAD of the system has been carried out in order to materialize the constructive solutions that will bring the concept into reality. Other constructive insights have been also treated, like the bearing selection, among others.

The selected approach consists on a three-legged surface that is attached to the motion platform of the simulator and serves as a base for the mock-up attachment. The orientation of the legs define the height of two coincident rotating axes (rolling and pitching), creating a mechanism able to rotate its surface around a desired center of rotation. When the rotation around those axes is fixed trough measuring elements, the rider-induced torques measuring system is enabled. By positioning said CoR at the height of the system's CoG, most of the measuring imprecisions that presents the current simulator are eliminated, since the greatest part of inertial forces generated by the platform motion have no longer an effect on the measuring data.

Table of Contents

Symbols and Indices

Latin letters:

Symbol	Unit	Term
a	$\frac{m}{s^2}$	Acceleration
d, D	mm	Diameter
f	Hz	Frequency
F	N	Force
h	mm	height
l	mm	Length
m	kg	Mass
M	Nm	Moment
r, R	mm	Radius
t	s	time
T	Nm	Torque
S	./.	Safety factor
v	$\frac{m}{s}$	Linear speed
X	*mm*	Space position, automotive sign convention
Y	*mm*	Space position, automotive sign convention
Z	*mm*	Space position, automotive sign convention

Greek letters:

Symbol	Unit	Term
δ	mm	Displacement
φ	°, rad	Roll angle
θ	°, rad	Pitch angle
ψ	°, rad	Yaw angle
ω	$\frac{rad}{s}$	Angular speed

Indices:

Symbol	Term
a	Axial
exp	Expected
meas	Measured
mec	Mecanism
max	Maximum
min	Minimum
r	Radial

List of Abbreviations

AHP	Analytic Hierarchal Process
CAD	Computer Aided Design
CoG	Center of Gravity
CoR	Center of Rotation
DoF	Degrees of Freedom
FEM	Finite Element Method
FFT	Fast Fourier Transform
FZD	Fahrzeugtechnik Darmstadt
IRA	Instant Rotation Axis
LC	Load-cell
TUD	Technische Universität Darmstadt
RA	Rotation Axis
VRA	Virtual Rotation Axis
WIVW	Würzburger Institut für Verkehrswissenschaften

List of Figures

List of Tables

1 Introduction

1.1 Motivation

The relevance of vehicle simulators has been amply proved during the past decades. Simulators are broadly used during the development phase of a vehicle in order to reduce prototype costs and shorten time to market, but they also serve as a safe testing environment that can provide useful information about its behavior and interaction with the driver/rider. The objective of these simulators is to create the closest experience to reality possible, in order to extract valid conclusions and observations.

The institute of Automotive Engineering (FZD) of the Technische Universität Darmstadt has a research collaboration with industrial partners in the topic of motorcycle simulators. One key element of this research is the force-based determination of rider motion. Unlike in most vehicles, rider motion does play an important role in the dynamics and is an important input to consider when developing a motorcycle simulator.

1.2 Task description

The object of this thesis is the design of a rider-motion measuring system to incorporate into the future FZD's motorcycle simulator. More specifically, the system should measure the two main outcomes of rider motion on a two-wheeled vehicle: the rider-induced roll and pitch torques. This measured data will be integrated into the vehicle dynamics model.

The specific results that were demanded as an output for this master thesis are the following:

- A demands list in order to define the system's functionalities
- Presentation of sub-solutions and evaluation criteria
- An evaluated system concept
- Manufacturing documentation
- Documentation of the applied development methodology and the abovementioned results including their critical discussion.

1.3 Work methodology

For the design of the measuring system, a standard product development methodology has been followed. After a research phase, the product has been defined through the elaboration of a request list. Then, a creative process has been carried out in order to come up with possible concepts and they have been later evaluated in order to choose the most suitable one. Finally, in the materialization design phase, the chosen concept has been defined constructively.

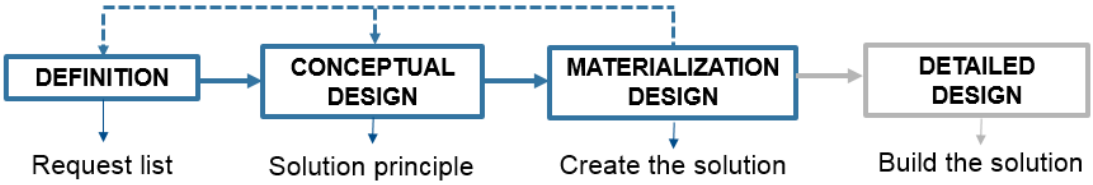

Figure 1-1: Product development steps, according to Riba Romeva[1]

However, the product development process does not finish with the abovementioned phase, but with the detailed design. In that final phase, the constructive solutions chosen in the materialization design are specified in depth and the actual manufacturing drawings are developed. For obvious time reasons, this last step is not treated on this thesis and will have to be performed afterwards.

As it will be clear along this paper, the thesis has a strong component of multibody analysis. To perform such analysis and simulate multibody systems it has been used MATLAB/Simulink with the extension of Simscape Multibody.

[1] cf. Riba Romeva, C.: Disseny de màquines V, p. 78.

2 State of the art

2.1 Rider influence on motorcycle dynamics

In the following section an explanation of the impact of rider motion on the motorcycle dynamic is done; it is not the purpose to present a deep analysis of two-wheeled vehicles behavior, just to highlight in which ways the rider's body motion can influence it.

In most vehicles, the effect of driver motion can be easily neglected in regards to the vehicle dynamics. Normally, driver's weight is much lower than the one of the vehicle and it is also true that in most cases, the driver is not able to move because he is resting on a seat. This statement, though, is not applicable to the case of motorcycles (or any other two-wheeled vehicle): rider's weight differs from the motorcycle weight by only one order of magnitude at most; the rider is also able to move on top of the bike because he is not tied down. It is remarkable, furthermore, how professional riders do not remain motionless on top of the bike, but they change their position and use it to vary the dynamic behavior. Thus, it is evident that rider motion is an important input to the dynamics of the bike and neglecting its effect would be too much of a simplification.

Rider motion can be presented in either *X*, *Y* or *Z* directions and each of those motions induce a different effect on the bike. To understand properly this phenomena a separated analysis of the above mentioned scenarios is presented.

Considering the vehicle under rectilinear motion, a rider motion in *X* direction constitutes an excitation causing the vehicle to rotate around its pitching axis; that means that the rider induces a torque around said axis. The pitching axis comes from the intersection of the squat line and the dive line, defined by the geometry of back and front suspension systems respectively. It is important to remember that the position of the pitching axis varies a lot depending on the constructive solution chosen, making the lever between rider and pitching axis very variable. [2]

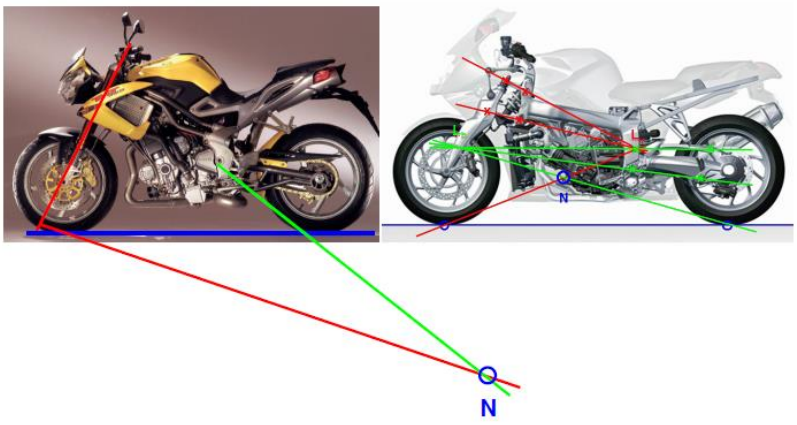

Figure 2-1: Different positions of the pitching axis[3]

[2] cf Weidele, A.; Klonecki, K.: VGU+FZD: Motorcycles 2015, pp. 111–119.

[3] Weidele, A.; Klonecki, K.: VGU+FZD: Motorcycles 2015, p. 118.

Nevertheless, not only rider motion generates a torque around this axis: the inertial accelerations generated by throttling and braking induce forces on all the masses of the vehicle, and thus, an overall torque is created. That torque is in reality traduced into a squat or a dive that can even get to the point of a wheelie or a stoppie (scenarios where the front or the rear wheels, respectively, loose contact with the ground). We can say that rider motion in *X* direction is, consequently, an added factor that could either magnify or counteract those effects. For instance, if a wheelie is wanted to be performed, the rider will move his body backwards, pull the handlebars and/or push the footpegs. If a stoppie is wanted instead, the opposite scenario will happen.

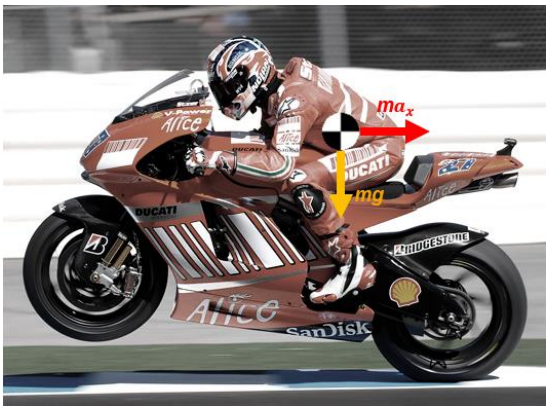

Figure 2-2: Effects of rider motion under rectilinear scenario

In the case of rider motion along the *Y* direction, we must consider the vehicle under turning motion. On a steady turning scenario, the centrifugal forces induced by cornering are counteracted by the forces on the tyres generated by camber thrust and slip. The ratio between the centrifugal force and the gravitational force defines the leaning angle of the bike. When a rider motion in *Y* direction appears, this equilibrium is lost and makes the bike to change the leaning angle until reaching a new equilibrium. Along with the steering angle, we can say that rider motion is the most important input in regards to the turning dynamics.

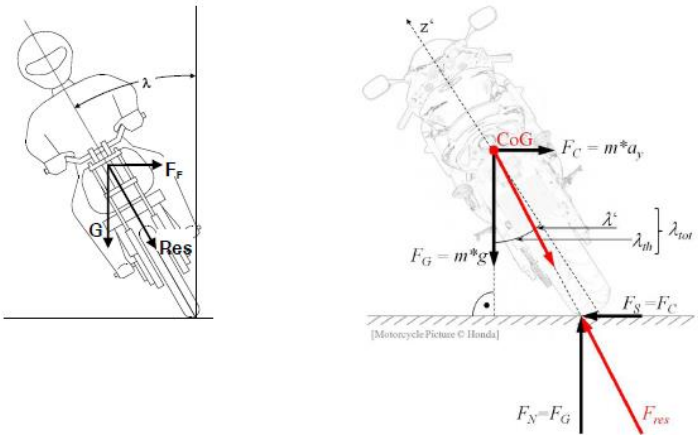

Figure 2-3: Free body diagram of a motorcycle under turning scenario[4]

[4] Weidele, A.; Klonecki, K.: VGU+FZD: Motorcycles 2015, p. 47.

Parallel to the previous scenario, in this case the rider motion generates a torque around the rolling axis. The position of this axis is not as clear as the one of the pitching, since it is not related with the suspensions or the chassis geometry. Until this very moment there is still an ongoing discussion about its real position, but the most extended version is as follows: the rolling axis starts as a horizontal line at ground height when the speed is 0, and moves upwards with speed until reaching the height of the vehicle's CoG. [5]

Finally, for the case of rider motion in the *Z* direction we must consider again the rectilinear scenario. In this case, no torque is generated but a vertical excitation of the sprung mass of the vehicle is induced, the so called bouncing motion. If we consider the vehicle as a mass connected to the ground through two springs that represent front and rear suspensions (including tyres), we can say that the first mode of vibration of such system corresponds to the bouncing motion, whereas the second one corresponds to the pitching.

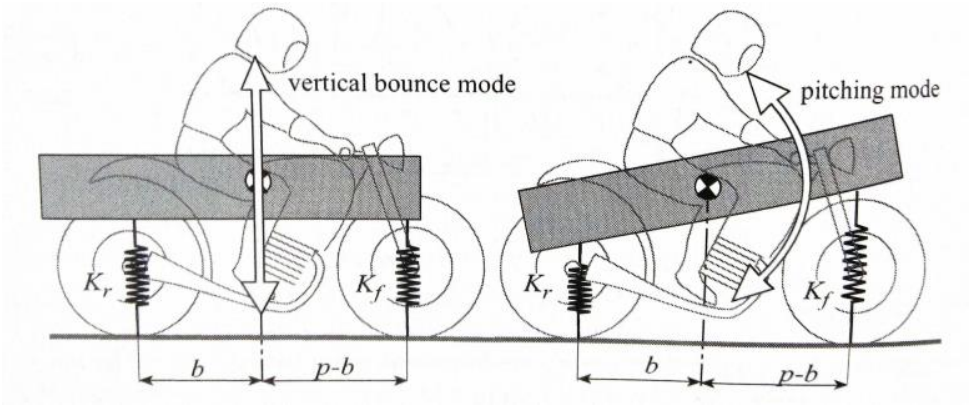

Figure 2-4: Modes of vibration of a motorcycle in the plain[6]

The importance of this last kind of rider motion is not as substantial as the previous ones, for the rider doesn't usually move in *Z* direction; only when he is getting feedback from the suspensions or stands up on the footpegs, which seldom happens. Furthermore, the bouncing motion is not relevant to the performance of the vehicle, as it is fully independent from *X* and *Y* direction dynamics. For these reasons, this last kind of motion does not belong to the ones that the measuring system has to consider as a requirement.

[5] cf. Foale, T.: Motorcycle handling and chassis design, 3.22–3.25.

[6] Cossalter, V.: Motorcycle dynamics, 172.

2.2 Competitor analysis

As for any kind of product, one of the early stages of its development is the analysis of the competence; knowing the technical solutions that other competitive products are using might give ideas on how to approach the development and also show the possible improvement fields in which the new product could outstand.

Therefore, an exhaustive analysis of the most important dynamic motorcycle simulators has been carried out, with focus on their rider-motion measurement solutions.

2.2.1 MotorcycleSim

MotorcycleSim is a research motorcycle simulator developed by the University of Nottingham. It takes as a base a complete chassis of a Triumph Daytona 675, including the wheels. This simulator only provides the rolling motion; it does not perform any pitch, yaw nor any linear displacement. It does work in static, dynamic and transient scenarios, providing the instability of the bike at low speeds and changing the behavior of the steering according to the speed (positive steering to counter steering).

In regards to the body-motion measurement, the MotorcycleSim neglects this input completely: as it does not even consider the pitching motion, so does with the rider-induced pitch-torque. In the case of roll motion, it only takes into account the change of the handlebar angle, and applies a leaning angle proportional to this input without considering any effect of the rider's body position.[7]

Overall, the immersion that this simulator offers is quite limited, due to the amount of dynamic simplifications that it assumes.

2.2.2 MDRG

Developed by the University of Padova, this simulator consists of a mock-up motorcycle with 4 degrees of freedom: lateral displacement, yaw, roll and pitch. The rider's effect on the pitch is neglected, so the pitching of the mock-up is only dependent of the longitudinal acceleration (throttling or braking). The roll motion is given only by the torque applied to the handlebars and does not consider the body-induced torque either.[8]

Once again, the omission of the rider-induced torques on the vehicle dynamics model translates into a poorly realistic experience.

[7] cf. Stedmon, A. W. et al.: 'MotorcycleSim': An Evaluation of Rider Interaction with an Innovative Motorcycle Simulator (2011).

[8] cf. Massaro, M. et al.: Using Simulators for the Assessment of Handling of Motorcycles.

2.2.3 SIMACOM

This simulator was conceived trough the collaboration of various technical laboratories from France: INRETS-MSIS, UEVE-IBISC and IEF-UPSUD. It uses as a mock-up the frame of a Yamaha YBR-125 and is able to procure yaw, pitch and roll motions but no linear motion. As in the previous cases, both rider-induced pitch and roll torques are completely neglected.[9]

2.2.4 MOTORIST

Developed by TU Delft and SIEMENS, this simulator is based on a complete Piaggio scooter fixed on a 6DoF Stewart motion platform. As in the previous cases, rider-induced torques are neglected.

2.2.5 KAIST bicycle simulator

The following is a bicycle simulator developed in South Korea. It consists of a bike frame fixed to a Stewart moving platform, which allows a 6 DoF motion. Although the original model didn't consider rider-induced torques, a further upgrade was made to take into account the effect of rider's body position. In this case, the same Stewart platform measures the forces/torques generated on its top and are compared to the values expected from a fixed stand rider. Thus, the rider effect is considered as a perturbation to the system. Later on, the perturbing forces and torques are translated into a net rider-induced torque for the vehicle dynamics software.[10]

This interesting solution presents, unfortunately, three pitfalls. First: an accurate estimation is found to be difficult due to the high sensitivity in estimation to the model uncertainties, so the working range of the simulator stays under a frequency of 1,5Hz; second: the reading forces are not very accurate due to the fact that the magnitude of those is very high; and third: because it needs a complex controller to compare the reading forces to the expected ones, the response time is quite long.

2.2.6 Cruden Simulator

This commercial simulator is developed by Cruden, a Dutch company that develops all sorts of vehicle simulators. In this case, a complete Ducati Panigale is mounted on a 6DoF moving Stewart platform. Both pitch and roll rider-induced torques are considered; with this purpose, two cameras are set on the front and the back of the bike, capturing the rider's upper body. Those cameras register the motion, which is later estimated as a torque for the vehicle dynamics model. The rider must not wear any special gear with optical points of reference, for the cameras and processor make an automatic estimation.[11]

[9] cf. Nehaoua, L. et al.: Motorcycle riding simulator: How to estimate robustly the rider's action?

[10] cf. Shin, J.-C.; Lee, C.-W.: Rider's net moment estimation using control force of motion system for bicycle simulator (2004).

[11] cf. Westerhof, B. E.: Evaluation of the Cruden Motorcycle Simulator.

The main problem with this optical solution is that the higher the accuracy we demand (i.e. more optical reference points), the slower is the response; so there must be always a compromise between the two. Besides, it only considers the upper body, and not the whole rider's body effect.

2.2.7 DESMORI simulators

Finally we arrive to FZD's current simulator: the DESMORI. This system consists of a mock-up frame fixed to a 6DoF motion Stewart platform. As a matter of fact, we should talk about twin simulators, for there are two of them: one located at the WIVW and another at BMW-Motorrad. Both of them use the same technologies and software, as well as the vehicle dynamics model behind them. The main difference between them lays, casually, on the way they measure the rider induced torque. It must be said that they only consider the torque induced to the rolling.[12]

The simulator located at BMW-Motorrad takes as a mock-up bike the frame of a BMW K1600 and to measure the rider-induced roll torque uses an optical system similar to the one of the Cruden simulator, but in this case the rider has to wear a jacket with optical reference points. The camera located at the back of the bike captures the motion of those references and, the data is later processed and translated into an estimated torque. As it happened with the Cruden simulator, the problem of this solution lays on the compromise between accuracy and time of response: if we wanted a higher accuracy we would need to add more reference points, which would make the processing work much slower.

The DESMORI simulator located at WIVW, which is the one that uses FZD for research purposes, uses as a mock-up bike the frame of a BMW F800s. The way in which this simulator calculates the rider-induced roll torque is by creating an actual rolling rotating axis and measuring the torque around that axis.

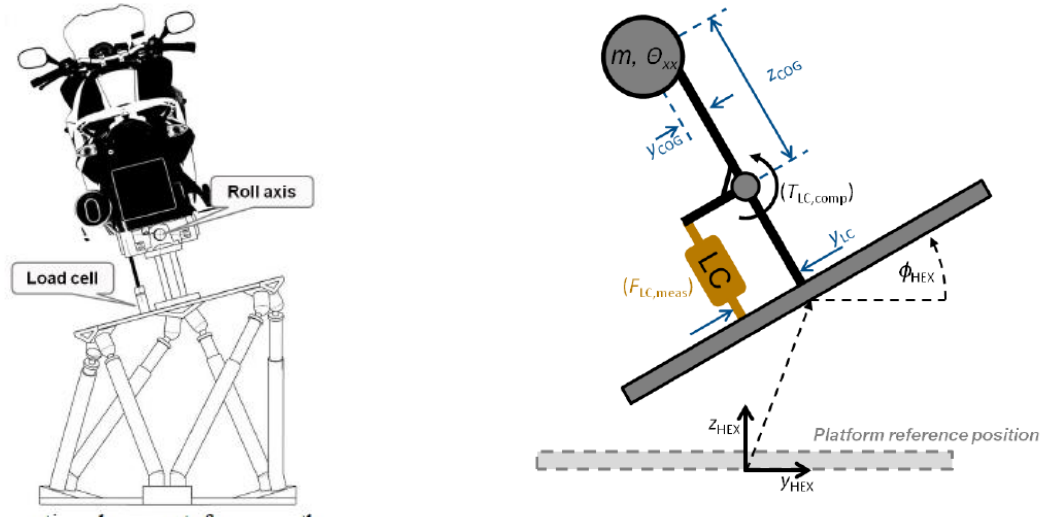

Figure 2-5: Schemes of Desmori simulator at WIVW[13]

[12] cf. Pleß, R. et al.: Approach to a holistic rider input determination for a dynamic motorcycle riding simulator.

[13] Pleß, R. et al.: Approach to a holistic rider input determination for a dynamic motorcycle riding simulator.

As it can be seen from the figures, the mock-up bike is not really stiff-connected to the motion platform, because between them there is a joint that allows the rotation of the mock-up in the direction of the roll axis. Nevertheless, this motion is fixed because a load cell is installed between the platform and the mock-up bike; this way, the load cell is able to read a force when a torque around that roll axis is generated. In conclusion: when the rider moves his body on the bike, a real torque is generated and a force on the load cell is readable. Having the chance of measuring a real torque implies having a much direct and faster response, which is crucial for an immersive experience.

Although this solution might be the most suitable of the ones presented until this point, it does have some problems or improvement fields. For construction reasons, the joint that allows the rotation around the roll axis is located just under the frame of the bike; that means that the torques generated around that axis include the inertial forces of the mock-up bike, and not only the forces created by the rider's change of body position. In this scenario, the measurements of the load-cell depend on the tilt angle of the motion platform and also on the accelerations generated. Therefore, the reading forces are considerably high (which means that the accuracy of the load-cells is not very precise) and they have to be corrected in order to dismiss the forces induced by the mock-up.

The solution to these problems would be to locate the rolling rotating axis at the height of the system's CoG, but it is clear to see that a physical rotating axis in that position would be constructively impossible.

2.2.8 Comparative table

Simulator	*Provided motion*	*Rider-induced pitch torque measurement*	*Rider-induced roll torque measurement*	*Measurement technology*
MotorcycleSim	1 DoF (roll)	No	No	-
MDRG	4 DoF (lateral displ, roll, pitch, yaw)	No	No	-
Simacom	3 DoF (roll, pitch, yaw)	No	No	-
Motorist	6 DoF	No	No	-
KAIST	6DoF	Yes	Yes	Perturbation estimation on the platform
Cruden	6DoF	Yes	Yes	Optical processing and estimation
DESMORI (BMW)	6DoF	No	Yes	Optical processing and estimation
DESMORI (WIVW)	6DoF	No	Yes	Physical rotating axis and direct measurement

Table 2-1: Comparative table between current motorcycle simulators; focus on rider motion measurement

2.3 Four-bar linkage system

The following section exposes the concept of the four-bar linkage system. During the research stage of the thesis, this technical system was introduced by the tutor and the possible application to the developing product was made manifest. The concept became of vital importance for the thesis and, for that reason, deserves its own section. It is mandatory to understand its nature before going any further because, as it will be seen, a big part of the conceptual designs are based on it.

The system consists on an articulated quadrilateral not parallelepiped, in which two of the opposed bars are coincident in the space. Although it is generically called four-bar linkage, in this case only three bars are considered since the missing one is substituted by direct constraints on the floor. The mechanism representation would be as follows:

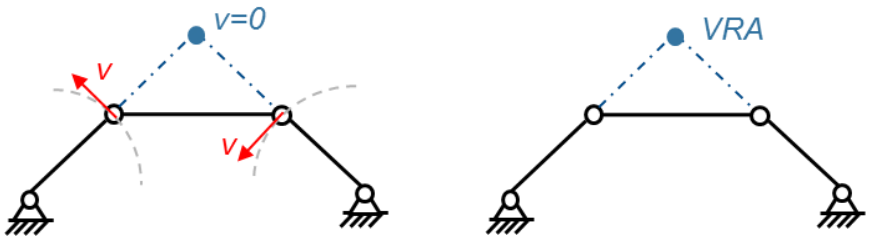

Figure 2-6: Finding the VRA on a four-bar linkage

The particularity of this system is that it allows the rotation of the surface around a given axis. This axis is positioned in the point where the lines created by the direction of the legs[14] meet in the space. It is what is called a virtual rotation axis.

We can imagine now that we attach this system to the motion platform of the simulator, and that attached to the system's surface we set a mock-up bike (represented as a vertical column in the figures). On top of the mock-up bike, there is the rider. Both mock-up bike and rider have a certain mass; as a simplification for this explanation, we will neglect the masses of surface and legs. Let's consider now that we aim the legs in such a way that the virtual rotation axis is at the very same position as the system's CoG. Under this scenario the rigid body created by surface, mock-up bike and rider is free to rotate around the VRA. However it will not do that, for the CoG and the VRA are coincident and no torque due to gravitational force is created. This statement is valid for any surface orientation.

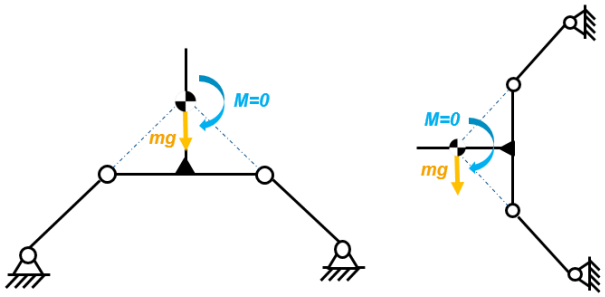

Figure 2-7: Scheme of the four-bar linkage system with different orientations, VRA and CoG on the same position

[14] For comprehensive reasons, from now on the upper bar will be called surface and the other two sustaining it will be called legs

Let's consider now that the rider is not fixed on top of the bike, but that has a certain horizontal motion. As soon as he/ moves away from the neutral position, the overall CoG will translate as well, and thus, a torque around the VRA will appear. If there is nothing that prevents the surface from doing it, it will rotate. Once the surface starts tilting, the legs will change their orientation and the VRA will move from its original position, increasing the lever in regards to the CoG and varying consequently the rotating torque.

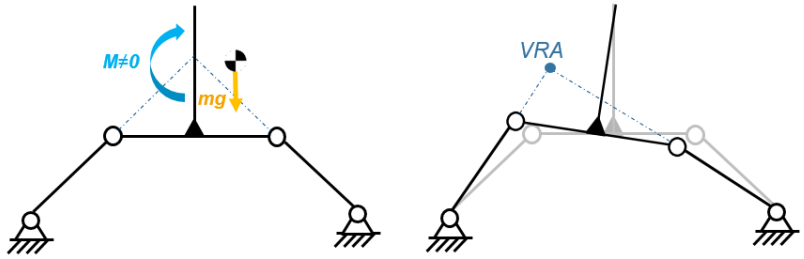

Figure 2-8: Displacement of the VRA when the surface rotates on a four-bar linkage system

Instead of letting this happen, it is possible to install a load-cell in such a way that it fixes the mechanism's degree of freedom; this way a measuring system is obtained, in which the motion of the rider is translated into a proportional load on the load-cell.

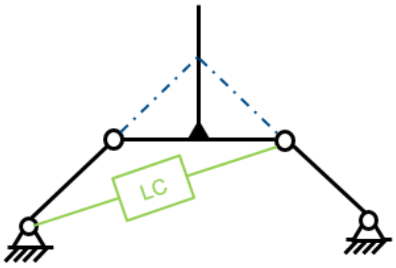

Figure 2-9: Example of position to install a load-cell to fix the rotation

Because the quadrilateral is fixed, the VRA stays in the same position; that means that the lever creating the gravitational torque remains always the same, and that the relation between rider motion and the reading load must be linear. In order to prove these statements, a simulation has been carried out using MatLab Simulink with Simscape Multibody extension.

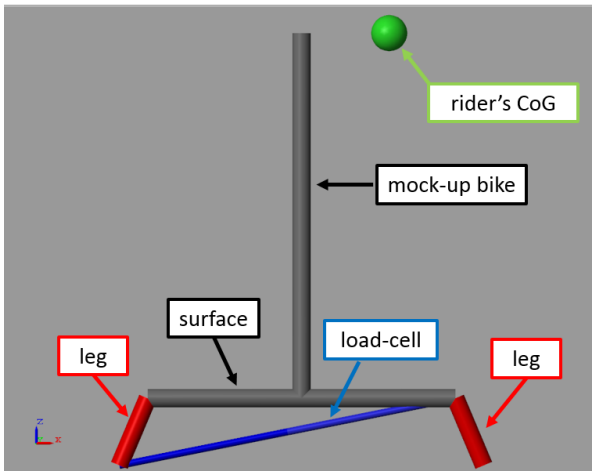

Figure 2-10: Screenshot of the four-bar linkage Simscape model showing the different components

The system consists on a four-bar linkage system with a load-cell fixing the degree of freedom, like just explained. A mass has been set at a certain height representing the rider (green ball on the previous figure), and it has been provided with a sinusoidal motion in *X* direction. In the following graph the Fast Fourier Transformation (FFT) of the rider motion is represented, showing different tested frequencies. The representation of the force read on the load-cell is shown as well. It can be already seen from this first graph that the relationship between both variables is linear, since both present the same frequencies.

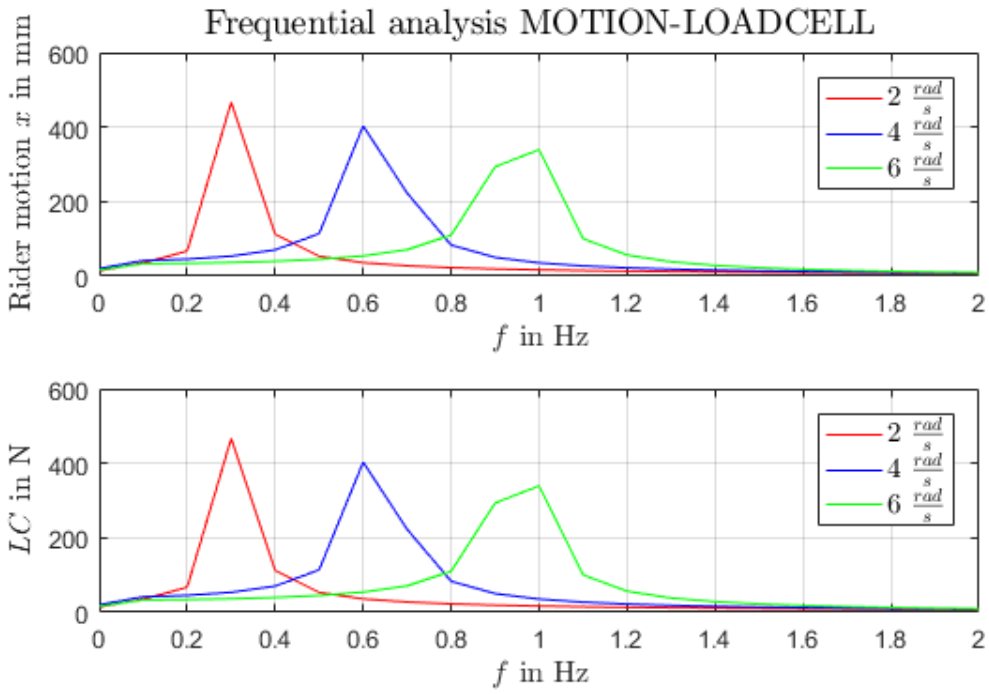

Figure 2-11: Frequency response of the four-bar linkage measuring system

To make it even clearer, a specific graph has been generated. We can see that the relationship between rider motion and load is completely linear and it does not depend on the frequency of the motion.

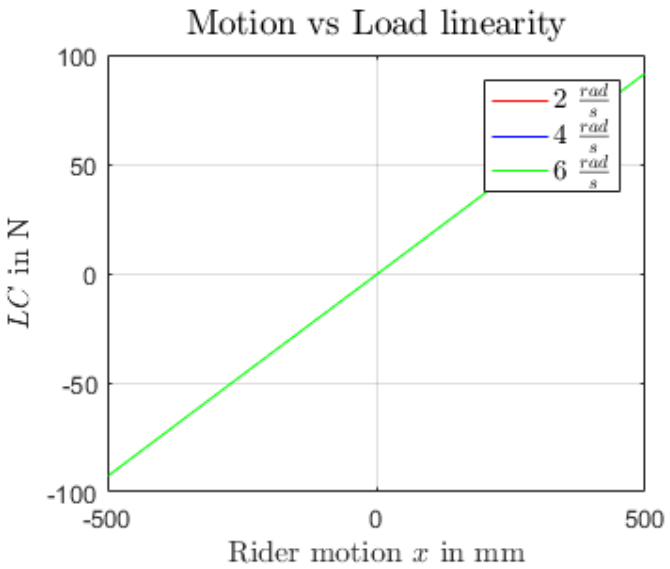

Figure 2-12: Measured load vs rider motion of the four-bar linkage system

From this analysis it is visible the potential of this concept as a measuring system: it processes low loads because only the influence of the rider's mass is measured and the relationship between motion and reading load is linear... As a reminder from the competitor analysis chapter: the main problem of the actual simulator of the department was that it measures also the inertial forces generated by the mock-up bike, making the measuring precision poor; being able to refuse this effect would make a great advance in terms of measurement performance. This is the reason why a lot of the designs discussed during the conceptual phase, as it will be seen, are based on this concept.

3 Product definition

Design of a motorcycle mount with roll-and-pitch-torque measurement						Sheet 1/1
Con-cept	N	FR RR TR W	Request list			Date
			Description	Values, Data	Comment	
Performance	1	FR	Roll-torque measurement precision	4Nm	light rider (40kg) moving 1cm "y"	01.10.2018
	2	FR	Pitch-torque measure-ment precision	10Nm	light rider (40kg) moving 2,5cm "x"	01.10.2018
	3	TR	Data acquisition - sensor positioning	linearity with CoG move-ment		02.11.2018
	4	TR	Measurement universal-ity	precision regardless of the bike		02.11.2018
	5	W	Roll-torque actuation		For higher frequency movements	12.10.2018
	6	W	Pitch-torque actuation		For higher frequency movements	12.10.2018
	7	W	Vertical Load measure-ment		Multibody system exci-tation	26.10.2018
	8	TR	Minimum disturbance motion platform			12.10.2018
Attachment	9	FR	Attachment to the moving surface		Hexapod platform or other	08.10.2018
	10	FR	Universal mock-up at-tachment		Any mock-up can be at-tached	08.10.2018
	11	RR	Payload	400kg	To consider in joints, bearings, etc.	26.10.2018
	12	FR	Stiff Connection to Frame		No suspensions over the platform	26.10.2018
	13	FR	Attachment of Swing Arm shaft		Consequence of (10) and (12)	26.10.2018
Ergonomics & Dimensions	14	FR	No interference with the rider		During operation nor mounting	08.10.2018
	15	RR	Maximum size of the sys-tem	800x800x300mm		08.10.2018
Scenario	16	FR	Stiff while riding		Stiffen progression from stand still	26.10.2018
	17	W	Freely Movable at stand still		Feeling of instability at stand still	26.10.2018
Production	18	TR	Budget	€4000,-		08.10.2018
	19	TR	Fabrication methods	Manufacturable in the workshop		02.11.2018

Table 3-1: Request list of the product

The first step in the design of any product is its definition. This is a fundamental stage in which, starting from an initial loose idea of the product, a complete set of expected features is carried out. After this stage a more specific idea of the product is obtained, easing the design process and also enabling to check the product performance once it is finished.

In order to clarify the expected features, a request list has been developed. This method consists of a list of solicitations that are asked to the future product. Information is classified into different categories: wishes (W), fixed requirements (FR), ranged requirements (RR) and target requirements (TR). Further information and divisions are given to complete the table.

The main requirements asked to the product are (1) and (2), which refer to the capability of the system to measure both roll and pitch induced torques with a certain precision. As it can be seen, the desired roll-torque measurement has been set with a higher precision, for the rider's body motion is considered to be more critical under that scenario.

Number (3) asks for linearity on the measured data with respect with the motion of the rider; having a linear relation between these two makes the understanding of the data easier and ensures that the precision of the system will remain stable.

Requirement (4) alludes to the fact that the precision of the measured data has to be independent of the mock-up bike mounted on the simulator and also of the rider. This means that even though the position of the global CoG might change for different tests, the precision of the system has to be under the ranges given in (1) and (2).

(5) and (6) show the wish of being able to use the system also as an excitation in order to obtain higher frequency motions; the motion platform is only able to provide low frequency ones. Wish (7) refers to the capability to measure not only pitch and roll torques, but also the rider's induced vertical motion (Z direction).

Requirement (8) aims to the fact that the platform motion should affect the minimum possible to the measured data. The system should only measure the torques due to the motion of the rider, and the inertial forces generated by the motion of the platform should have a minimum effect on those readings.

(9) to (13) are related to the system's attachment and other constructive concerns. It is asked to the system to be attached to the motion platform and that the connection to the mock-up bike should be stiff and universal, in order to be able to mount any kind of bike. The system should be able to carry a total weight of 400kg; the sum of weights of mock-up bike, rider and own weight of the system.

Requirements (14) and (15) relate to the dimensions of the product and its ergonomics. The maximum size of the measurement system is given by the dimensions of the motion platform and by the fact that no interference with the rider is wanted. In order to maximize the immersion of the rider in the simulations, the rider should not notice the existence of such system, in the sense that he/she should be able to move on the motorcycle (and even mount or dismount the mock-up bike) without being restricted by any obstacle.

(16) and (17) show the wish of considering the instability phenomena at low speeds in which the bike is not able to maintain the neutral position (0^o roll angle) because it tends to fall down. As a wish it is presented that the product should be able to provide a variable rolling stiffness to provide this experience: the bike should be freely movable at standing still and then increase the stiffness gradually until the speed reaches the point in which the gyroscopic forces make the bike stable (around 30km/h).

Finally, requirements (18) and (19) refer to production issues. An estimated fabrication budget is given and as a limitation it is said that the different parts of the product should be feasible to manufacture in TUD's workshops.

4 Conceptual design

Conceptual design starts from the expected specifications obtained during the product definition stage and provides as an output an accepted principle of solution. During this step, several possible solutions are proposed and evaluated; the most suitable one is the one that will be carried out.

4.1 Functional structure

One of the most important tools during conceptual design is the analysis of the functional structure[15]. The so called functional structure is a block diagram in which every block represents a function that the product must perform regardless of the specific solution that is being adopted. Arrows represent fluxes of energy, materials or signals that go between the blocks, serve as global inputs or outputs. Depending on the complexity of the product, the diagram can be divided into different sub-functions.

In this particular case, the functional structure is quite simple. Following the main requirements of the list, the following diagram has been developed:

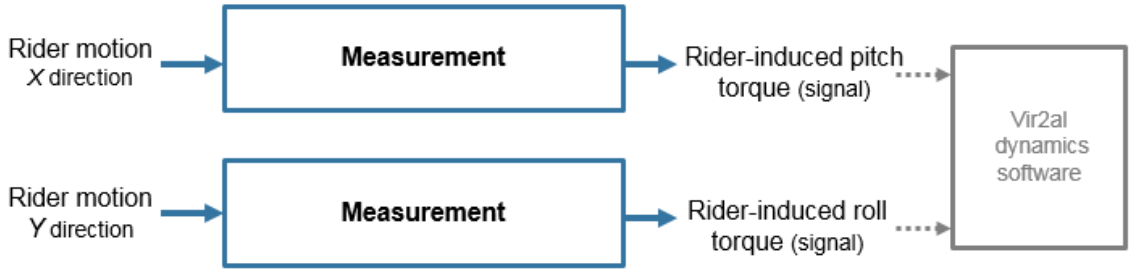

Figure 4-1: Functional structure of the product

The basic function of the product is to measure the rider motion in *X* and *Y* directions and translate this data into overall rider-induced pitch and roll torques. These torques will be added into the vehicle dynamics model.

[15] cf. Riba Romeva, C.: Disseny de màquines V, p. 127.

4.2 Creative process

The creative process involves the generation of possible solutions to a given problem. It is said that creativity comes from three different sources: first, the knowledge and the skills in the working field; second, the motivation to solve the problem; and third, the experience and intuition related to the problem and its particular circumstances.[16] Unlike other activities, it's difficult to ensure results during the creative process, for it is not an exact science. Nonetheless, it is not a spontaneous activity either, it requires preparation and organization.

For this exact reason there has been developed several methods that help stimulate creativity. Those can be divided into different categories: conventional methods (such as research, analogies, or competence analysis), intuitive methods (brainstorming, Delphi method, sinectics…) and discursive methods (scheme classification, inverted variations…).

The creative process followed during this thesis can be explained through the next scheme:

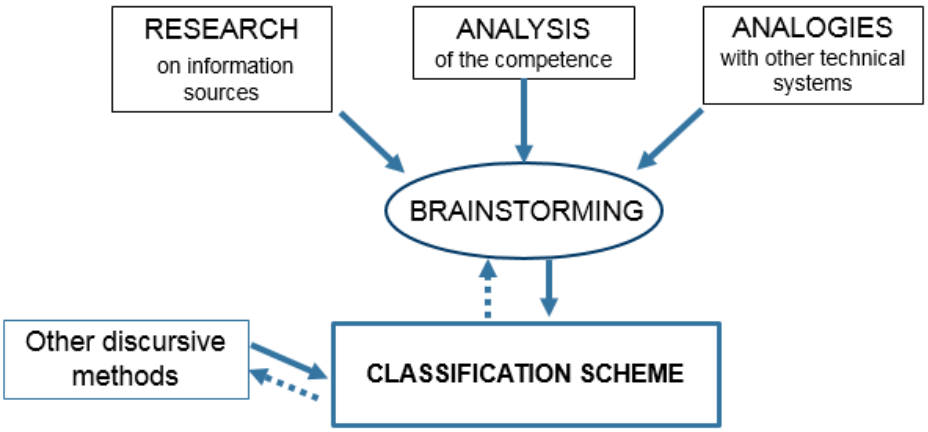

Figure 4-2: Scheme of the creative process followed

The process started with traditional creative methods: first of all, doing research in order to obtain a sufficient knowledge on the field of motorcycle dynamics and vehicle simulators in general. Then, through an exhaustive analysis of the competence to know what the state of the art was and which solutions were being used by the existing simulators. With the help of the above mentioned methods (and also others like finding analogies with other technical systems) it was possible then to perform an intuitive method. Through a kind of brainstorming procedure, several possible solutions were obtained.

Nevertheless, the most important method and the one that vertebrates all the creative process was a classification scheme. This discursive method consists in organizing the obtained possible solutions into a tree-like scheme sorting the designs into common characteristics and features. It is really easy to see this way, in which areas it is possible to improve and still find more possible solutions.

[16] Riba Romeva, C.: Disseny de màquines V, pp. 92–95.

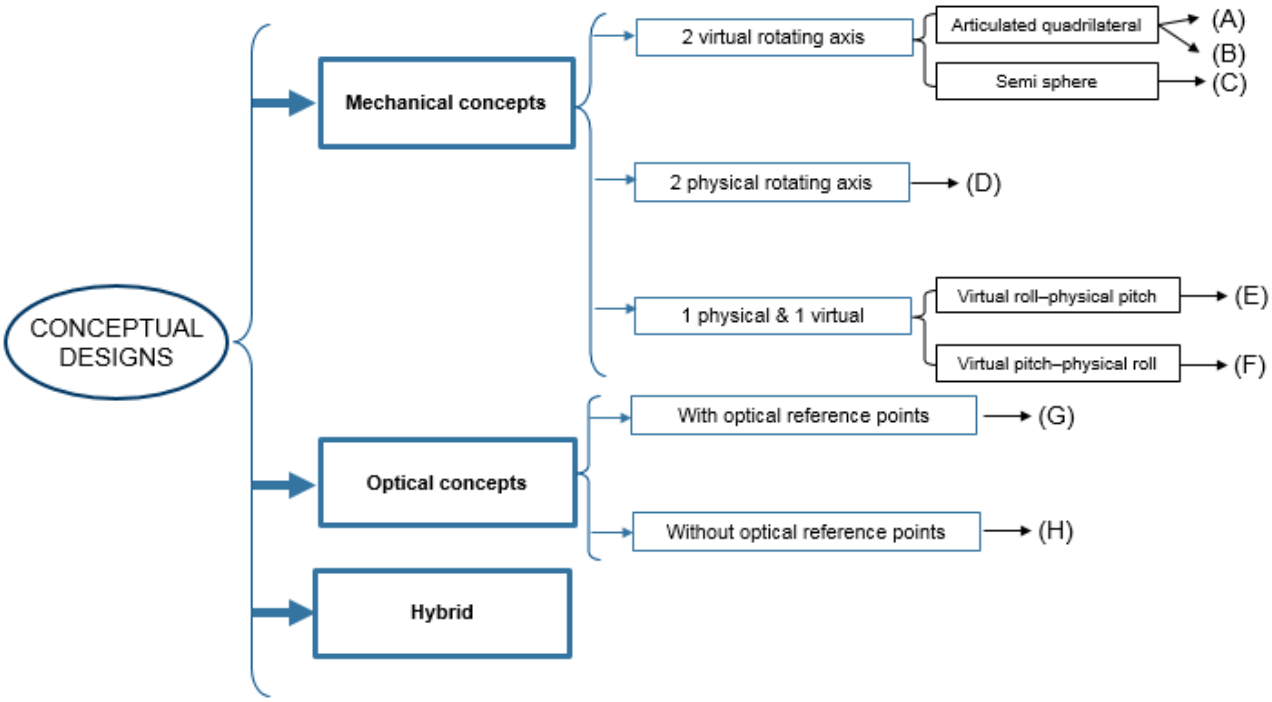

Figure 4-3: Classification scheme used during the conceptual design phase

The biggest division is the one that splits the design into mechanical concepts and optical concepts; mechanical concepts are the ones that involve a physical system that enables the direct measure of a force, torque or displacement. Optical concepts are the ones that implicate technologies involving cameras, sensors and processing images in order to estimate the torque. Since we are considering the measure of two independent torques, a hybrid solution would also be possible, in which one torque would be measured through a mechanical system and the other through an optical one.

Inside the category of optical concepts we can divide the solutions into the ones that use optical reference points (like in the case of Desmori simulator at BMW) and the ones that estimate all the upper body of the rider without wearing any reference (like in the Cruden motorcycle simulator).

Since mechanical concepts should allow the direct measure of a torque, it implies that they should allow the rotation around an axis. Nevertheless, that does not mean that the mock-up bike will have a relative motion on top of the motion platform (one of the requirements was to have a stiff connection between the motion platform and the mock-up). The rotation around that axis would be fixed through a measuring element, such as a load-cell. When the rider moves on top of the bike, a torque around that axis will be generated and the measuring element will support a certain load because it will be fixing the rotation. It's the basic idea that materializes the actual FZD simulator when measuring the roll.

However, this does not mean that all mechanical concepts should involve a physical rotating axis like in the Desmori at WIVW. We can divide mechanical concepts into the ones that use physical rotating axes, the ones that use virtual rotating axes and the ones that use one of each.

A virtual rotating axis is the one that doesn't have an actual shaft or any other physical rotating system coincident with the rotating axis. The rotation is accomplished by allowing the system to move in such a way that it describes a rotating motion around the desired virtual axis. The reason to use this kind of system rather than a physical one is that it allows to position the rotating axis exactly in the desired place without having all the constructive problems that would come along with building a shaft in that very place. It also offers more modularity, for it makes it easier to vary this position. As explained in the state of the art section, one of the problems of the Desmori simulator at WIVW is that the rotating axis cannot be in its optimal position for those constructive reasons; ideally, the rotating axis should be in the same position as the overall CoG of the system. This way, the effect of the masses of the mock-up bike would be discarded on the measuring data.

Although there are other possible ways to accomplish this, the simplest option is a bar-linkage. For its importance along this thesis and also because it will make it easier to understand further and more complex designs, an in-depth explanation of the four-bar linkage system was also presented in a state of the art section.

From all the possible conceptual designs that came into view during the creative process, the following eight represent the most appropriate ones. The selection process will be done between these concepts.

- **(A) 2 DoF surface (roll+pitch)**

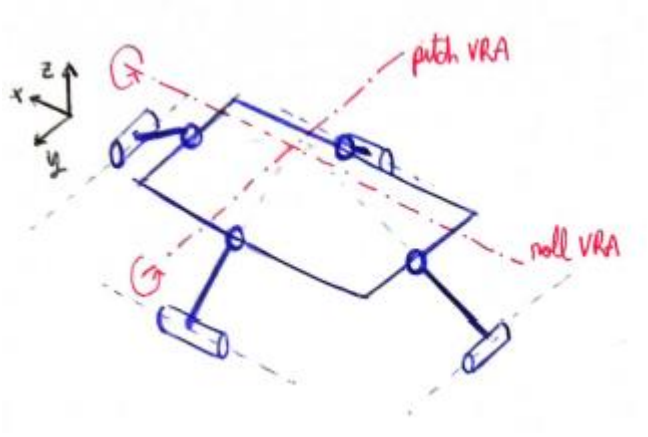

Figure 4-4: Sketch of a 2 DoF mechanical measuring system based on a moving surface

This concept is based on the idea of the 1 DoF four-bar linkage system, but this time adapted to a 3D surface that could allow both rotations around roll and pitch axes. Although the 2D four-bar linkage is a simple system and it can be easily designed, a 3D surface that allows only the mentioned rotations is much more challenging and, for that reason, the feasibility of this concept is not granted before a further analysis is done. Nevertheless, it is valuable as a concept to work on, which is why it is considered as a possible design.

- **(B) 2 superposed 1 DoF surfaces**

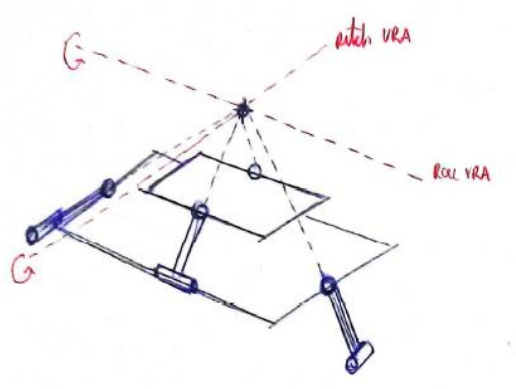

Figure 4-5: Sketch of a 2DoF mechanical measuring system based on two superposed four-bar linkage systems

For the reasons exposed on the previous design, another approach to enable two rotating axes is presented. This one, although much more complex in construction and not that optimal in terms of design has the feasibility granted; it is based on two simple one-degree rotating surfaces, one over the other, providing each of them the rotating motion around one axis.

- **(C) Spherical platform**

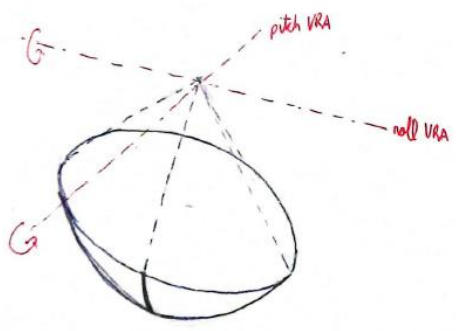

Figure 4-6: Sketch of a 2DoF mechanical measuring system based on a spherical platform

In this case, in order to allow the desired two rotations, a spherical platform is proposed. Although it is a solution that ideally works and the feasibility is theoretically granted, it is obvious that it would be a very complex (and for that reason, expensive) approach.

- **(D) 2 physical rotating axes**

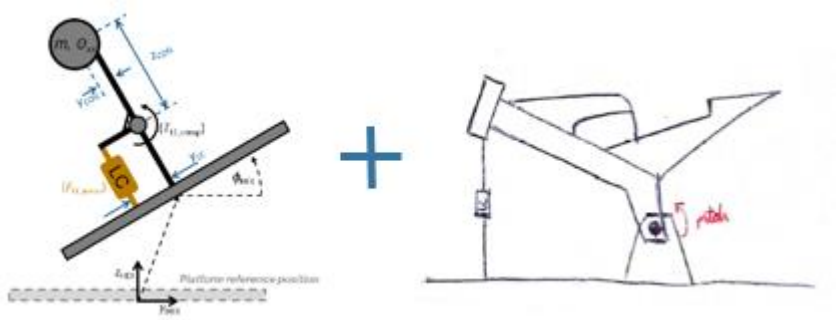

Figure 4-7: Scheme showing the idea of incorporating two physical rotating axes[17]

In this case the solution would be to incorporate an actual rolling axis on the mock-up bike, like in the case of the Desmori at WIVW, and another one that could allow the rotation around the pitching axis. For instance, the swing-arm of the mock-up could be easily used as such.

- **(E) 1 DoF surface (roll) + physical pitching axis**

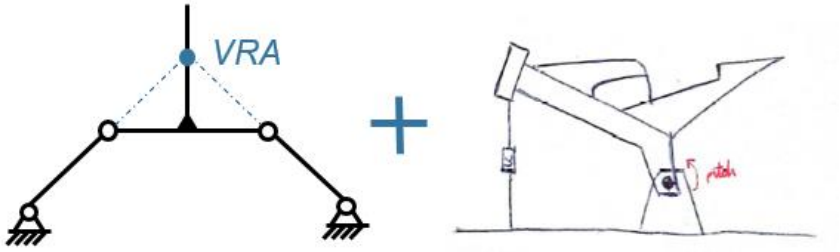

Figure 4-8: Scheme showing the idea of having a VRA for rolling and a physical RA for pitching

The following concept is a mix of ideas: uses a physical pitching axis (that could be placed in the swing-arm axis) and a 1DoF platform based on the four-bar linkage system.

- **(F) 1 DoF surface (pitch) + physical rolling axis**

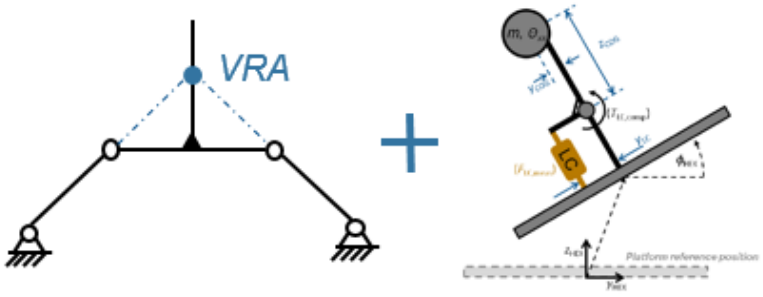

Figure 4-9: Scheme showing the idea of having a VRA for pitching and a physical RA for rolling [18]

[17](Adapted from) Pleß, R. et al.: Approach to a holistic rider input determination for a dynamic motorcycle riding simulator, p. 7.

[18](Adapted from) Pleß, R. et al.: Approach to a holistic rider input determination for a dynamic motorcycle riding simulator, p. 7.

This one is the complementary of the previous concept; physical axis is the one that allows the rolling and the surface creates a virtual rotating axis around the pitch.

- **(G) Optical system with reference points**

Using different cameras around the simulator and with the help of optical reference points placed on the rider's body, this system could analyse the images and process them in order to translate the data into torques.

- **(H) Optical system without reference points**

Similar to the previous concept, but without the need of placing optical reference points on the body of the rider, for the processing system would estimate them directly from the images, like in the case of the Cruden motorcycle simulator

4.3 Concept selection

In order to evaluate these concepts and choose the most valid one, a selection procedure called AHP (Analytic Hierarchy Process) has been carried out. In this procedure, a set of comparative tables are developed and each solution is faced against the others in regards to different criteria.[19] A given solution (or criteria) is confronted to another one (rows vs. columns), and is evaluated if it's better (1), equivalent (0,5) or worse (0).

The first step is the ponderation of the evaluating criteria. Following the procedure just explained it is found how important those criteria are in relation to the rest. In this case the following evaluating criteria have been considered:

- Simplicity: the concept must be as simple as possible. The lesser moving parts and the lower the complexity of those, the easier (and cheaper) it will be to be conceived and built.
- Versatility: as it has been stated on the request list, the system must be able to attach different mock-up bikes and to adapt its geometry in order to maintain the desired precision even though the CoG position changes.
- Measurement accuracy: also asked on the request list, it is the most important evaluating criteria
- Measurement directness (processing speed): it is well-know that in simulators the response time is critical in order to provide to the rider a fast response and, thus, grant a realistic experience. The system must be able to compute the torques and send them to the vehicle dynamics model as fast as possible.
- Adaptability to accomplish wishes: it is also considered the capacity of the design to potentially adapt so that wishes on the request list can be accomplished.

[19]cf. Riba Romeva, C.: Disseny de màquines V, p. 59.

The following table shows the ponderation of these criteria:

CRITERIA	Simplicity	Versatility	Accuracy	Directness	Adaptability	∑+1	Pondered
Simplicity		0,5	0	0,5	1	3	0,20
Versatility	0,5		0	0,5	1	3	0,20
Accuracy	1	1		1	1	5	0,33
Directness	0,5	0,5	0		1	3	0,20
Adaptability	0	0	0	0		1	0,07
					SUM	15	1

Table 4-1: AHP criteria evaluation table

The next step is the evaluation of the different concepts in regard to the different criteria, starting with simplicity:

SIMPLICITY	A)	B)	C)	D)	E)	F)	G)	H)	∑+1	Pondered
A)		1	1	1	1	1	0,5	0,5	7	0,19
B)	0		1	1	1	1	0,5	0,5	6	0,17
C)	0	0		0,5	0	0	0	0	1,5	0,04
D)	0	0	0,5		0	0	0	0	1,5	0,04
E)	0	0	1	1		1	0	0	4	0,11
F)	0	0	1	1	0		0	0	3	0,08
G)	0,5	0,5	1	1	1	1		0	6	0,17
H)	0,5	0,5	1	1	1	1	1		7	0,19
								SUM	36	1

Table 4-2: AHP simplicity evaluation table

As we can see, the simplest designs are the ones of the 2DoF surface (A) and the optical system without optical references (H). They are closely followed by the 2 superposed 1DoF surfaces (B) and the optical system with optical references (G). Without any doubt, the most complicated designs are the spherical platform (C) and the 2 physical rotating axes (D).

VERSATILITY	A)	B)	C)	D)	E)	F)	G)	H)	∑+1	Pondered
A)		0,5	1	1	1	1	0,5	0,5	6,5	0,18
B)	0,5		1	1	1	1	0,5	0,5	6,5	0,18
C)	0	0		0	0	0	0	0	1	0,03
D)	0	0	1		0	0	0	0	2	0,06
E)	0	0	1	1		0,5	0	0	3,5	0,10
F)	0	0	1	1	0,5		0	0	3,5	0,10
G)	0,5	0,5	1	1	1	1		0,5	6,5	0,18
H)	0,5	0,5	1	1	1	1	0,5		6,5	0,18
								SUM	36	1

Table 4-3: AHP versatility evaluation table

From the previous table we can see that sorted by its versatility, concepts (A), (B), (G) and (H) stand out. If there is a change of the mock-up or the rider, systems (A) and (B) can change easily the position of the rotating axis in order to maintain the desired precision. This could be accomplished by changing the length of their legs or the position in which they are attached. (G) and (H), since they rely on optical systems, the change of those characteristics has no influence on the performance. Of course, the least versatile design is the one coming from the spherical platform (C), because to change the position of the virtual rotating axis the radius of the sphere has to be changed, which is highly unfeasible.

The following one shows the comparison in regards to measurement accuracy. The most accurate concepts are the ones that provide a virtual rotating axis. As they can locate the rotating axes very close to the CoG, the readings on the load-cells can be much lower, and thus, use measurement systems with much precision. Overall, the concepts involving optical recordings perform the poorest in this respect, because they are based on estimations (in the case of no optical references) or rely in very few reference points.

ACCURACY	A)	B)	C)	D)	E)	F)	G)	H)	∑+1	Pondered
A)		0,5	0,5	1	1	1	1	1	7	0,19
B)	0,5		0,5	1	1	1	1	1	7	0,19
C)	0,5	0,5		1	1	1	1	1	7	0,19
D)	0	0	0		0	0	1	1	3	0,08
E)	0	0	0	1		0,5	1	1	4,5	0,13
F)	0	0	0	1	0,5		1	1	4,5	0,13
G)	0	0	0	0	0	0		0	1	0,03
H)	0	0	0	0	0	0	1		2	0,06
								SUM	36	1

Table 4-4: AHP accuracy evaluation table

According to the directness of measure, all mechanical solutions perform well because they measure a force; the only processing needed before sending the recorded data to the vehicle dynamics model is correcting the signal if inertial forces are measured. In the case of optical systems, the processing is much longer and complex and the more reference points they consider, the higher the precision but also the slower the response.

DIRECTNESS	A)	B)	C)	D)	E)	F)	G)	H)	∑+1	Pondered
A)		0,5	0,5	0,5	0,5	0,5	1	1	5,5	0,15
B)	0,5		0,5	0,5	0,5	0,5	1	1	5,5	0,15
C)	0,5	0,5		0,5	0,5	0,5	1	1	5,5	0,15
D)	0,5	0,5	0,5		0,5	0,5	1	1	5,5	0,15
E)	0,5	0,5	0,5	0,5		0,5	1	1	5,5	0,15
F)	0,5	0,5	0,5	0,5	0,5		1	1	5,5	0,15
G)	0	0	0	0	0	0		1	2	0,06
H)	0	0	0	0	0	0	0		1	0,03
								SUM	36	1

Table 4-5: AHP directness evaluation table

Finally, the following table is about the adaptability of the design to accomplish request wishes. Both (A) and (B) are very suitable to incorporate further requirements such as high frequency excitation, just replacing measurement items for exciting ones.

ADAPTABILITY	A)	B)	C)	D)	E)	F)	G)	H)	∑+1	Pondered
A)		0,5	1	1	1	1	1	1	7,5	0,21
B)	0,5		1	1	1	1	1	1	7,5	0,21
C)	0	0		0,5	0,5	0,5	1	1	4,5	0,13
D)	0	0	0,5		0,5	0,5	1	1	4,5	0,13
E)	0	0	0,5	0,5		0,5	1	1	4,5	0,13
F)	0	0	0,5	0,5	0,5		1	1	4,5	0,13
G)	0	0	0	0	0	0		0,5	1,5	0,04
H)	0	0	0	0	0	0	0,5		1,5	0,04
								SUM	36	1

Table 4-6: AHP adaptability evaluation table

The last step of the AHP is pondering the results by the ratios found in the first table; this way we are able to see the final performance of every concept and develop a ranking:

EVALUATION	Simplicity (x0,2)	Versatility (x0,2)	Accuracy (x0,33)	Directness (x0,2)	Adaptability (x0,07)	∑	**Ranking**
A)	0,03889	0,03611	0,06481	0,03056	0,01389	0,18426	**1**
B)	0,03333	0,03611	0,06481	0,03056	0,01389	0,17870	**2**
C)	0,00833	0,00556	0,06481	0,03056	0,00833	0,11759	**4**
D)	0,00833	0,01111	0,02778	0,03056	0,00833	0,08611	**8**
E)	0,02222	0,01944	0,04167	0,03056	0,00833	0,12222	**3**
F)	0,01667	0,01944	0,04167	0,03056	0,00833	0,11667	**5**
G)	0,03333	0,03611	0,00926	0,01111	0,00278	0,09259	**7**
H)	0,03889	0,03611	0,01852	0,00556	0,00278	0,10185	**6**
					SUM	1,00000	

Table 4-7: AHP final evaluation table

According to the previous table, the most suitable design is the 2 DoF surface (A), followed closely by the 2 superposed 1 DoF surfaces (B). After a quick analysis of the AHP, it can be seen that both have an exact performance on all criteria, except for simplicity. It is clear that an only moving surface is a much simpler and finer solution than having two of them one on top of the other, but as it has been said before, the feasibility of such a system is not granted. For that reason, when this point of the design was reached during this thesis, the following objective was pointed: to ensure the feasibility

of a linkage system that allows 2 specific DoF (pitch and roll) on a surface. If finally it was found that it was not possible to create such a system, concept (B) would be the option carried out.

4.4 Concept feasibility

The aim of this section is to ensure that the chosen concept design can be implemented in reality. In order to show the process followed during the thesis, the different approaches that came up to materialize the concept are presented.

The concept is a bar-linked surface system that allows two specific degrees of freedom: rolling and pitching. These DoF will be fixed afterwards by load-cells, obtaining a measuring system of the rider induced torques around those axes. The rotating axes shall be located at a desired position changing the geometry of the multibody. It is, as a matter of fact, a 3D extrapolated concept of the four-bar linkage system presented before.

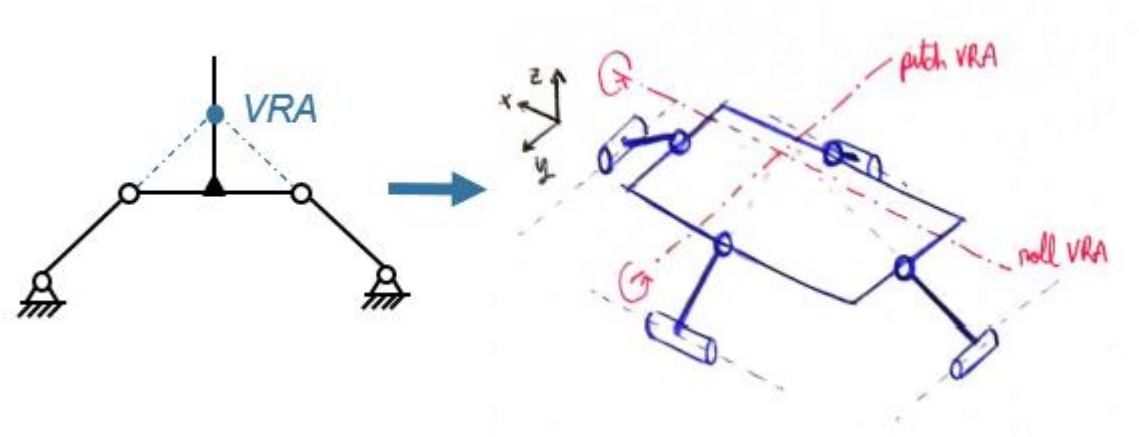

Figure 4-10: Scheme showing the relationship between the four-bar linkage system and the 2DoF surface

To ensure the feasibility of this concept means, in this case, to find if there is a viable way to obtain a moving surface with the desired degrees of freedom. To find the right kinematics of a given mechanism, the common approach is to try to find the right joint types that allow the desired motion for the given bodies.

The total number of DoF of a mechanism is defined by the number of bodies multiplied by 6 (maximum DoF for a solid body in the space) and then subtracting the degrees of freedom fixed by the chosen joints:

$$DoF_{mec} = (n_{bodies} \times 6) - \sum_{i=1}^{j} (n_{j-joints} \times fixed\ DoF_j) \tag{4-1}$$

As an extrapolation of the 2D four-bar linkage system, the process started considering a surface and four legs; the idea was to create each rotating axis by the confronting legs. Aiming the four of them

at the same point would enable to have a general center of rotation where both pitch and roll axes meet.

- **Approach 1:** 1 surface, 4 legs and 8 spherical joints

The first idea was to use spherical joints on all the unions, which only fix the three degrees of freedom related to linear motion and allow the three possible rotations.

$$DoF_{mec} = (5 \times 6) - (8 \times 3) = 6 \tag{4-2}$$

As it can be seen from the count of DoF, this approach is far under-constrained, allowing the motion in 4 more DoF than needed. For this reason, it was discarded.

- **Approach 2:** 1 surface, 4 legs, 4 spherical joints and 4 revolute joints

In order to reduce the amount of DoF, it was proposed to replace the joints on the bottom of the legs by revolute joints, which only allow 1 DoF: the rotation around one axis.

$$DoF_{mec} = (5 \times 6) - (4 \times 3) - (4 \times 5) = -2 \tag{4-3}$$

In this case the system would be over-constrained and was, thus, rejected too.

- **Approach 3:** 1 surface, 4 legs, 4 spherical joints and 4 cylindrical joints

For the next approach the revolute joints were substituted by cylindrical joints, which also allow a linear motion.

$$DoF_{mec} = (5 \times 6) - (4 \times 3) - (4 \times 4) = 2 \tag{4-4}$$

According to the count, this approach would enable the correct amount of DoF. To check if the given ones correspond to the desired rolling and pitching, a first analysis of the kinematics was done. Let's consider that the platform is rotating around either axis. The velocity experienced by the system can be seen in the following figure, representing the platform seen in the direction of the rotating axis. As it can be seen on the right figure, such rotating motion would not be possible because it will be re-strained by the length of the central legs.

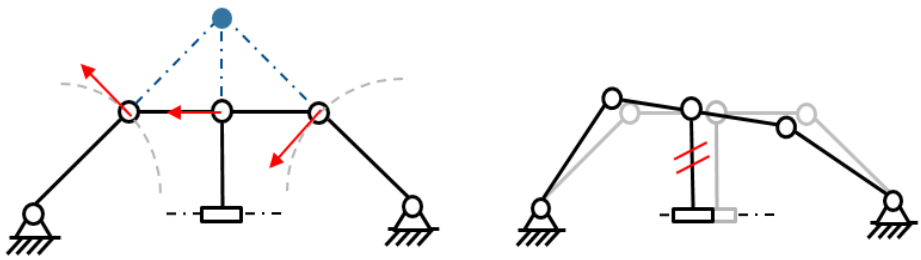

Figure 4-11: Scheme showing the restricted motion done by the central legs on the Approach 3

It is demonstrated then, that the DoF's performed by this approach are not the ones desired and this option is also not the right one. However, the kinematic analysis developed gives important information and constitutes the base of the following approach: considering extendable legs.

- **Approach 4:** 1 surface, 4 legs (x2 parts each), 4 prismatic joints, 4 spherical joints and 4 universal joints

The main idea of this approach is to consider legs with extendable length, which in the mechanism model it means having legs divided into two parts linked through a prismatic joint. This way, the motion that was constricted in the previous approach would be enabled.

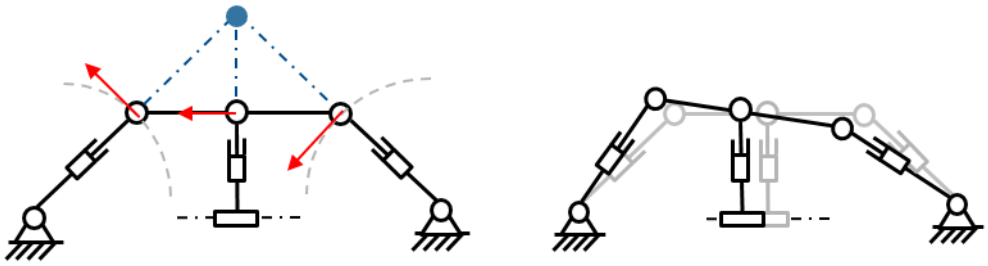

Figure 4-12: Scheme showing the enabling of the roation through the use of extendable legs

In order to obtain only 2 DoF it is necessary to replace the spherical joints that are on top of the system by universal joints that only allow two rotations.

$$DoF_{mec} = (9 \times 6) - (4 \times 5) - (4 \times 4) - (4 \times 4) = 2 \tag{4-5}$$

It is important to remind that in reality the degrees of freedom will be fixed by load-cells, which means that the motions experienced will be infinitesimal. Having only infinitesimal changes on the length of the legs means that, in reality, these changes could be assumed by the bearing plays or an elastic union, and that having an actual division of the legs would not be necessary.

Although at first sight it seems that this approach would accomplish the requirements, a simulation with Simscape has been carried out to make sure that it behaves the way it is asked.

On the Simscape model, the DoF have already been fixed by substituting two of the cylindrical joints (one in each direction) by simple revolute joints and enabling the reading of the constraint force in the axial direction. In reality this would mean having two load-cells fixing the axial motion of two of the cylindrical joints. This should allow to measure a force proportional to the motion of the rider, like in the case of the four-bar linkage system. A mass representing the rider has been also set in the model, and this time allowing it to move in both X and Y directions. To implement the extendable legs, a prismatic joint with a very high stiffness has been used.

The following figures show the effects of a rider motion in X direction.

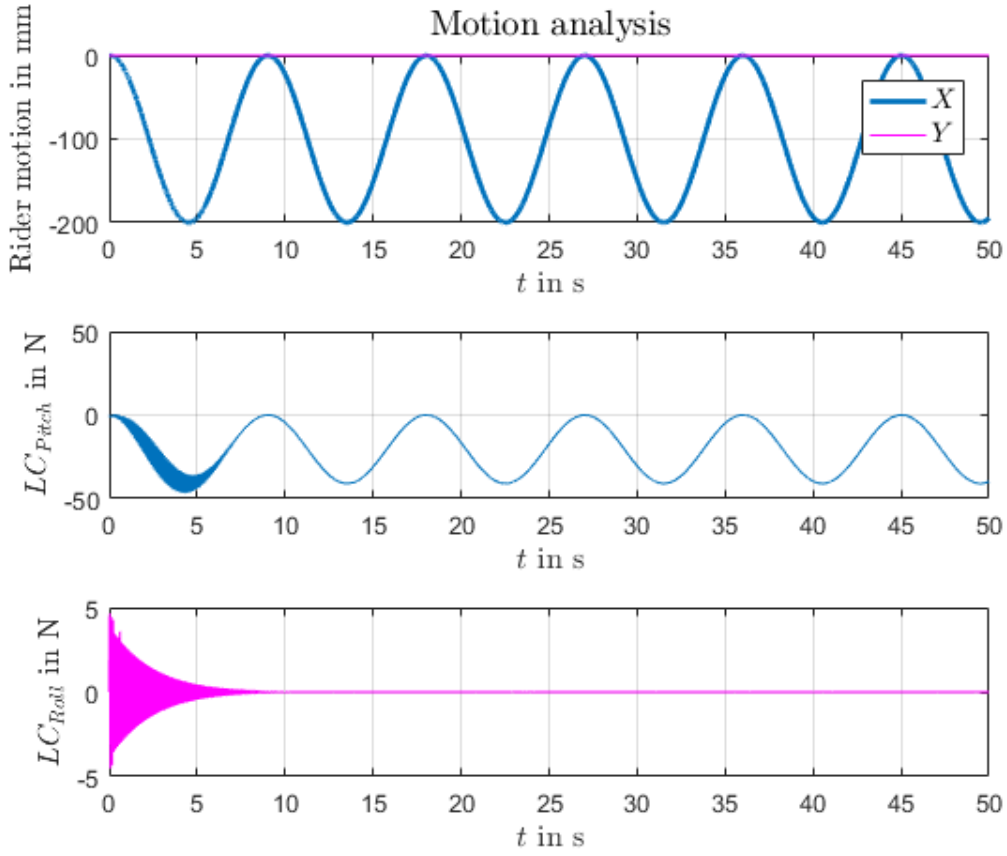

Figure 4-13: Dynamic analysis of approach 4 under rider excitation along *X* direction

Ignoring the initial noise that comes from considering a very high stiffness on the prismatic joints, we can see that the system behaves as expected. The load-cell measures a force proportional to the displacement of the rider's mass.

The following figure shows the relationship between the both, and we can see that it is completely linear.

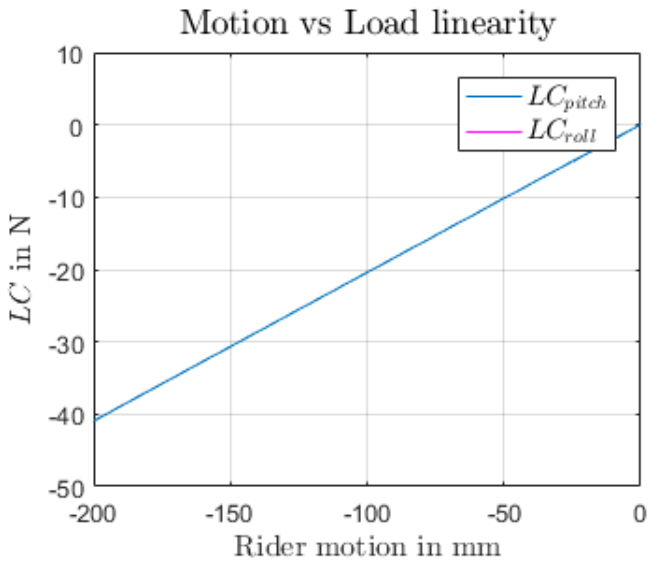

Figure 4-14: Measured load vs rider motion of approach 4 under rider excitation along *X* direction

When the excitation is done in Y direction, the results are akin:

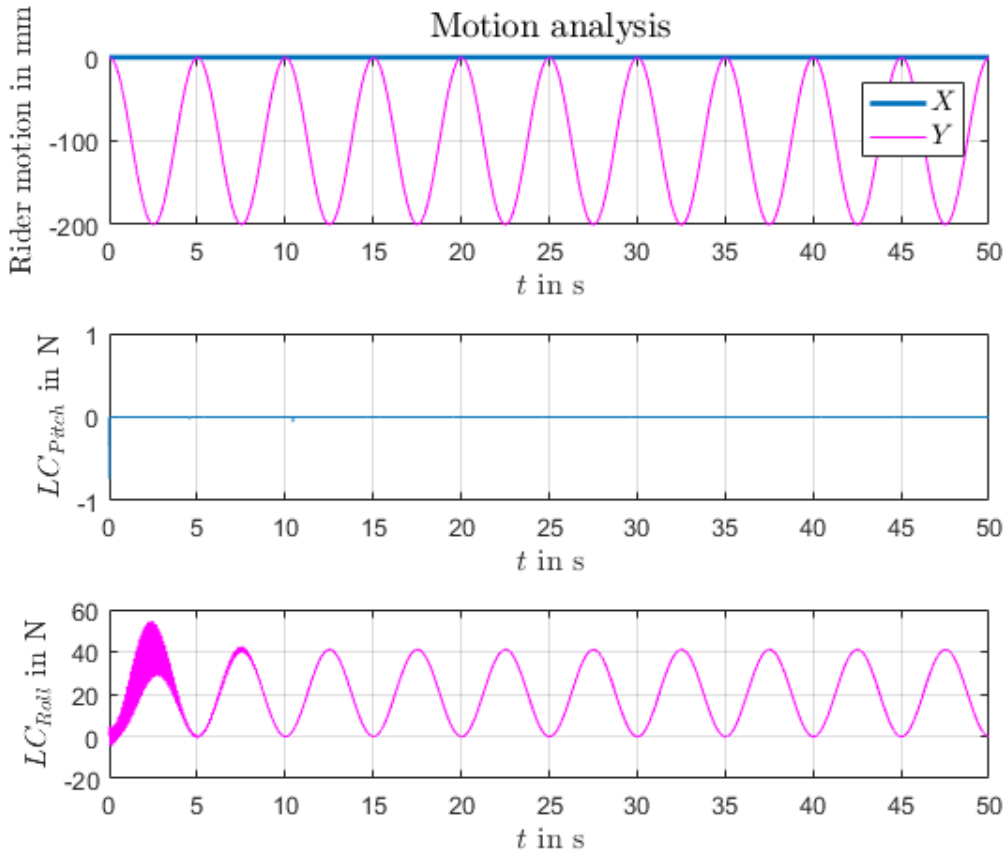

Figure 4-15: Dynamic analysis of approach 4 under rider excitation along *Y* direction

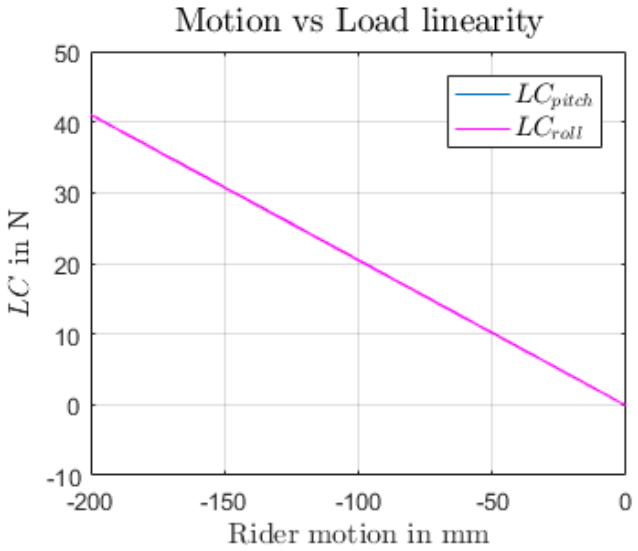

Figure 4-16: Measured load vs rider motion of approach 4 under rider excitation along *Y* direction

Finally, a test having an excitation in both directions was performed.

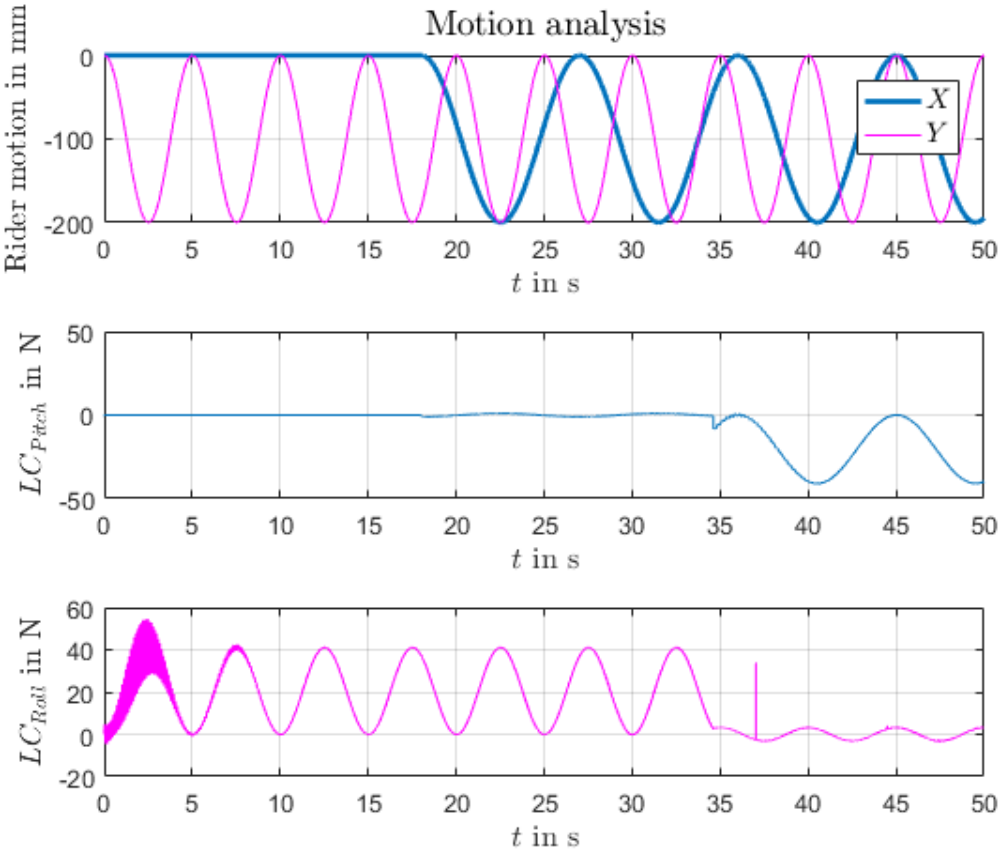

Figure 4-17: Dynamic analysis of approach 4 under rider excitation along *XY* directions

This time we can see that the system is not behaving in the expected manner. During the first part of the simulation, only the *Y* excitation is enabled and the measuring system works just fine, measuring a proportional force on the roll load-cell. When the motion in *X* direction appears, the system does not show any reading on the pitch load-cell, until a certain point, in which the readings on the pitch load-cell appear and the ones on the roll disappear. We can see that this change occurs when the rider's motion component of the current showing force is in neutral position, whereas the other one is far from it.

Apparently this approach is able to provide the two required DoF's but only separately. Only in neutral position is the mechanism able to rotate around both axes, but as soon as it starts to rotate around one of them and the neutral position is lost, it is not able to perform a rotation around the other axis. Only when the neutral position is reached once again, the mechanism is able to change the rotating axis.

For this reason, it lays demonstrated that approach 4 is not a viable concept either. At this point of the thesis, the following question came up: is it really necessary to have four legs (2 vs 2) to create the required rotating axes? Or is it possible to accomplish that with only three legs? The following approaches were considered to answer this very question.

- **Approach 5:** 1 surface, 3 legs, 3 cylindrical joints, 2 spherical joints and 1 universal joint.

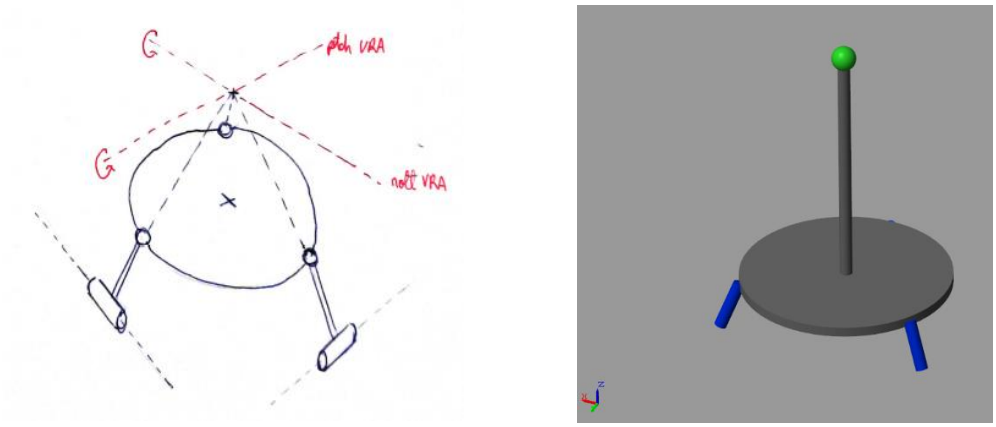

Figure 4-18: Sketch (left) and screenshot of the Simscape model (right) of approach 5

Approach 5 discards the idea of extendable legs because in the case of tripods, since the motion of the legs is not orthogonal, the rotation around one axis is not restrained by the length of a leg. For the moment, it is considered that the legs create a regular tripod: oriented 120º from each other.

In this case, 3 cylindrical joints have been considered on the bottom of the legs, whereas on the top we have 2 spherical joints and 1 universal joint (the position in which this last one is placed is, for the purposes of this explanation, irrelevant).

$$DoF_{mec} = (4 \times 6) - (3 \times 4) - (2 \times 3) - (1 \times 4) = 2 \tag{4-6}$$

Following the path of the previous approaches, two of the cylindrical joints will have their axial motion fixed by load-cells in order to constrain the DoF's and enable the measuring. Like in the case of the position of the universal joint, the choice of which cylindrical joints are fixed it is considered, so far, trivial.

Having a tripod instead of a quadripod means that the measurement on the load-cells has not a direct connection to the rider induced torques, for the orientation of the load-cells is no longer orthogonal. However, with a simple trigonometrical conversion it is possible to obtain the desired information.

The following figure shows the results of the analysis of this approach performed with Simscape, this time performing a riding motion on both *X* and *Y* directions. As we can see, the measuring system works accordingly to the requirements, having a clear lecture of both pitch and roll rider induced torques.

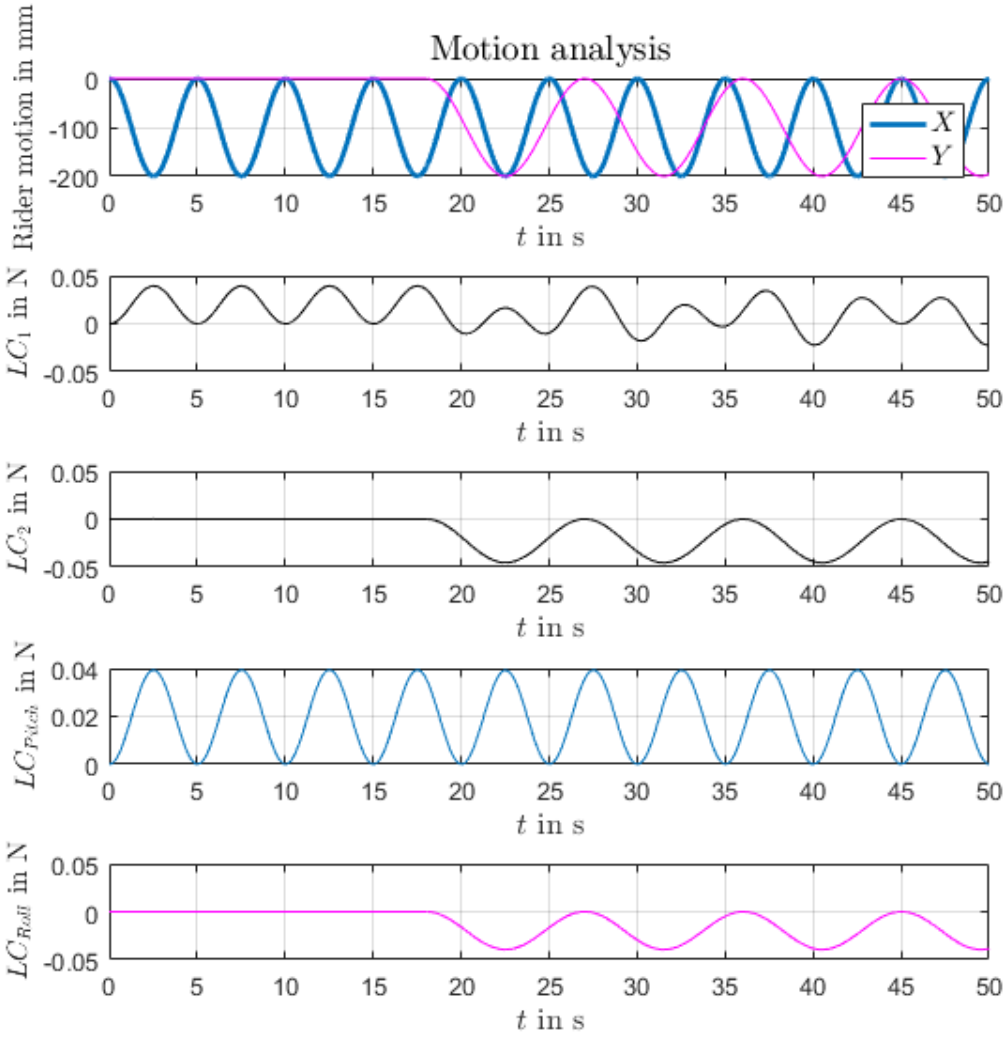

Figure 4-19: Dynamic analysis of approach 5 under rider excitation along *XY* directions

We can also see from the following graph, that the relationship between the motion and the measurement for both cases is completely linear.

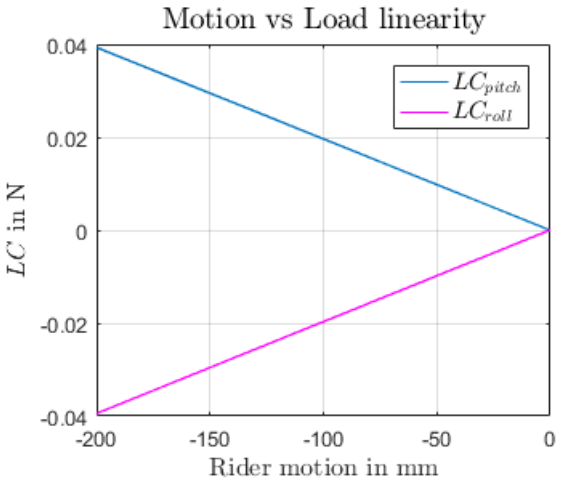

Figure 4-20: Measured load vs rider motion of approach 5 under rider excitation along *XY* directions

This means that approach 5 provides the right kinematics for a 2DoF motion platform that enables the measuring of rider induced roll and pitch torques. Therefore, the feasibility of the concept chosen in the previous chapter is demonstrated.

Although it could have been enough with this last approach, during the development another possible tripod mechanism configuration aroused:

- **Approach 6:** 1 surface, 3 legs, 3 cylindrical joints and 3 spherical joints

The particularity of this approach is that it is completely symmetrical, and each leg has the same constraints. In this case, not 2 DoF have been considered but 3, in order to install a load-cell on each of the cylindrical joints.

$$DoF_{mec} = (4 \times 6) - (3 \times 4) - (3 \times 3) = 3 \tag{4-7}$$

The analysis with Simscape gave the following results. It is remarkable that this option works well too and would be a valid approach for the materialization of the rider induced measurement system.

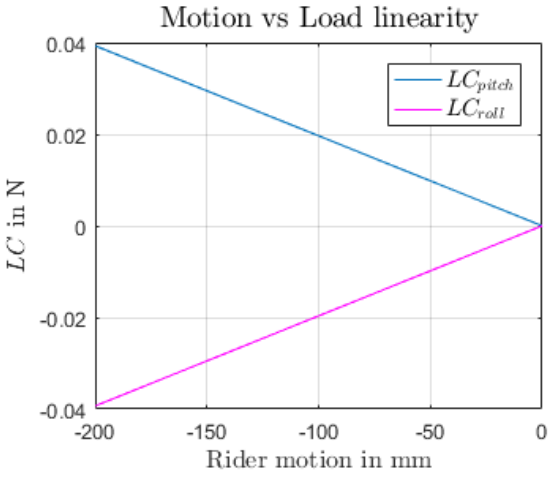

Figure 4-21: Measured load vs rider motion of approach 6 under rider excitation along *XY* directions

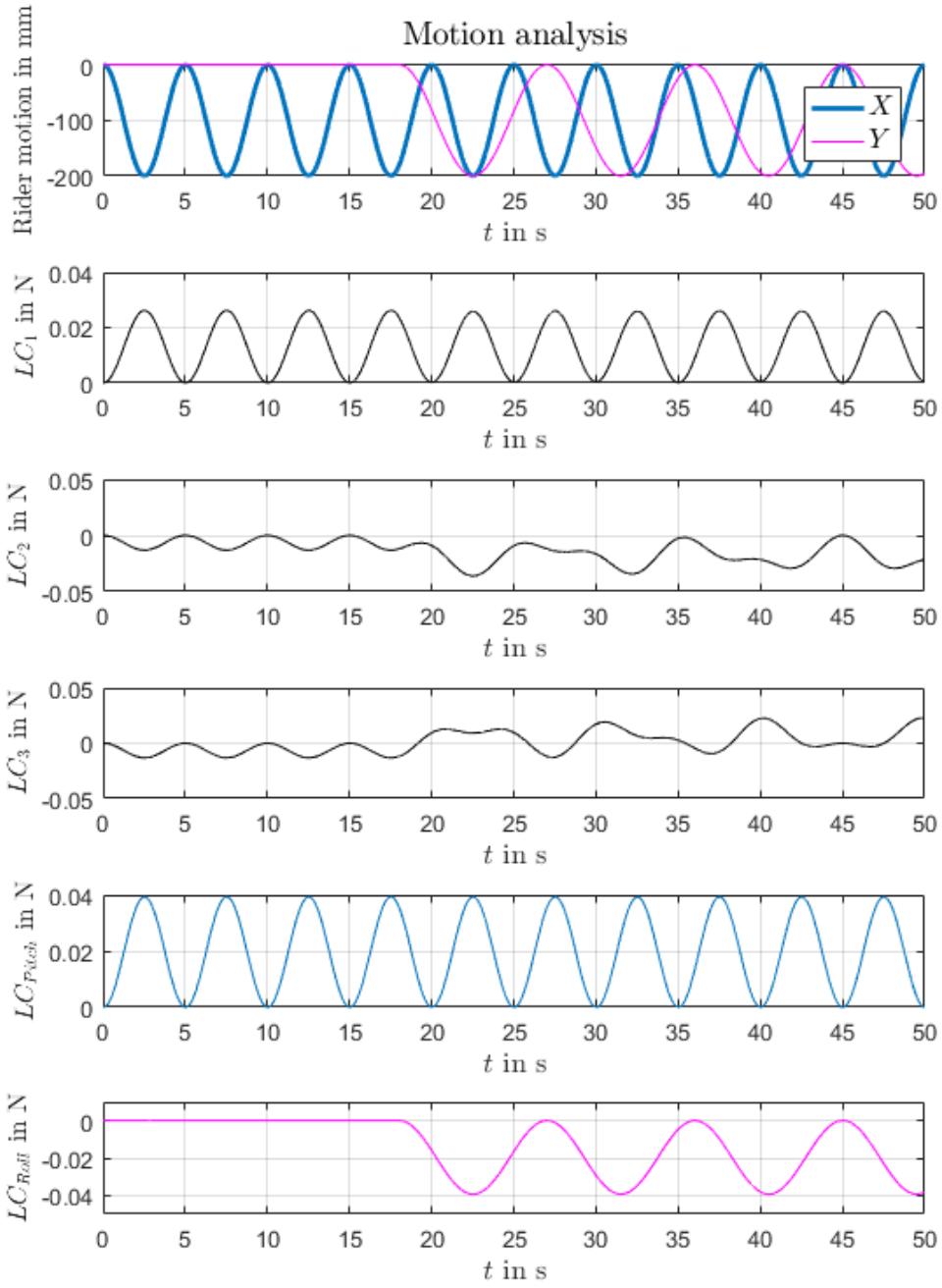

Figure 4-22: Dynamic analysis of approach 6 under rider excitation along *XY* directions

Therefore, it is verified that the feasibility of the chosen conceptual design is granted; and not only with one possible configuration, but with two. Cinematically speaking both approaches 5 and 6 perform exactly the same because they both create the desired rolling and pitching axes on the mechanism.

4.5 Two vs. three load-cells

The final step of the conceptual design stage is choosing one of the two valid approaches found in the previous part (approaches 5 and 6) in order to develop the solution according to it. As stated before, both are valid cinematically because they provide the required DoF's that are later fixed by load-cells, enabling this way the measurement of the rider induced torques. However, they present constructive and performance differences, and those will determine which one will be chosen.

The first difference has to do with the magnitude of the reading loads. Having only two load-cells implies that the reaction forces created by these in order to counteract rider-induced torques will have to be greater than in the case of having three load-cells. Note that, as it has been shown, after pertinent trigonometric transformations, both approaches read the same equivalent rider-induced forces; however, that does not mean that the particular forces experienced by each of the load-cells is the same for the two approaches. Measuring higher loads implies getting a worse precision, which is something we want to avoid.

The following example shows the behavior of approaches 5 and 6 under a rider-induced roll torque, considering the orientation shown on the following picture:

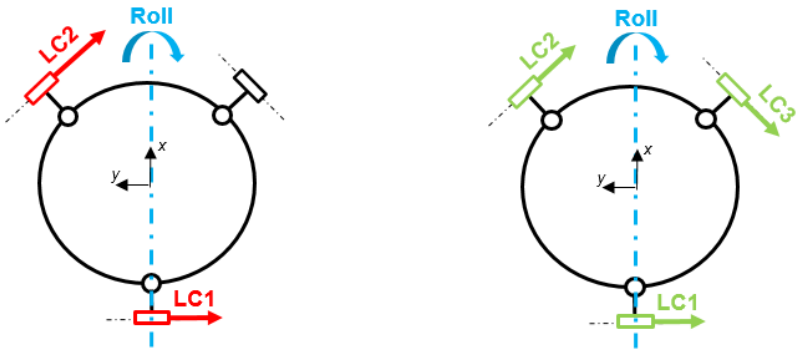

Figure 4-23: Scheme of the load-cells under induced roll for approach 5 (left) and approach 6 (right)

The next graphs show the performance of both approaches under this scenario, and also the specific loads read on every load-cell. It is visible how in the case of approach 5, the magnitude read on LC2 is much bigger, since all the rider-induced torque is counteracted by this only load-cell. As it handles bigger loads, it means that the precision of the readings will be lower than in the case of the load-cells if approach 6.

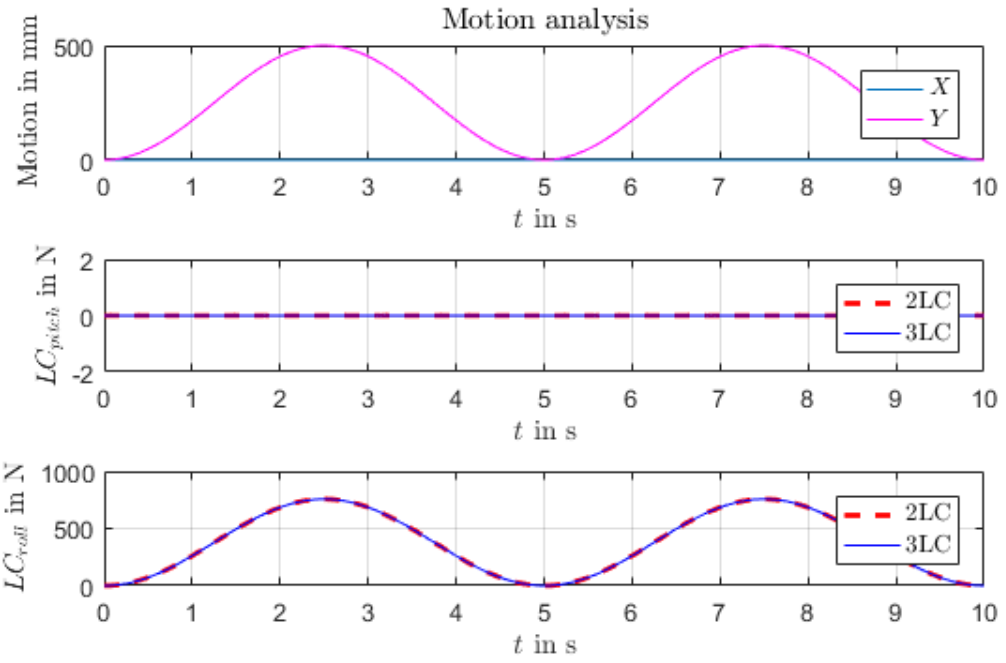

Figure 4-24: Dynamic analysis of approach 5 and 6 under rider excitation along *Y* direction (induced roll)

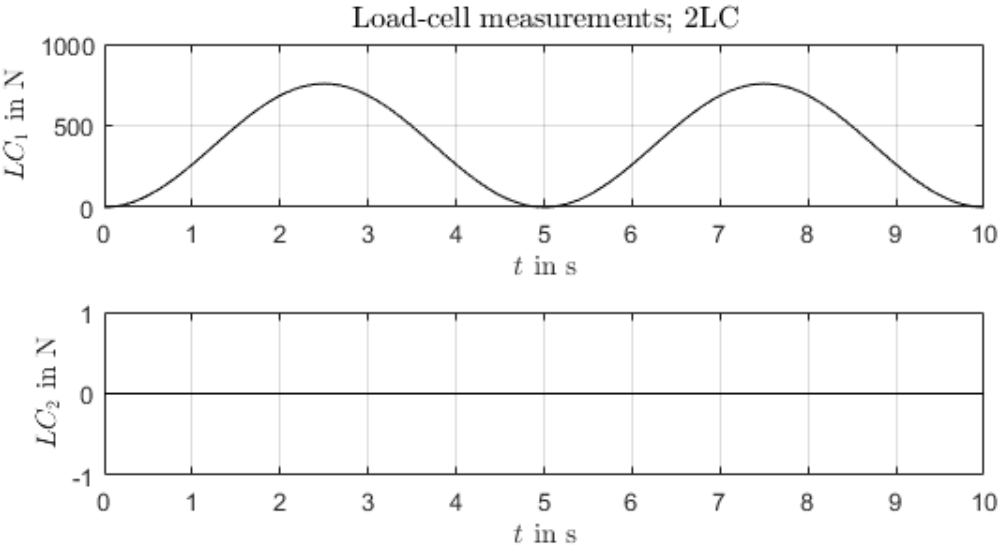

Figure 4-25: Load-cell measurements of approach 5 under rider excitation along *Y* direction (induced roll)

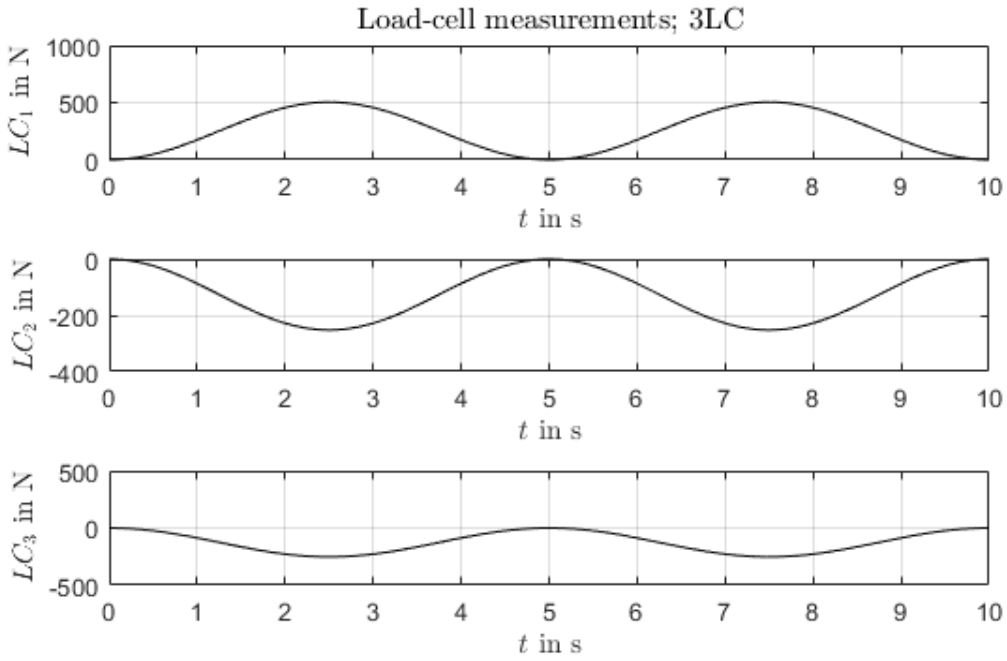

Figure 4-26: Load-cell measurements of approach 6 under rider excitation along *Y* direction (induced roll)

The analogous case in which a pitching rider-induced torque is applied is also shown. The conclusions stated for the previous scenario are applicable for this one as well.

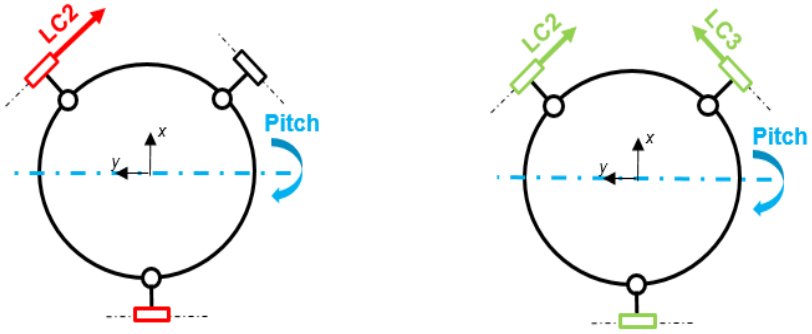

Figure 4-27: Scheme of the load-cells under induced pitch for approach 5 (left) and approach 6 (right)

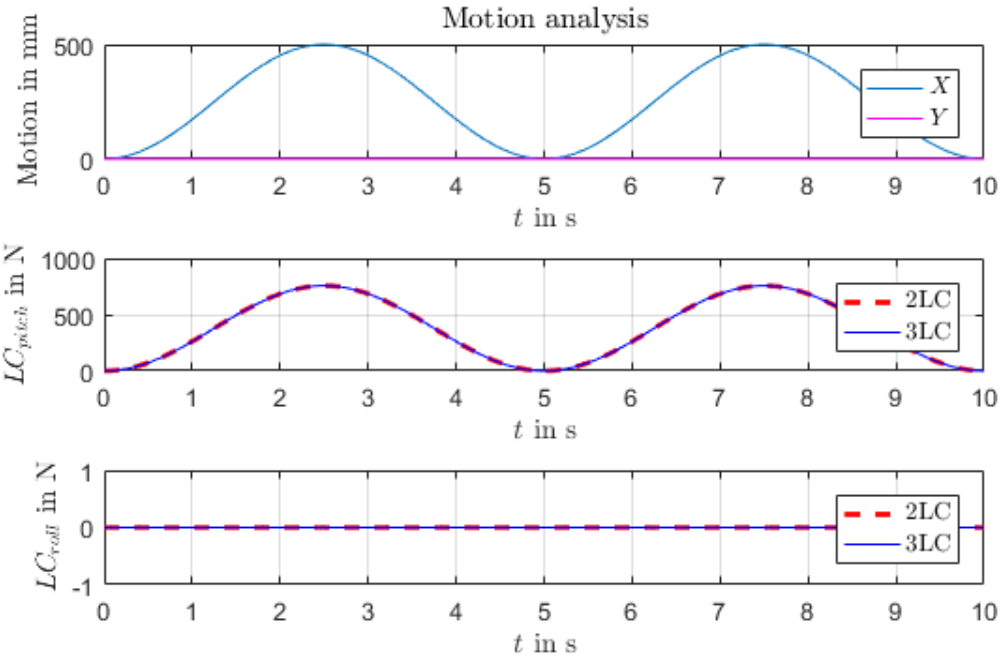

Figure 4-28: Dynamic analysis of approach 5 and 6 under rider excitation along *X* direction (induced pitch)

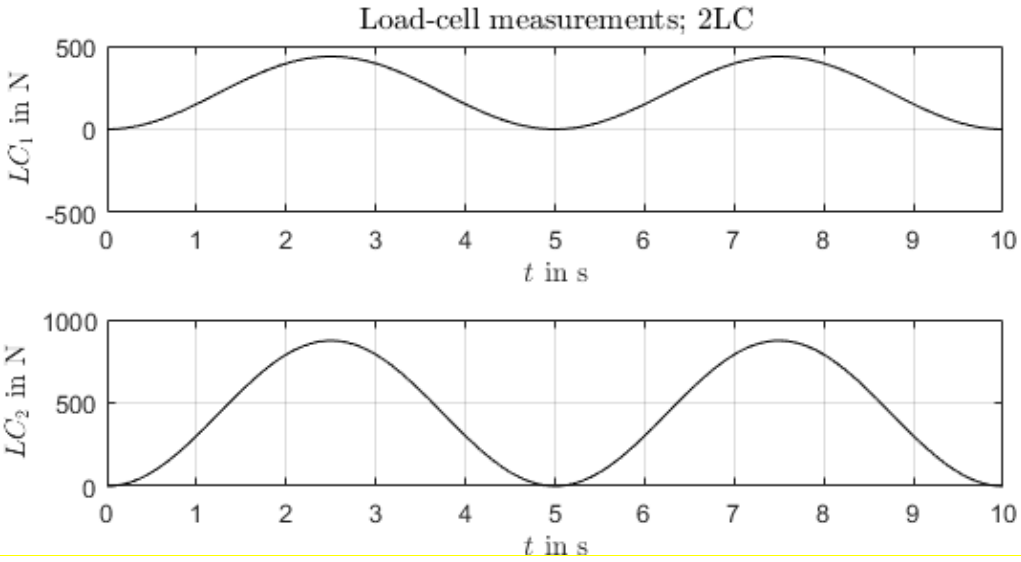

Figure 4-29: Load-cell measurements of approach 5 under rider excitation along X direction (induced pitch)

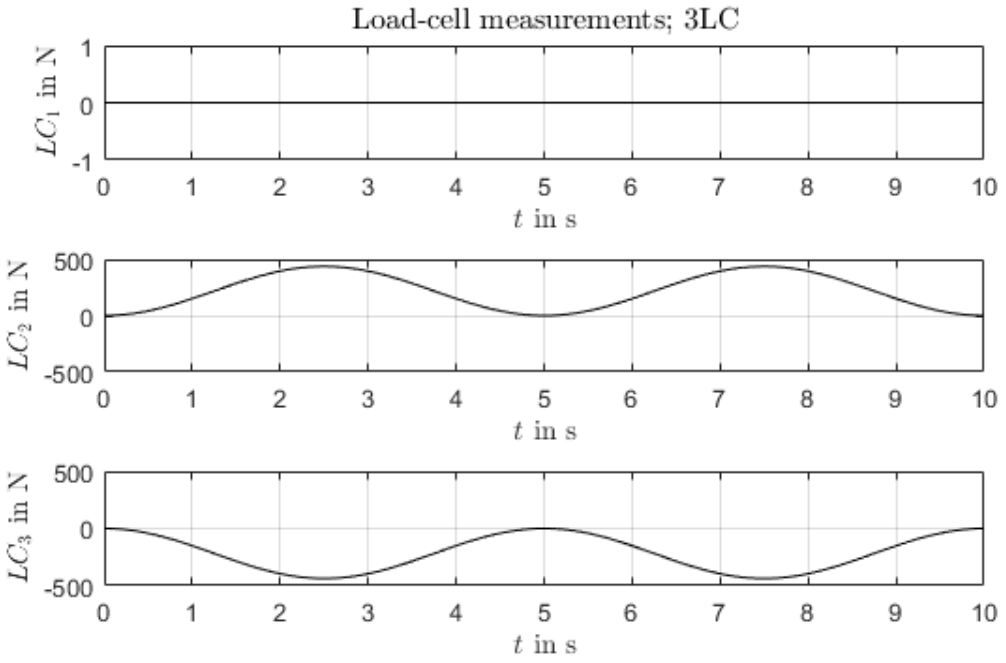

Figure 4-30: Load-cell measurements of approach 6 under rider excitation along *X* direction (induced pitch)

It is important to mark the following fact: the magnitude of the loads read on the load-cells could be lower if the orientation of the legs wasn't regular; playing with different orientation angles could provide lower magnitudes, and consequently, better precision. Nevertheless, it has been tested that not having 120º orientation between the legs generates rotating axes at different heights. This means that both axes would not be coincident and that no global center of rotation would be enabled, ruining the kinematics. Therefore, the only viable option is to have a regular leg disposition.

Although until this point it would seem fair to choose directly approach 6 since it provides a better precision on every possible scenario, there is also another factor that contrast both approaches and that must be taken into account: the constructive solutions used.

The particularity of approach 5 in regards to this factor, is that one of the legs has mounted on top a universal joint instead of a spherical one (like the other legs do). To materialize a universal joint what it is usually used is what is called a cardan; in those cases though, the desired performance of such a joint is to transfer a torque, like in the case of automotive transmission shafts. In our case no torque is transferred and high axial forces will have to be supported, which makes a cardan not suitable for this application. To reduce the supported forces on the universal joint and being able to use a cardan, it could be possible to have a non-regular leg disposition; if the leg mounted with the U-joint was closer to the CoR, the forces supported by it would be lower. Still, having this scenario has been tested that would lead into the same problem as having a not regular leg orientation, compromising the kinematics of the system. Hence, the only option would be to design a specific constructive solution using different shafts and a couple of sets of bearings, which would be highly complex.

Approach 6, on the other hand, does not present this problem either. Once again, its strongest point relays in its symmetry and regularity, making approach 5 look too complicated in comparison. That being said, it is clear that from the two last standing concepts, approach 6 is the most suitable one and, for that reason, it is the one that has been developed in this thesis.

5 Dynamic analysis of the concept

5.1 Simulation model

Once the conceptual design phase was accomplished by selecting the most suitable alternative to be developed, a rigorous simulating model was elaborated. The main purpose of it was to have a useful tool that could help trough the design and development phase of the thesis. In this chapter, an exhaustive analysis of the model is presented.

The Simscape model could be seen as a system with certain inputs and outputs. The inputs of the model are the motion of the rider and the motion of the platform (hexapod or any other solution). The main output is the measured data on the load-cells, but for reasons that will be shown later, also the constraint forces and torques generated on the joints.

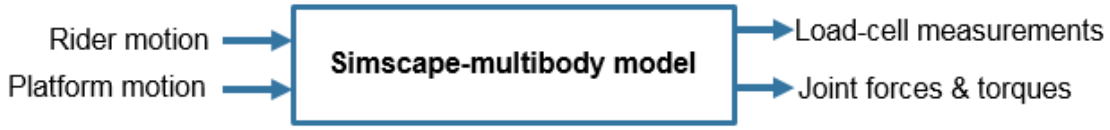

Figure 5-1: Functional scheme of the Simscape model

The scheme is highly reminiscent of the functional structure of the product, this time adding as an input the platform motion and the joint forces as an output. Actually, the platform motion could be considered as a disturbance input, which could potentially induce errors on the load-cell measurements.

To incorporate the platform motion to the model, six independent inputs were created: *X*, *Y* and *Z* linear motions; and the equivalent rotations around those axes (corresponding to roll, pitch and yaw respectively). This way, all the possible movements of the platform could be implemented. In the model, those inputs were variables coming from the Workspace, and were integrated consequently into different motion-actuated joints that support the motion platform body.

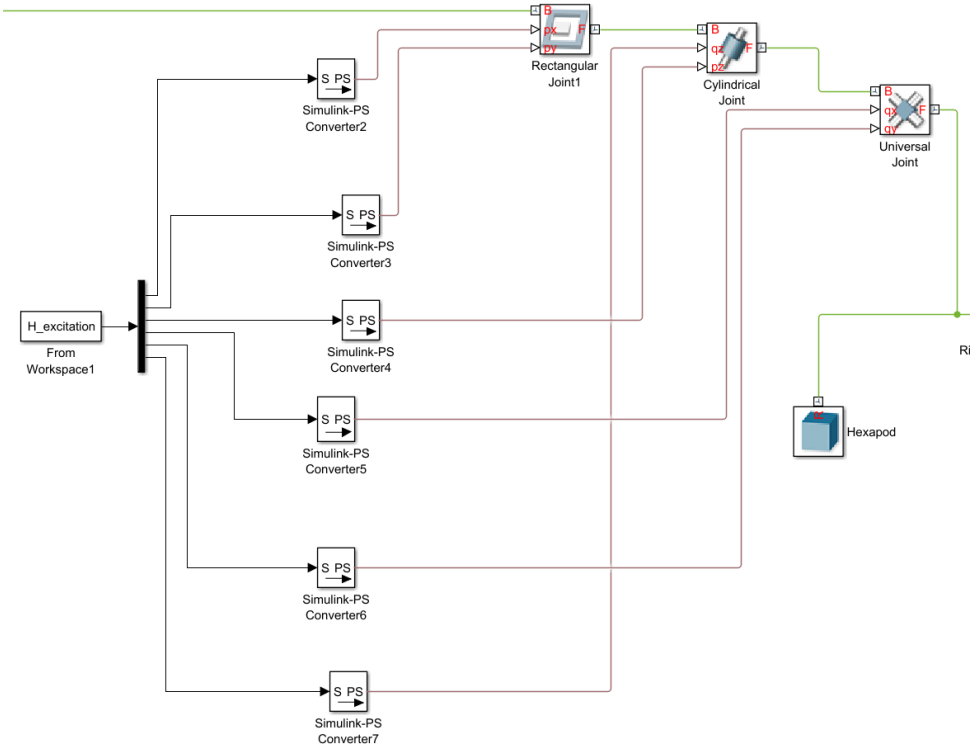

Figure 5-2: Screenshot of the Simscape model showing the inputs related to platform motion

The rider motion is provided in an analogous manner, considering *X* and *Y* displacements as Workspace inputs. Signals are added to a motion-driven joint that handles, on the other side, a sphere with a mass correspondent to the rider's. This way, the rider-motion input enables the movement of this sphere, representing the motion of the rider's CoG.

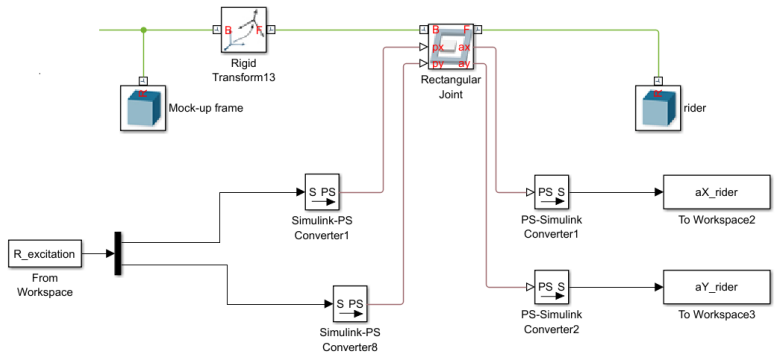

Figure 5-3: Screenshot of the Simscape model showing the inputs related to rider motion

The three equal legs are designed as cylinders that are linked on top by spherical joints to the system's surface. On the bottom, they are attached to the motion platform through revolute joints.[20] All the constraint forces and torques are registered and submitted as Workspace outputs.

[20] Note that in the concept design it was considered cylindrical joints with the axial displacement fixed by load-cells, which is the same as considering directly revolute joints and measuring the axial constraint force

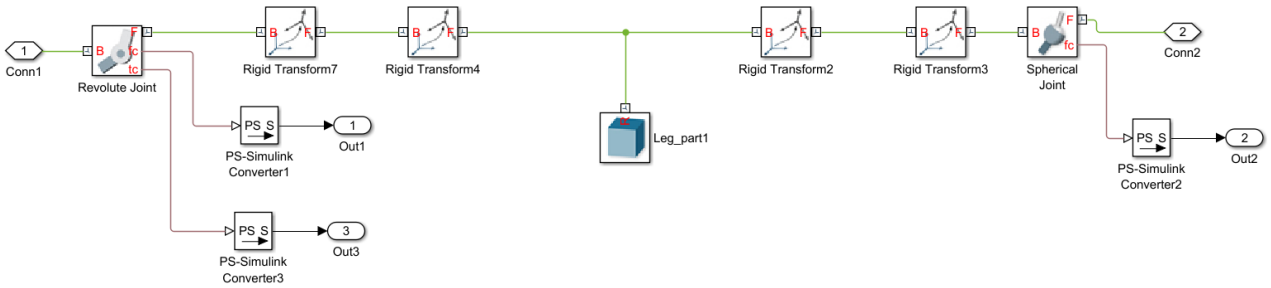

Figure 5-4: Screenshot of the Simscape model showing the subsystem of the legs

Finally, between the system's surface and the sphere that represents the rider, a cylinder body that constitutes the mock-up bike is attached.

The geometrical and dynamic properties of the model are set through an external script. In it, the different masses of the conforming bodies are defined. The masses considered for the dynamic analysis are the ones shown here. The rider mass has been set to only 50kg because it has been considered that not all the body is in motion, just a fraction of it (mostly the upper body).

```
%DYNAMIC PARAMETERS
rider_mass=50; %kg

hexapod_mass=50;
rod1_mass=10;
rod2_mass=10;
rod3_mass=10;
surface_mass=50;
mockup_mass=200;
```

Figure 5-5: Script parameters related to masses

The script calculates all the geometrical dimensions using as an input the following variables:

```
%Intrinsecal system parameters
rider_CoG_H=1000;
platform_R1=320;
platform_R2=platform_R1;
platform_R3=platform_R1;
rod_L1=150;

delta_12=(2*pi/3); %2pi/3 (symmetrical) to work propperly
delta_13=(2*pi/3);
```

Figure 5-6: Script parameters related to geometrical properties

Being the rider_CoG_H, the height of the rider's CoG in riding position; Platform_R are the radiuses in which the legs are fixed to the surface, rod_L1 is the length of one leg and delta_12, and delta_13 are the leg orientation. Note that, although it is already discussed that the system only works cinematically well when the orientation between the legs is 120º and their attachment radius is the same for all of them, the script enables to play with these values and obtain an unsymmetrical solution. It is thanks to this feature, that it was proved that the system only worked properly having a regular geometry.

The most interesting part of this script is the height calculation of the overall CoG. It has already been said in several times that the ideal position of the CoR is the same as the one of the system's CoG, in order to reduce the effect of the system's inertial forces on the load-cell measurements. Therefore, the system's legs should be aiming to the CoG position. But, how is the CoG position calculated? First of all, the following assumption is embraced: the CoG lays in the exact center of the surface, so that the only unknown is its height. Since we are measuring the torque around a rotating axis, the overall mass of the system includes all the fixed bodies that rotate from the CoR. This overall system's CoG includes the masses of the rider, the mock-up bike, the surface and a fraction of the weight of the legs, because they are attached to the surface.

Knowing the fraction of the weight of the legs that lay on the surface is not an easy task, because it depends on its inclination; the inclination, on the other hand, is given through the aiming of the CoG, which is exactly what we are looking for. As it can be seen, it's not a linear problem that could be solved directly, so another way of calculating the CoG height has been elaborated: through iteration.

```
while abs(force_error)>1e-6
    S=fsolve(@(x)tripod_system(x,CoR, platform_R1, platform_R2, platform_R3, rod_L1),
    platform_H=S(1);
    base_R1=S(2);
    base_R2=S(3);
    base_R3=S(4);
    alpha=S(5);
    beta=S(6);
    gamma=S(7);
    rod_L2=S(8);
    rod_L3=S(9);


    H_excitation.time=[0:0.01:t_sim]';
    H_excitation.signals.values(:,1)=0*(cos(H_excitation.time*2*pi/5)-1);
    H_excitation.signals.values(:,2)=0*(cos(H_excitation.time*2*pi/5)-1);
    H_excitation.signals.values(:,3)=0*(cos(H_excitation.time*2*pi/5)-1);
    H_excitation.signals.values(:,4)=pi/2;
    H_excitation.signals.values(:,5)=0;
    H_excitation.signals.values(:,6)=0*(cos(H_excitation.time*2*pi/6));

    R_excitation.time=[0:0.01:t_sim]';
    R_excitation.signals.values(:,1)=0*(cos(R_excitation.time*2*pi/5)-1);
    R_excitation.signals.values(:,2)=0*(cos(R_excitation.time*2*pi/5)-1);
```

Figure 5-7: Script showing the iterative method to find the system's CoG (part1)

```
    sim('tripod_neat_3LC_20190307');

    Loadcell_pitch=Loadcell_Force_2.signals.values*sin(delta_12);
    Loadcell_roll=Loadcell_Force_1.signals.values+Loadcell_Force_2.signals.values*cos(delta_12);
    force_error=mean(Loadcell_roll);
    if force_error>CoR/2
        CoR=CoR-CoR/4;
    elseif force_error<CoR/2 && force_error>0
        CoR=CoR-force_error/10;
    elseif force_error>-CoR/2 && force_error<0
        CoR=CoR+force_error/4;
    elseif force_error<-CoR/10
        CoR=CoR+CoR/4;
    end

    iter=iter+1;
end
```

Figure 5-8: Script showing the iterative method to find the system's CoG (part2)

The script begins the iteration with an initial CoR height and calculates the geometry according to it. Afterwards, it simulates the model giving a fixed displacement to the motion platform roll of $\frac{\pi}{2}\ rad$, which means laying the system horizontally. For the rider is not moving, if the CoR height was the same as the system's CoG, the rider induced measurement would show a value of 0N. The script compares the readings of the rider induced torques with the stipulated error range, and if the first one is bigger, an according modification of the CoR height is performed before running the next iteration. When the measured rider induced torques are inside the error range, the iterative process stops. This way, the CoR can be positioned exactly where the CoG is.

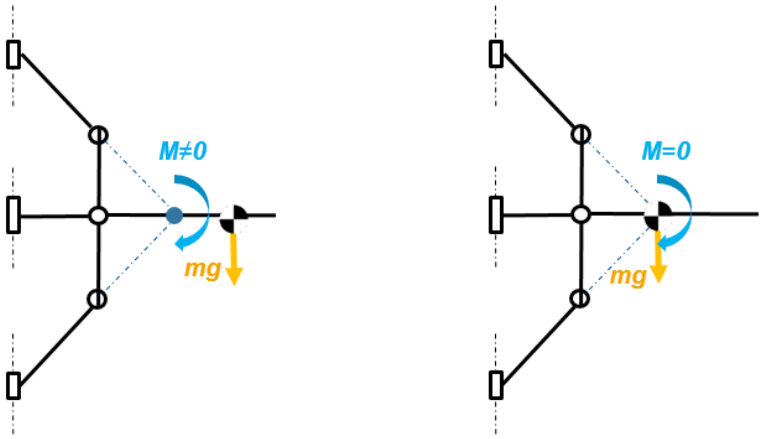

Figure 5-9: Scheme showing how the iterative method finds the CoG

Hence, all the geometric and dynamic parameters are set and the simulations are ready to be performed. With the aim of not having to run this script every time a simulation is performed, the Workspace created by this script is saved.

Another script that is designed to run the simulations uses as an input said Workspace. In it, the different excitations of the hexapod and the rider can be set, even taking real data acquired from the current simulator of the department. This script also processes the acquired data and prepares the figures to be shown.

5.2 Analysis of the different motion scenarios

In the following section, a dynamic analysis of all the motion scenarios is done in order to test the performance of the design. As stated in the previous part, we can consider the simulating model as a system with two inputs: rider motion and platform motion. The main output is the measurement data on the load-cells. Ideally we would like to have a direct and linear relationship between rider motion and measured data, but the platform motion is a disturbance input that can alter this desired relationship. The aim of this section is to analyse how this disturbance affects the readings under all possible motion scenarios, comparing the expected data (the ideal signal that we would get if there was no disturbance effect) and the real one.

First of all, an explanation of how the expected data is calculated is presented. The torque created by rider motion around the rotating axes comes from two different sources. First, the relative position of the rider's CoG in regards to the CoR creates a torque due to the gravitational force; the further it gets from the CoR, the higher is the torque. And second, the lateral accelerations of the rider when he changes his position also create a torque around said axis.

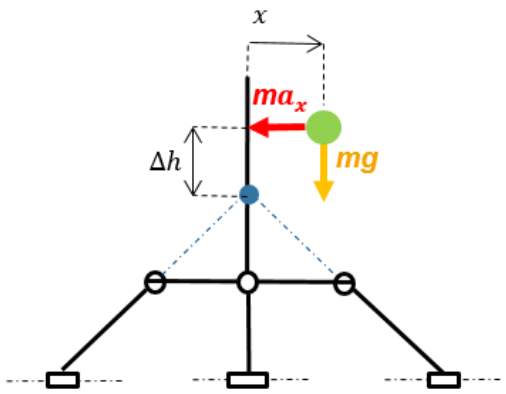

Figure 5-10: Scheme showing the two sources for rider-induced torque

With that being said, and knowing the position of the rider's CoG and the system's CoR, the expected rider induced torque follows the next expression[21]:

$$T_{exp} = mgx + ma_x\Delta h \tag{5-1}$$

Translating this torque into the expected value of the measured load-cell loads is a simple calculation knowing the height of the CoR:

$$LC_{exp} = \frac{T_{exp}}{CoR\ height} \tag{5-2}$$

[21] The expression shown is the one corresponding to the expected rider induced pitch torque. The case of the rider induced roll torque is analogous.

In order to check the performance of the design, the studied scenarios constitute the harshest motions that the system will have to handle. These scenarios are the following ones:

1. Rider motion *X* direction; no platform motion:
   - The rider's CoG position is set through a sinusoidal signal of 250mm of amplitude and a frequency of 1Hz in the *X* direction.
2. Rider motion *Y* direction; no platform motion:
   - The rider's CoG position is set through a sinusoidal signal of 250mm of amplitude and a frequency of 1Hz in the *Y* direction.
3. No rider motion; platform motion *X* direction
   - The platform motion is set through a sinusoidal signal of 500mm of amplitude and a frequency such that creates a maximum acceleration of 1,5G in the *X* direction.
4. No rider motion; platform motion *Y* direction
   - The platform motion is set through a sinusoidal signal of 500mm of amplitude and a frequency such that creates a maximum acceleration of 1,5G in the *Y* direction.
5. No rider motion; platform motion *Z* direction
   - The platform motion is set through a sinusoidal signal of 500mm of amplitude and a frequency such that creates a maximum acceleration of 1,5G in the *Z* direction.
6. No rider motion; platform roll motion.
   - The platform motion is set through a sinusoidal signal of $\frac{\pi}{6} rad$ of amplitude and a frequency of $\frac{\pi}{2} \frac{rad}{s}$ around the *X* axis.
7. No rider motion; platform pitch motion.
   - The platform motion is set through a sinusoidal signal of $\frac{\pi}{6} rad$ of amplitude and a frequency of $\frac{\pi}{2} \frac{rad}{s}$ around the *Y* axis.
8. No rider motion; platform yaw motion.
   - The platform motion is set through a sinusoidal signal of $\frac{\pi}{12} rad$ of amplitude and a frequency of $\frac{\pi}{2} \frac{rad}{s}$ around the *Z* axis.
9. Rider motion *X* and *Y* directions; platform motion *X* direction
   - The rider's CoG position is set through a sinusoidal signal of 250mm of amplitude and a frequency of 1Hz for both *X* and *Y* directions.
   - The platform motion is set through a sinusoidal signal of 500mm of amplitude and a frequency such that creates a maximum acceleration of 1,5G in the X direction.
10. Rider motion *X* and *Y* directions; platform motion *Y* direction
    - The rider's CoG position is set through a sinusoidal signal of 250mm of amplitude and a frequency of 1Hz for both *X* and *Y* directions.
    - The platform motion is set through a sinusoidal signal of 500mm of amplitude and a frequency such that creates a maximum acceleration of 1,5G in the *Y* direction.
11. Rider motion *X* and *Y* directions; platform motion *Z* direction
    - The rider's CoG position is set through a sinusoidal signal of 250mm of amplitude and a frequency of 1Hz for both *X* and *Y* directions.

- The platform motion is set through a sinusoidal signal of 500mm of amplitude and a frequency such that creates a maximum acceleration of 1,5G in the *Z* direction.

12. Rider motion *X* and *Y* directions; platform roll motion.
    - The rider's CoG position is set through a sinusoidal signal of 250mm of amplitude and a frequency of 1Hz for both *X* and *Y* directions.
    - The platform motion is set through a sinusoidal signal of $\frac{\pi}{6} rad$ of amplitude and a frequency of $\frac{\pi}{2}\frac{rad}{s}$ around the *X* axis.
13. Rider motion *X* and *Y* directions; platform pitch motion.
    - The rider's CoG position is set through a sinusoidal signal of 250mm of amplitude and a frequency of 1Hz for both *X* and *Y* directions.
    - The platform motion is set through a sinusoidal signal of $\frac{\pi}{6} rad$ of amplitude and a frequency of $\frac{\pi}{2}\frac{rad}{s}$ around the *Y* axis.
14. Rider motion *X* and *Y* directions; platform yaw motion.
    - The rider's CoG position is set through a sinusoidal signal of 250mm of amplitude and a frequency of 1Hz for both *X* and *Y* directions.
    - The platform motion is set through a sinusoidal signal of $\frac{\pi}{12} rad$ of amplitude and a frequency of $\frac{\pi}{2}\frac{rad}{s}$ around the *Z* axis.

All the complete graphs of the different scenarios can be found in the appendix; of each one of them there is a representation of the excitation under which they are subjected, and also the comparison between the expected value and the real one of both pitch and roll forces on the load-cells. It is represented in the time domain and also in the frequency domain (the Fast Fourier Transform has been used in this case).

Next, the most important insights of the different scenarios are presented:

- **Scenarios 1 and 2: rider motion; no platform motion**

These two scenarios represent the basic ones, in which the rider is moving in either *X* or *Y* directions and there is no disturbance coming from the platform because it is not moving. Since the design of the system has been developed through the test of these two scenarios, it is obvious that the obtained response is the one desired. Leaving aside the noise coming from the measured data or other marginal differences, from the frequency graph we can see clearly that the magnitude and frequency of the expected and real data are equal.

- **Scenarios 3, 4 and 5: no rider motion; linear platform motion**

The following scenarios represent the effect of a direct disturbance coming from linear motion of the platform, without any input from the rider. Therefore, we would expect ideally that the measured roll and pitch forces to be 0. Once again, if we neglect the noise and other low amplitude oscillations that possibly come from solver issues, we can see that the expected roll and pitch forces are virtually 0 in all these cases, as expected.

- **Scenarios 6 and 7: no rider motion; roll & pitch platform motion**

Under these two scenarios, the desired response would also be to have no roll or pitch loads since the rider is not under motion. However, we can see clearly in these cases that not negligible loads appear. When the roll excitation is set on the motion platform, an oscillation on the roll-load reading appears with the same frequency as the one of the platform excitation (0,25Hz).

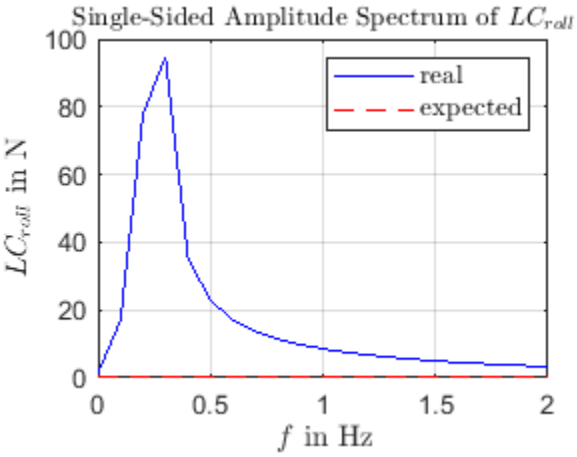

Figure 5-11: Close-up of the frequency analysis of the system under platform rolling excitation

In the case of pitch excitation, the effect is analogous.

The reason for this effect is that the rotational acceleration created by the platform motion induces an inertial rotation on the system. It is well known that if a free body is subjected to a rotational force field, it will induce a displacement of the body's CoG and also a rotation around that point. In our case, that the body is fixed, the motion of the CoG does not represent any effect on the load-cell readings, but the rotation of the body does because it induces a torque. Therefore, a force on the load-cells appears.

We see then, that on those two cases the effect of the disturbance input has a real effect on the output. To solve this problem, the measured data will have to be corrected subtracting the effect of rotational acceleration. It is not a complex procedure because the motion of the platform is always controlled and it would be easy to estimate this effect in order to correct the data. Unfortunately, this will make the response of the system to be slower, for it has to do further processes and is no longer a direct measuring procedure.

- **Scenario 8: no rider motion; yaw platform motion**

Under this scenario, although a rotational acceleration is also induced, the measuring system is not influenced by the torque around the *Z* axis. This means that, as expected, the measured roll and pitch loads are virtually 0.

- **Scenario 9 and 10: rider motion; *X* and *Y* linear platform motions**

The following scenarios are tested to see if there is any kind of coupled effect coming from the action of both rider and platform motions. On scenarios 9 and 10, we can see that the measuring system

behaves as expected; from the frequency graph it is visible that the platform motion has no effect on the output data, since the only response is the one coming from the rider motion.

- **Scenario 11: rider motion; *Z* linear platform motion**

Under this particular scenario an undesired effect appears on the measured data due to the coupling between the rider's CoG position and the acceleration of the platform on the Z direction. From the frequency diagram it is easily visible the difference between the expected and the real loads, since the later presents two unexpected peaks.

When the rider leaves the neutral position, the system's CoG displaces accordingly and a torque around the CoR due to gravitational force is created; this is how the measuring system works. The problem appears when a vertical acceleration is induced, because the effect of gravitational torque is altered. Hence, this is another particular case in which a disturbance input impacts on the measured data; yet again, this effect can be corrected because it can be easily estimated but it implies a slower processing speed.

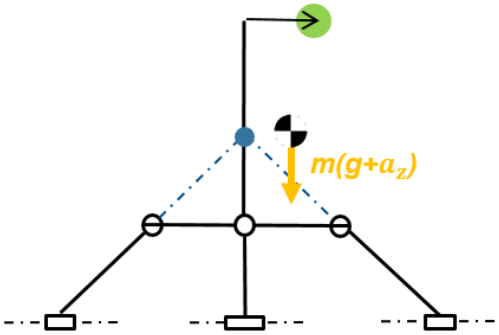

Figure 5-12: Scheme showing the coupling effect of rider motion and platform motion along *Z* direction

- **Scenarios 12 and 13: rider motion; roll & pitch platform motions**

Although it has already been proved that roll and pitch motions alone imply an important error to the measured data even when the rider is not moving, a further effect appears when the rider is under motion. At first sight we can easily see on the frequency diagram the effect of rotational acceleration described on scenarios 6 and 7, because a peak at the platform excitation frequency appears. However, if we take a closer look, we can also see smaller peaks at frequencies over 1Hz, that is the one coming from rider motion.

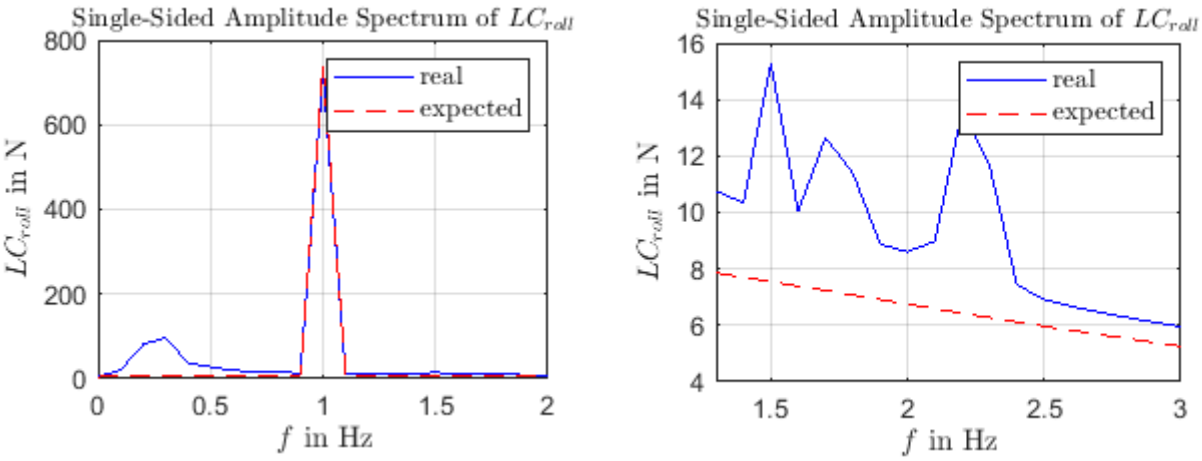

Figure 5-13: Close-ups of the frequency analysis of the system under rider motion and platform rolling motion

This effect is due to the centrifugal force created by the rotational speed of the motion platform. When the rider is in neutral position, this force does not create any torque around the CoR because the lever is 0; but as soon as the position of the rider changes, a lever is generated and, with it, a torque. Although, in comparison, this implications of this effect seem to have a small impact on the measured data, it would be better if it was also corrected subtracting its estimated effect before adding it to the motorcycle dynamics model.

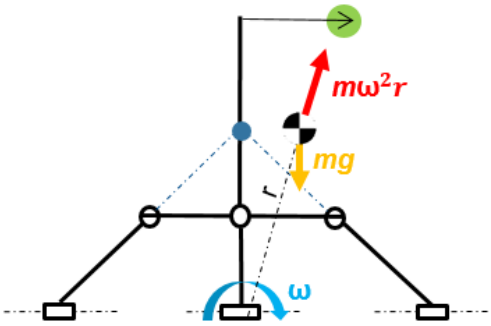

Figure 5-14: Scheme showing the coupling effect of rider motion and platform rolling or pitching motion

- **Scenario 14: rider motion; yaw platform motion**

It is visible from the frequency diagram that two small unexpected peaks appear in this case. Under this scenario, a phenomena similar to the one explained for the scenarios 12 and 13 is happening: it is due to the effect of the centrifugal force. As long as the rider is in neutral position, it lays on the rolling axis and no centrifugal force is created. However, when the rider moves away from there, the centrifugal force appears, creating a torque that alters the desired measured data.

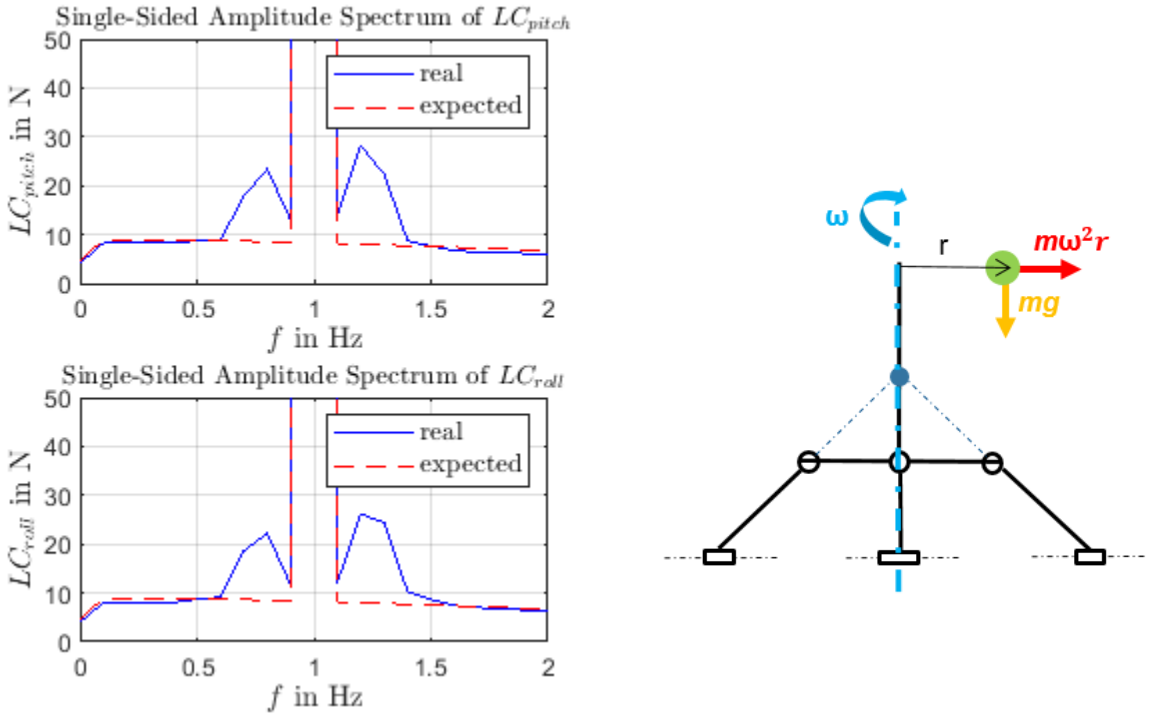

Figure 5-15: Close-up of the frequency analysis of the system under rider motion and platform yawing motion (left) and scheme showing the coupling effect (right)

5.3 Real platform motion scenario

This following section is an analysis of the system's performance under a real life scenario. What has been done is considering as an input for the motion platform an actual recording of the hexapod's parameters of the current FZD's motorcycle simulator. Said recording corresponds to an experiment performed to check the behavior of the simulator under harsh accelerations and violent changes; this makes it suitable to use it as an input for the current simulation, since we want to see the performance of the system under the most severe conditions that it is going to experience. For that exact reason, it has been set to the rider a sinusoidal excitation along both *X* and *Y* directions with 250mm of amplitude and 1Hz for each (the same conditions set on the previous experiments).

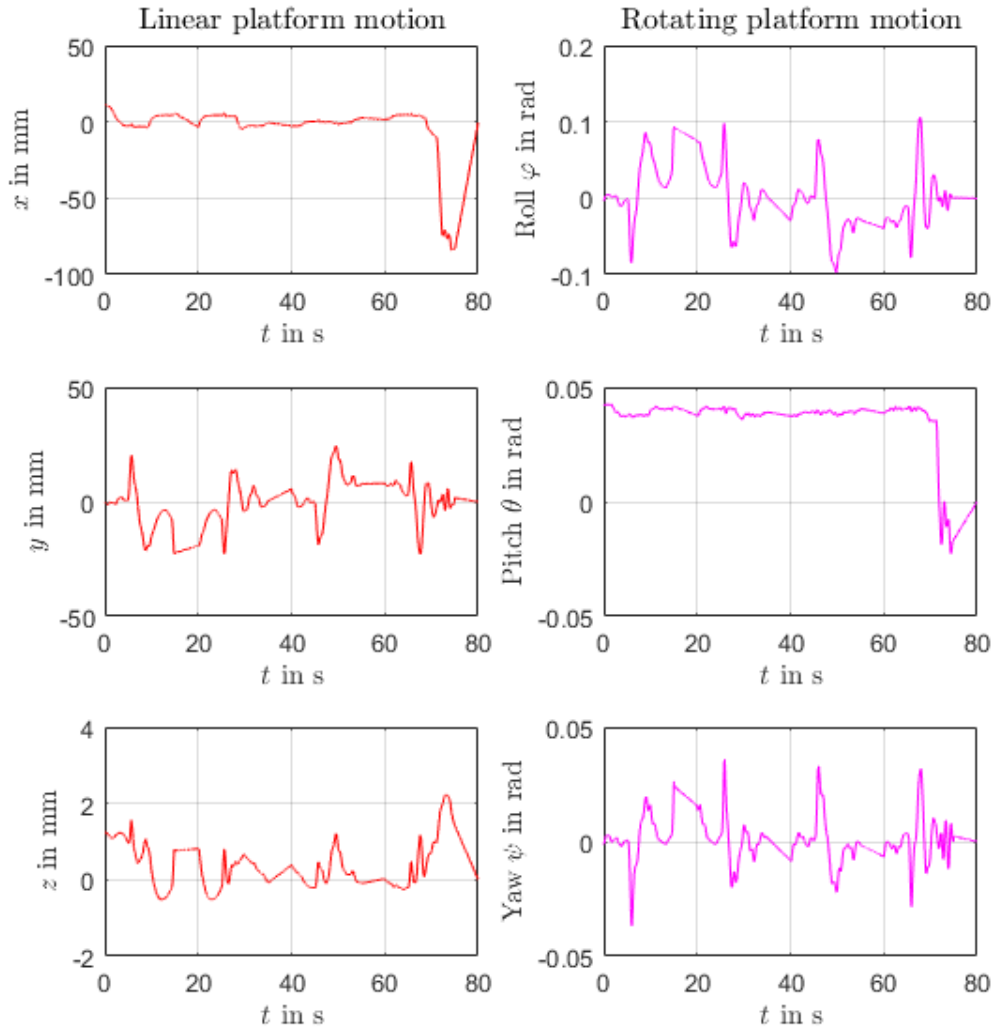

Figure 5-16: Excitation graph of the motion platform under real input data

The following graphs show the comparison between the expected roll and pitch load-cell forces and the real ones measured in the simulation. This comparison is shown on both time and frequency domains in order to analyse the data more easily.

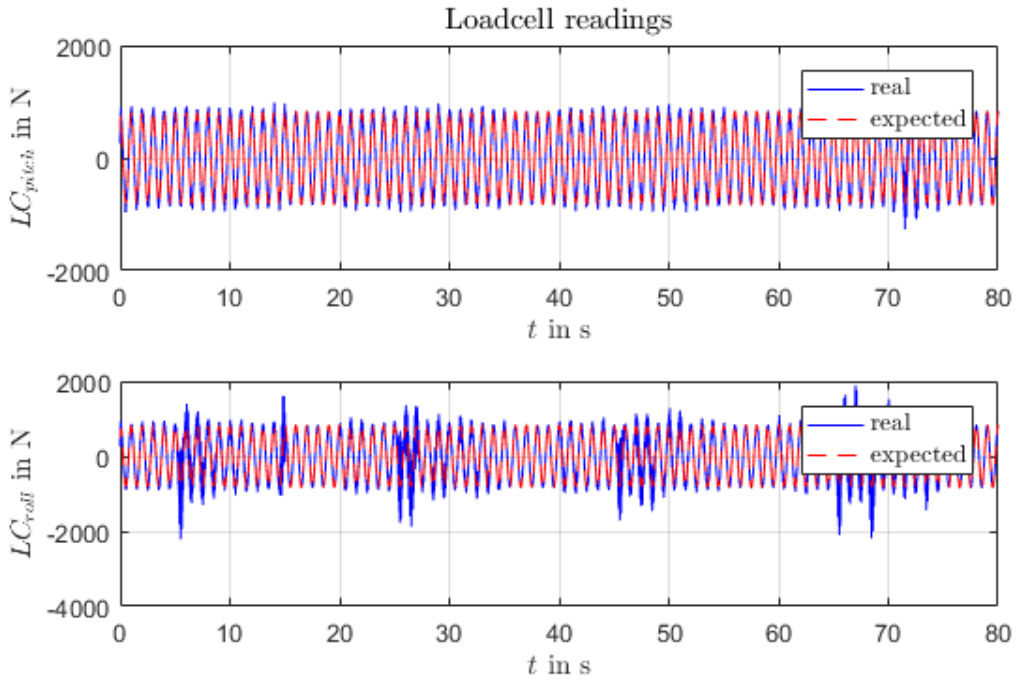

Figure 5-17: Time domain dynamic analysis of the system under real platform motion

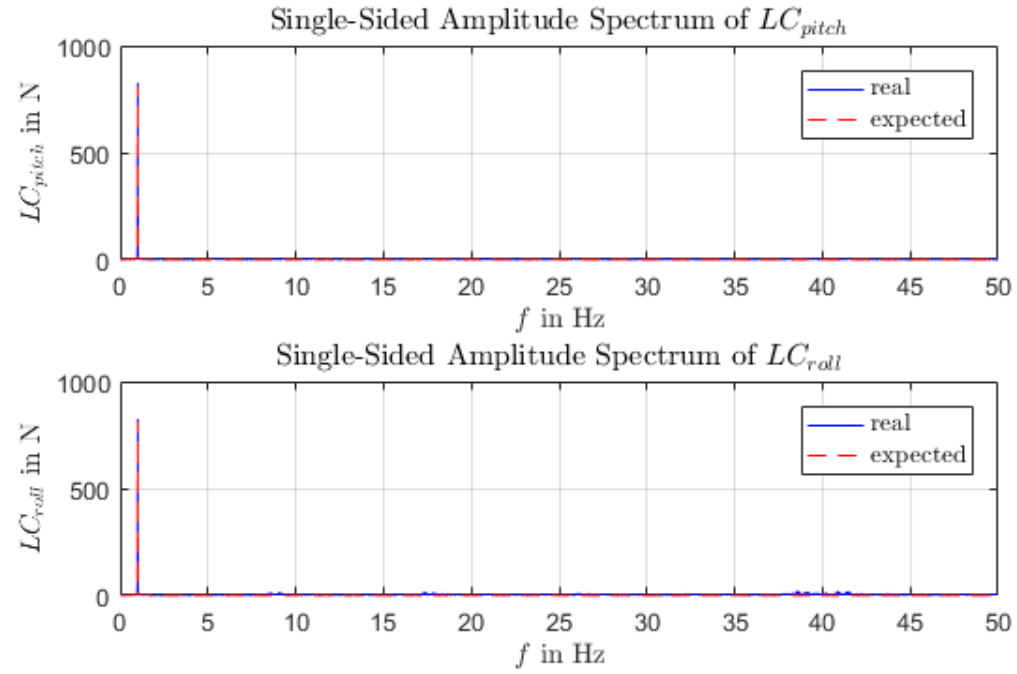

Figure 5-18: Frequency domain dynamic analysis of the system under real platform motion

From first sight it is difficult to see on the frequency graph any important effect other that the one caused by the actual rider motion, which is the main peak. This could be a good sign meaning that the effect of the platform motion has little effect on the overall measuring data, but we must not forget that the platform motion in this case is not excited by sinusoidal signals; that means that the spectre of frequencies is highly distributed, and that the sum of those little effects on different frequencies can cause a significant disturbance at a given moment. Plus, on the time domain graph, it is visible that the measured data presents obvious differences in regards to the expected.

In order to see this fact more clearly, the error between the expected and the measured data is plotted next. We can extract now significant information; the maximum error at any given moment coming from the pitch load-cell is 496N, and the one belonging to the roll is as high as 1207N. Considering that the maximum expected forces are 840N on both cases, that makes a percentage error of 59% and 143% respectively for pitch and roll.

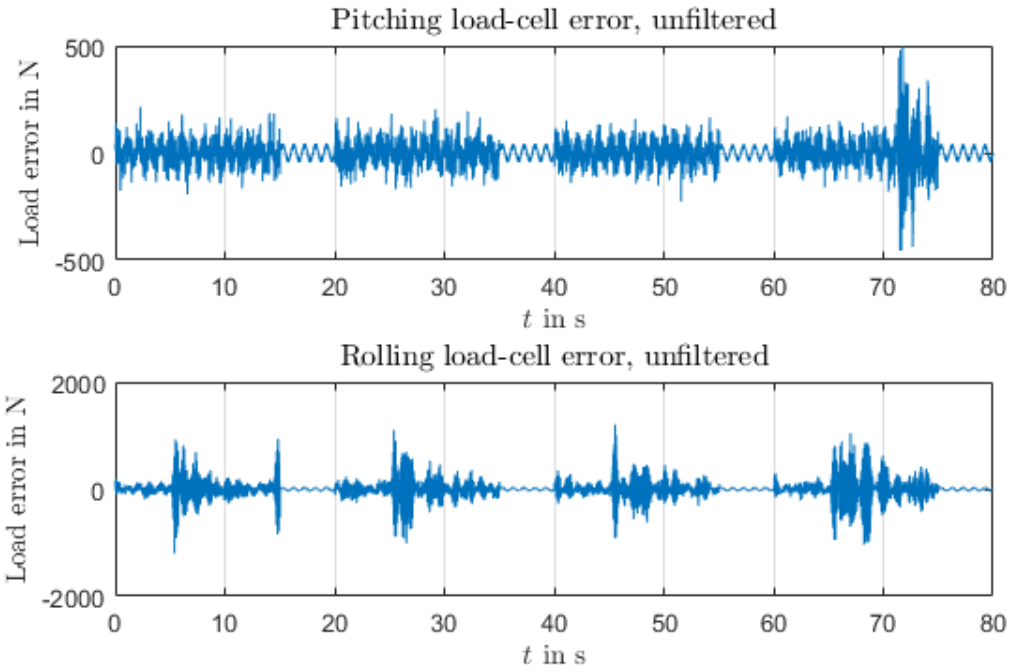

Figure 5-19: Measuring error of the system under real platform motion in time domain

However, if we take a look at the spectral error or scale up the measured data we can see that the highest effects come from very high frequencies, which can easily be recognized as noise.

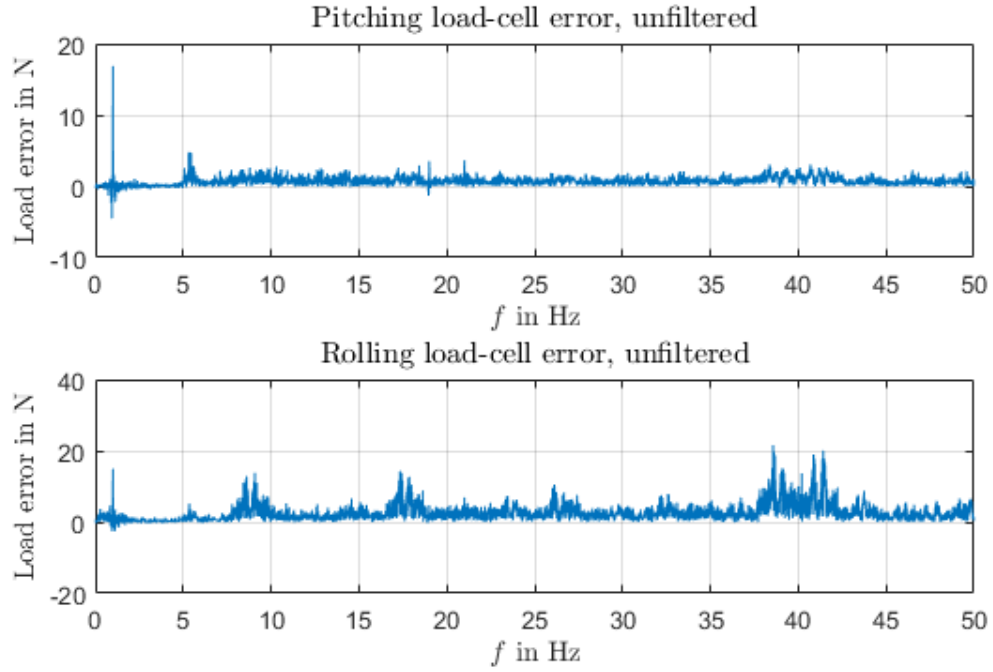

Figure 5-20: Measuring error of the system under real platform motion in frequency domain

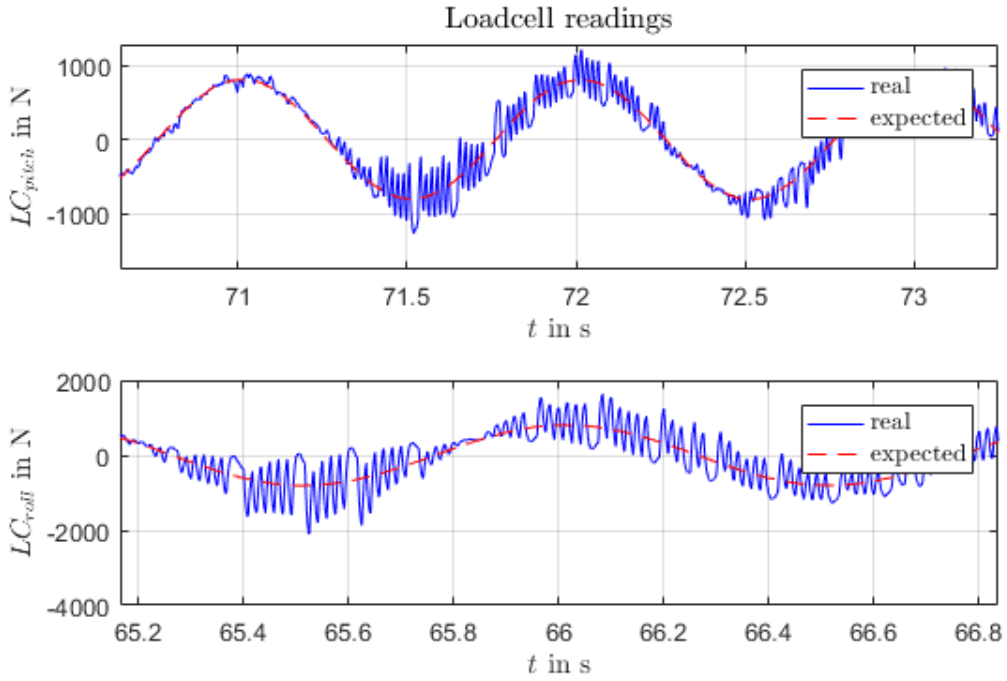

Figure 5-21: Close-up of the Time domain dynamic analysis of the system under real platform motion

After a deep analysis of the system it has been found that the most part of the noise comes from the Simulink-Simscape conversion of the input motion data, given that it calculates automatically the derivatives of the signal. Since the motion of the system cannot provide frequencies higher than 20Hz, it makes no sense to obtain frequencies that high. With the aim of discarding this noise, a 20Hz low-pass filter has been set on the input motion data.

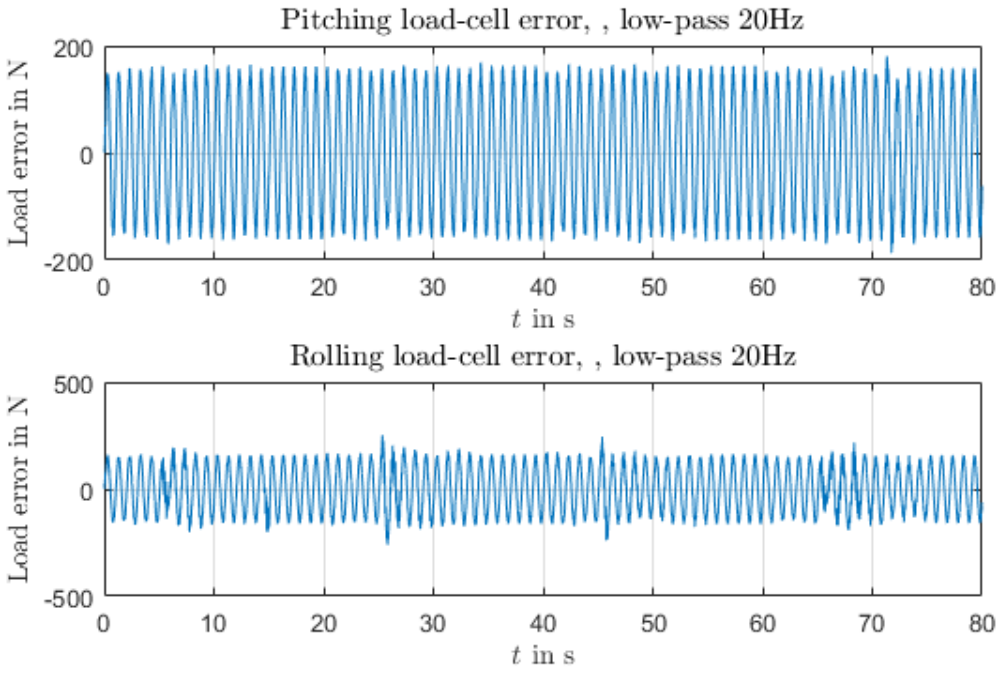

Figure 5-22: Measuring error of the system under real platform motion (filtered 20Hz) in time domain

It is visible now that the error has reduced significantly presenting an error of only 180N in the case of the pitch and 260N in the case of the rolling measurement. Although the obtained errors after all these considerations are still very high (260N represent nearly 30% of percentage error), it is remarkable that, as stated on the previous chapter, these errors can be further corrected by estimation. It is important to remember also, that even though the error can be corrected, it is always preferable to have a smaller one because it makes the measuring load lower, and consequently, the precision can be enhanced.

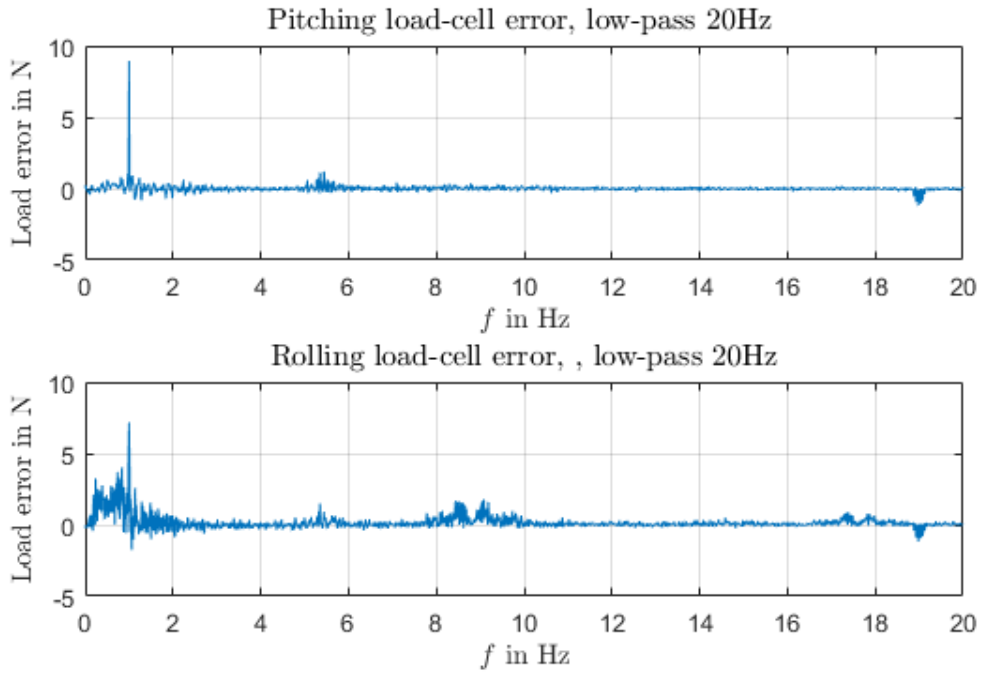

Figure 5-23: Measuring error of the system under real platform motion (filtered 20Hz) in frequency domain

From the frequency graph we can see that the highest error appears at 1Hz, which is the excitation frequency of the rider. Taking into account the observations made in the previous section, this fact bears out what was seen: Apart from the error due to the pitch and roll accelerations, the rest come from the coupling effect between the rider's CoG position and the platform excitation.

5.4 CoG/CoR height deviation

As explained before, the basis of this system lays on the idea of having the CoR in the same position as the CoG. But, what would happen if the CoR was not aimed exactly to the CoG and a deviation was created? This scenario can easily happen if there is any kind of error during the CoG calculation, or also if the constructive solution chosen does not provide enough precision to aim the legs exactly at the desired position. The aim of this section is to find the answer to this question and to analyse the system's behaviour under this possible situation. For this discussion, only a deviation on the height is contemplated, considering that both CoG and CoR are exactly in the center of the motion platform.

Analytically speaking, having a height deviation induces a further error on the measured data in the following three ways:

First: a torque is generated as soon as the motion platform leaves the vertical position; when the platform presents a certain tilt angle (roll or pitch), even if it does not experience any motion, a torque around the CoR is created due to gravitational force. (This scenario is actually the one used to calculate the right position of the CoR in the code, as stated on the pertinent chapter).

Second: linear platform motions along *X* and *Y* directions induce a torque due to inertial accelerations. If there is no deviation, the inertial force does not create any torque because the lever is 0; but as soon as there is a lever, a torque is generated.

Third: all the possible error sources inherent to the ideal system presented on the previous chapter are aggravated by the fact of having a deviation. Levers are generated or magnified, which induce a higher error on the measured loads.

In order to quantify these effects, a simulation considering the real data of the current hexapod under harsh conditions has been taken into account (the same conditions of the previous simulation, with low-pass filter of 20Hz) and different height deviations have been applied: 0, 50, 100and 200mm.

The different errors (difference between the expected and the measured loads) have been calculated and the following graph shows the maximum error for each kind (pitch and roll) of measure, depending on the height deviation:

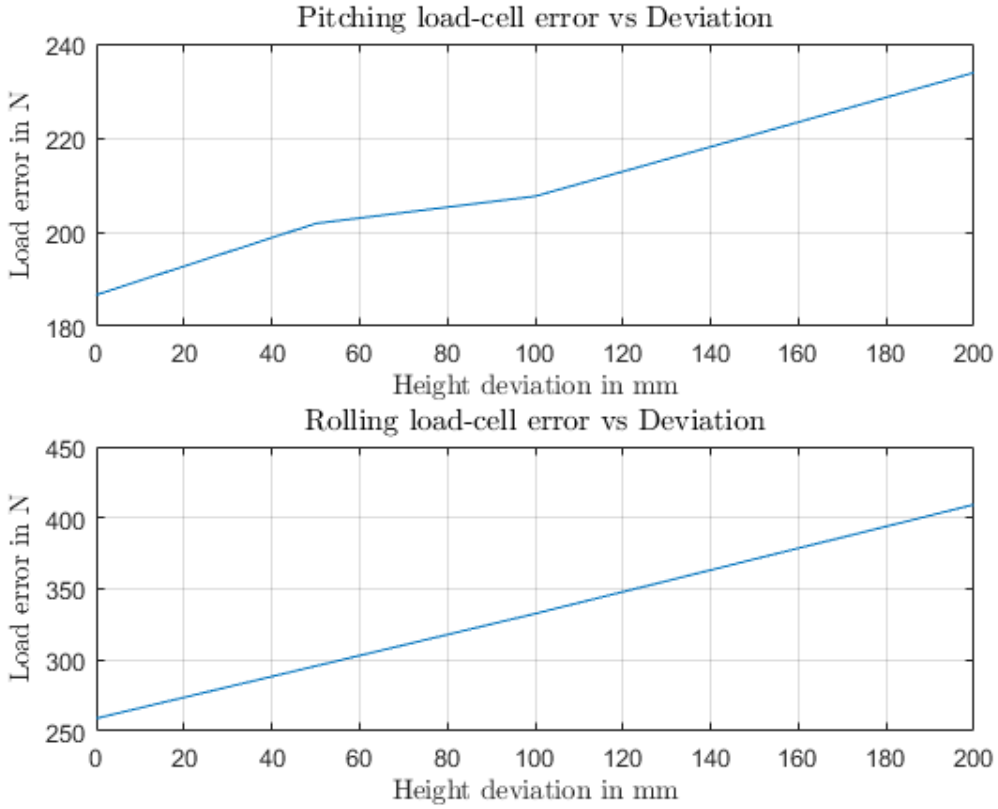

Figure 5-24: Measuring error vs height deviation for real platform motion scenario

We can see the increasing tendency of the error with the height deviation. Having a 200mm distance between the CoG and the CoR magnifies the error from originally 186N (22% percentage error) to 234N (27,9%) in the case of the pitch, and from 259N (30,83%) to 409N (48,7%).

5.5 Coupling of the rider motion effects

There is an effect on the measuring that lays undisclosed and that has an important relevance: the impossibility to distinguish the two possible sources of the rider-induced torques. As stated in previous sections, the rider-induced torques come from the position of the rider's CoG (creating a torque due to gravitational force) and the lateral acceleration of the rider due to its motion. Since the proposed system measures directly the generated torque, there is no way to know which part of it comes from gravitational force and which one comes from the lateral acceleration.

This fact is a problem, because it means that a correction of the measuring data specific for each source is, to the best of the writer's knowledge, not possible. But, why would it be necessary to correct the data separately?

Positioning the CoR at the same height as the system's CoG is highly beneficial in terms of reducing the effect of inertial forces on the measurement, as it has been shown. However, locating the rotational axes at a position that is not the one on a real motorcycle entails significant setoffs. Consider the following case:

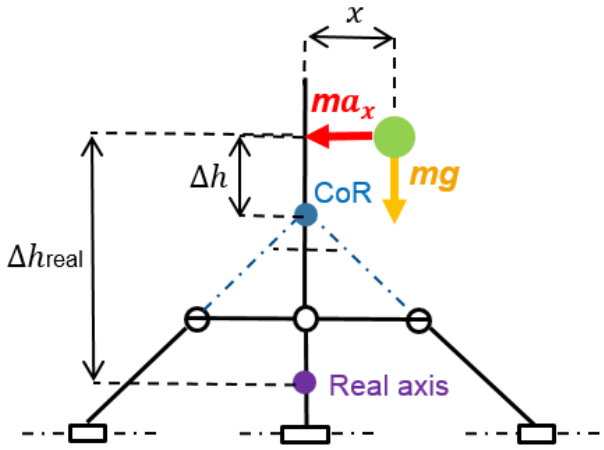

Figure 5-25: Scheme showing the difference on the position of the CoR and the real axes

The measured rider-induced torque would be, in this case:

$$T_{meas} = mgx + ma_x\Delta h \tag{5-3}$$

However, on a real motorcycle, the real pitch or roll axis will not be in that position (as explained in the state of the art, pitch and roll axes position can vary a lot), meaning that the real torque experienced on the motorcycle would be:

$$T_{real} = mgx + ma_x\Delta h_{real} \tag{5-4}$$

As it can be seen, in this case the torque that comes from the rider's CoG position is the same for both cases, but the one due to lateral acceleration changes because the lever is different. Before sending the torque to the vehicle dynamics model of the simulator, the measured torque should be corrected in order to fix this effect. Nonetheless, it is not possible to do so because we are measuring the whole torque and we would only need to correct the part that comes from lateral acceleration.

Although this problem appears also in the current FZD motorcycle simulator, having the CoR height so close to the rider's CoG would induce for this solution even bigger effects, since the lever that creates the torque that comes from lateral acceleration is very small.

6 Materialization design

6.1 Constructive solutions

The main objective of the materialization design is to choose the constructive solutions that will make the design a reality; the aim of this chapter is to present and analyse them. In order to help with this task, a basic CAD of the system has been developed. It is important to remark that this is only a possible implementation of the concept and that other possibilities might also be valid; however, to the best of the writer's knowledge, this represents the most suitable one.

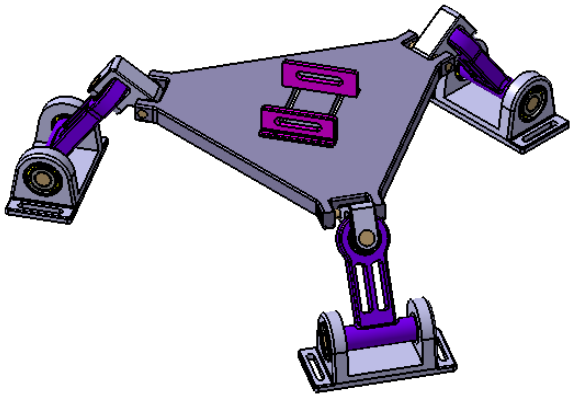

Figure 6-1: CAD model of the system

The first insight to explain is how the forces are measured. During the conceptual design phase, the system was presented with three load-cells fixing the axial motion of the cylindrical joints that were positioned on the base of the system. However, a literate materialization of this concept would lead to a very complex design that could, also, lead to stiffness issues. Like in the Simscape model, the load-cells fixing the axial motion of the cylindrical joints are substituted by revolute joints, which are far easier to materialize. However, unlike in the Simscape model, in which the rider-induced loads could be directly measured on the joint, in reality this is not possible and another way of accomplish the measurement is needed; the solution chosen is based on the incorporation of strain gauges on the legs.

Under rider motion, the legs will be subjected to two identical opposite forces in the axial direction of each bearing (this fact can be proved seeing the recorded data of any Simscape simulation).

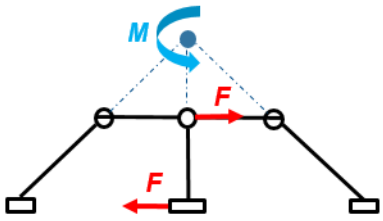

Figure 6-2: Free body diagram of a leg under rider-induced torque

Therefore, legs support a bending moment that cause a certain strain. Incorporating strain gauges in the legs, it is possible to obtain an electrical signal proportional to the rider-induced torques, enabling this way the measuring system. Note that for the design of the legs, the zone in which the strain gages are installed should be the one with lowest stiffness in regards to the direction of the rider-induced forces. Hence, the bending moment experienced will cause a strain only in that exact area, providing an accurate measurement of the loads.

Figure 6-3: CAD of a leg with proposed position for the strain gauges

The next point to explain is the materialization of the joints. The revolute joints on the bottom of the legs are presented as a back-to-back angular contact ball bearing disposition. [22]

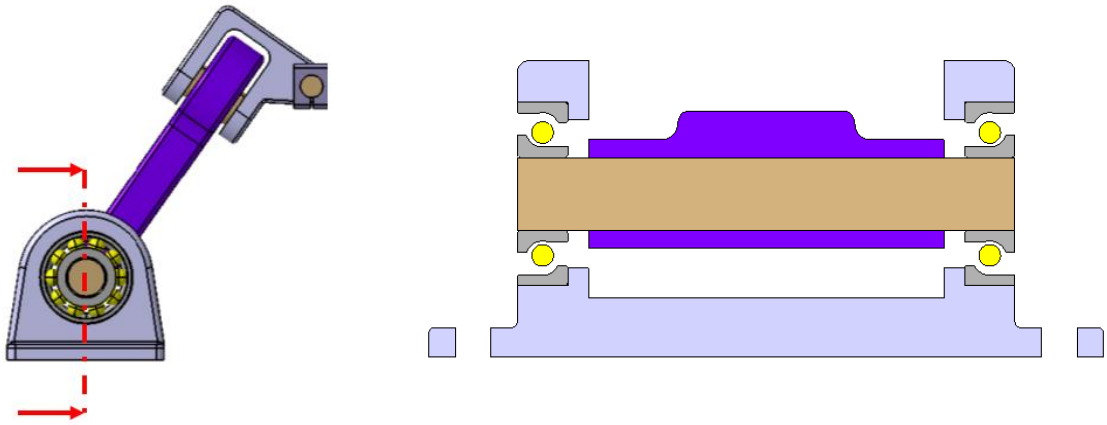

Figure 6-4: Cut detail of the constructive solution proposed for the revolute joints

The bearings are positioned on an external housing and are set on back-to-back disposition in order to support better the torques coming from the system. Since all the degrees of freedom are fixed, meaning that the bearings will not rotate, the most appropriate way of mounting the bearings would be with an adjusted arrangement, leaving both bearings fixed with the help of a preload during mounting. The selection process of the actual bearing models is treated on a further section.

[22] Note that the CAD shown is only a first approximation in order to choose the constructive solutions; it does not contain all the necessary parts or details to function properly

The shaft will pass through the leg hole with a certain interference; for example using an H7s6 adjustment, which requires mounting the shaft on a press.

For the implementation of the spherical joints located on top of the legs, it is proposed to use a spherical roller bearing. Spherical joints are normally implemented through ball linkages, such as the ones used in steering or suspension systems for cars. However, since the motion needed for this application is technically nonexistent and the loads to support are high, to use a spherical roller bearing was chosen instead. These bearings let the inner ring to misalign from the outer ring until between 3º and 5º, providing ideally the desired degrees of freedom. The disposition of the bearing has been set following the criteria of accomplishing the highest stiffness possible for the leg, in order to ensure the performance of the measuring system.

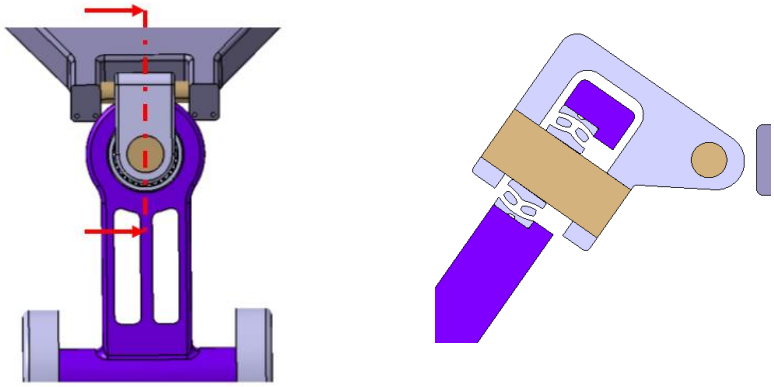

Figure 6-5: Cut detail of the proposed constructive solution for the spherical joint

The constructive challenge that presents this implementation is that a special design will have to be developed in order to fix the inner and outer rings from both sides without compromising the integrity of the linkage.

The possibility of adjusting the height of the CoR to match the system's CoG is accomplished through the capacity of varying the base diameter in which the legs are attached. The inferior bearing housing presents grooves for that purpose.

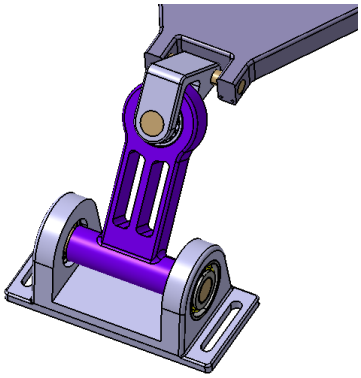

Figure 6-6: Proposed modular attachment to the motion platform

Since the leg orientation changes also with the height of the CoR, the yoke retaining the upper bearing is mounted on a fixed shaft that allows varying the leg angle. The shaft is fixed using an opened hole that can be tightened through screws. This solution presents the benefit of being able to set any desired orientation, but because the fixing is accomplished through friction (or deformation), the adequacy of this solution will have to be tested through FEM simulation. If it is found that the experienced loads make the shaft to rotate and not maintain the desired orientation, another solution would be to have different yokes to attack directly to the surface for different leg angles; this solution is obviously less ideal, for it implies working inside height error ranges for every yoke used (the effect of having a height deviation between the CoR and the CoG has already been presented).

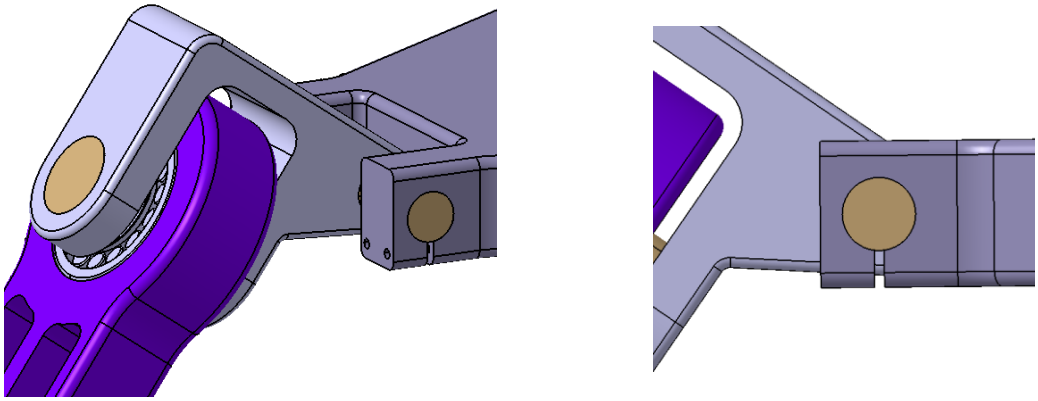

Figure 6-7: Proposed solution to provide variable leg inclinations

The final constructive concept to present is the attachment of the mock-up bike to the surface. As specified on the request list, the mock-up bike should be attached to the surface through the swing-arm axis. For that purpose, a modular system has been incorporated, which allows to fit different swing-arm shaft widths and also lets to adjust the mock-up on the *X* direction in order to position the sytem's CoG exactly at the center of the surface. The mock-up will have to be attached through another point in the surface in order to be fixed properly.

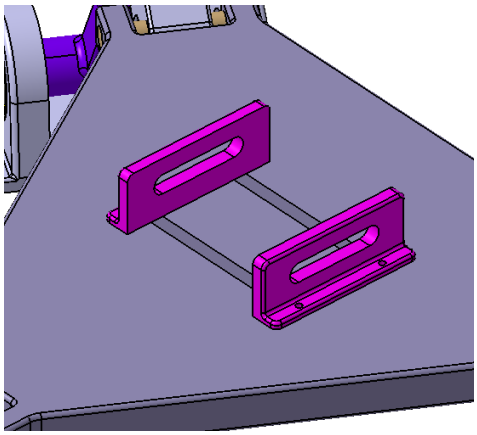

Figure 6-8: Proposed swing-arm attachment

6.2 Basic dimensions

Since the new FZD motorcycle simulator is being conceived at the same time through the work of students that develop different parts of it, it was important to show the proposed dimensions of this system in order to create a concordant overall design of the simulator. It has already been shown that the system proposed has the ability to adapt its geometry in order to change the height of the CoR. Therefore, the dimensions of the system change too.

As it will be seen in the bearing dimensioning chapter, two different scenarios with two extreme mock-up seat heights were considered to evaluate the loads. These two scenarios change the vertical orientation of the legs from 55º to 60º. However, not only the seat height has an effect on the position of the system's CoG, for all the weights of the system play a role in it. When dimensioning the bearings, a heavy scenario is considered in order to obtain the highest loads on the bearings possible. In reality, the masses can be lower, meaning that the leg angle range can be broader. In fact, the exact range will only be known after the detailed design phase is over, and the exact mass of the system is known. As a first approximation, though, it has been considered a leg angle range between 52º and 62º.

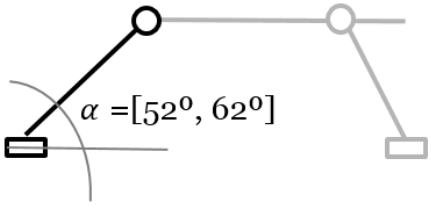

Figure 6-9: Angle range for the leg inclination

Note that the change of the CoR is accomplished by varying the diameter in which the lower part of the legs are attached to the motion platform and, adjusting the leg angle accordingly. The leg's length or the system's surface dimensions always remain the same.

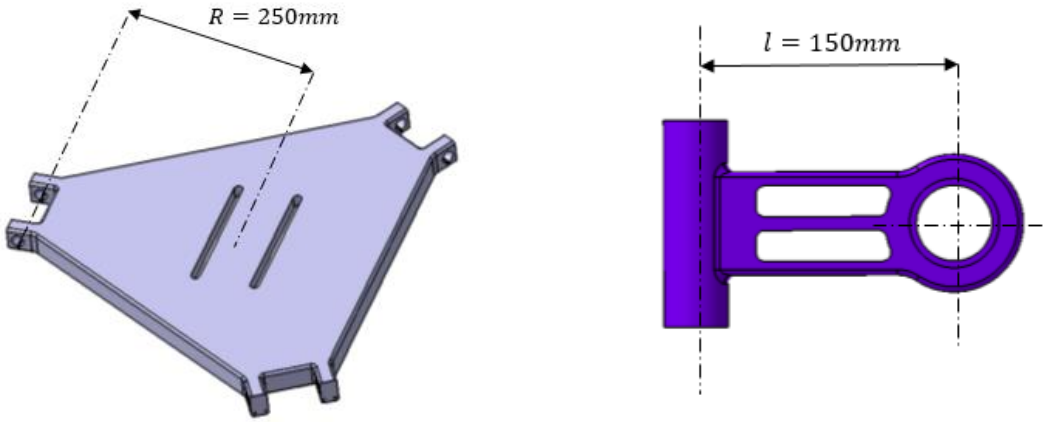

Figure 6-10: Basic dimensions of the surface (left) and the legs (right)

The dimensions that do change and that are shown next are: base radius, surface height, overall width and overall height. The design is a regular tripod, so all the lengths are the same regardless of the orientation shown.

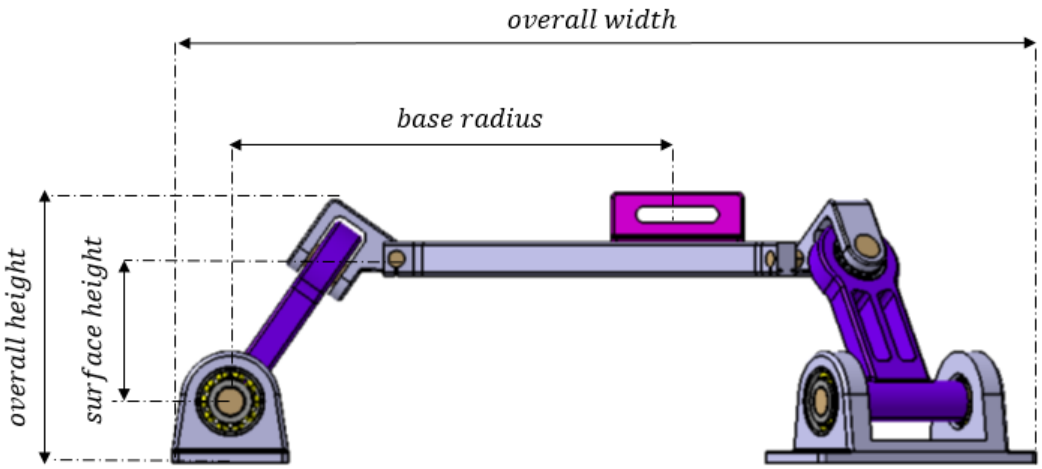

Figure 6-11: Basic dimensions of the system

The values for these variables under the two extreme scenarios are shown in the following table:

Leg angle	*52º*	*62º*
Base radius	412mm	389mm
Surface height	120mm	146mm
Overall width	794mm	758mm
Overall height	231mm	247mm

Table 6-1: Range of values of the system's basic dimensions

6.3 Strain gauge selection methodology

The actual selection of the strain gauges is something that will have to be performed during the detailed design phase, after the work of this thesis is over. The reason for this is that to choose the specific gauge model it is mandatory to know the stiffness of the legs, and this is something that cannot be known before a detailed CAD of the system is done. However, in this short chapter the recommended methodology to follow in order to choose them is presented.

The selection process has to be developed in parallel with the design of the legs: the legs should present the right stiffness to generate the sufficient strain to create an electrical signal on the gauges when the rider is inducing a torque. According to the request list, a 4Nm torque around the roll axis and 10Nm around the pitch axis are the desired precisions; meaning that when this torques occur, a sufficient strain on the legs has to be generated in order to have a signal on the strain gauges. However,

it is not sufficient with designing a very flexible leg since it must be strong enough to support the maximum bending moments without reaching the yield strength.

The most appropriate approach to this methodology is to perform FEM simulations of the legs and varying the design until finding the right compromise between flexibility and enough strength. Once the leg design is optimized, it will be possible to choose the strain gauges and see if the desired precision set on the request list is viable or not.

6.4 Bearing selection

Next, the process followed to choose to the bearings is presented. As stated in the dynamic analysis, it has been set as an output of the Simscape model all the constraint forces and torques experienced by the joints; thanks to that, it has been possible to dimension the bearings and linkages.

Since the system's geometry changes according to the position of the CoG, so do the loads experienced by the joints. For this reason, in order to dimension the bearings, two distinctive scenarios have been considered: a low rider position and another one high. The input motions considered are the same used for the real data simulation, since it contains the harshest motions that the system will encounter. The mass of the rider has been set to 80kg in order to reach the requested load of 400kg total. The rest of parameters are the ones considered for said simulation. It is important to remark that, since the bearings will not rotate and will be under maximum intermittent loads, the suited criteria to dimension the bearings is based on the maximum static load admissible.

- **Scenario 1: rider CoG height of 1000mm**

For the first scenario, it has been considered that the mock-up bike was a small bike, like the Honda Monkey, which has a seat height of 750mm. Considering that the CoG of a person is somewhere around the waist, it has been set a rider's CoG height of 1000mm.

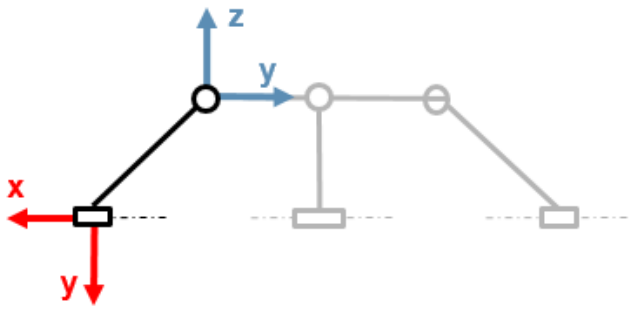

Figure 6-12: Sign convention used for each joint, coming from the disposition in the Simscape model

Although the loads on the bearings vary depending on the leg, in order to ensure the integrity of the system and as part of the safety factor, for the bearing calculation it has been considered always the highest loads and that they appear at the same time. The maximum and minimum loads on the joints are presented in the following table. Once again, with the aim of obtaining a safe design, the highest load in absolute value of every kind has been taken into account for the bearing calculation.

Constraint loads (1000mm)	*Maximum*	*Minimum*
Revolute Fz (load-cell)	750N	-730N
Revolute Fx	2100N	-650N
Revolute Fy	3100N	-900N
Revolute Mx	89Nm	-92Nm
Revolute My	63Nm	-61Nm
Spherical Fx	750N	-730N
Spherical Fy	650N	-2100N
Spherical Fz	1000N	-3000N

Table 6-2: Maximum and minimum loads registered on the joints for the scenario of a rider height of 1000mm

Starting with the revolute joint, the radial forces that will have to support the bearings are defined by the following expressions:

$$F_{r_A} = \sqrt{(\frac{F_x}{2} + \frac{2\,M_y}{l})^2 + (\frac{F_y}{2} + \frac{2\,M_x}{l})^2} \tag{6-1}$$

$$F_{r_B} = \sqrt{(\frac{F_x}{2} - \frac{2\,M_y}{l})^2 + (\frac{F_y}{2} - \frac{2\,M_x}{l})^2} \tag{6-2}$$

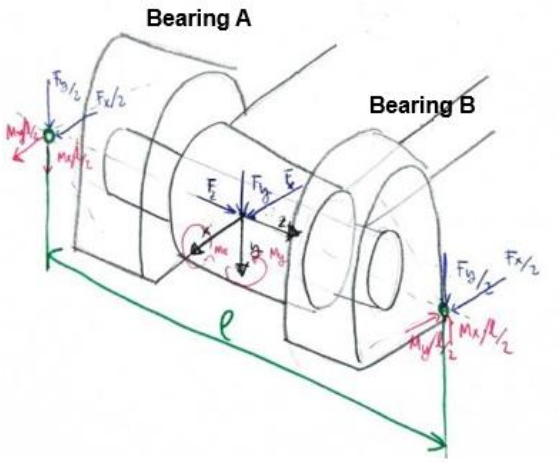

Figure 6-13: Sketch of the forces experienced by the angular bearings

In regards to the axial forces: considering that the bearing disposition will be back to back, the worst scenario possible is that all the external axial load is supported by only one bearing and that the axial load generated by the own bearing is in the same direction. In this case, the axial forces are calculated the following way:

$$F_{a_A} = \frac{0.5\, F_{r_A}}{Y_A} \quad , \quad F_{a_B} = F_{a_A} + F_z \qquad (6\text{-}3)\,,\ (6\text{-}4)$$

For this application, in which the bearings will experience important intermittent axial loads in both directions, the most suitable solution would be to use angular contact bearings. The following ball bearing has been selected: 7305 BEP by SKF (the specification sheet can be found in the appendix). A roller bearing could have been used instead, if the presented loads were too high. Knowing the bearing parameters and considering a length between the pressure points l of 220mm, it is possible to calculate the above-said loads.

$$F_{r_A} = 2{,}89kN \quad , \quad F_{a_A} = 2{,}78kN \qquad (6\text{-}5)\,,\ (6\text{-}6)$$

$$F_{r_A} = 2{,}89kN \quad , \quad F_{a_A} = 2{,}78kN \qquad (6\text{-}7)\,,\ (6\text{-}8)$$

$$F_{r_B} = 0{,}86kN \quad , \quad F_{a_B} = 3{,}53kN \qquad (6\text{-}9)\,,\ (6\text{-}10)$$

The equivalent static load can be now also calculated:

$$P_0 = F_r + Y_0 \cdot F_a \qquad (6\text{-}11)$$

$$P_{0_A} = 2{,}89 + 0{,}52 \cdot 2{,}78 = 4{,}34kN \qquad (6\text{-}12)$$

$$P_{0_B} = 0{,}86 + 0{,}52 \cdot 3{,}53 = 3{,}53kN \qquad (6\text{-}13)$$

Knowing that the highest equivalent static load is the one supported by the bearing A, the final step is calculating the safety factor. Because the system has to ensure the integrity of the user, a quite safety factor was desired (between 3 and 5). As it can be seen, the chosen bearing satisfies the expectations.

$$S_0 = \frac{C_0}{P_0} = \frac{14}{4{,}34} = 3{,}22 \qquad (6\text{-}14)$$

In the case of the spherical joint, first a projection of the measured loads has to be performed in order to obtain the loads in the orientation of the bearing.

$$F_y' = F_y \cdot \cos(\alpha) + F_z \cdot \sin(\alpha) \quad , \quad F_z' = F_z \cdot \cos(\alpha) - F_y \cdot \sin(\alpha) \qquad (6\text{-}15)\,,\ (6\text{-}16)$$

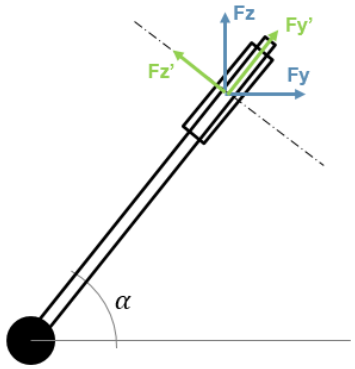

Figure 6-14: Base change used to calculate the loads on the spherical roller bearing

Considering that in the current disposition α takes a value of 55º, the abovementioned projected loads are:

$$F_y' = 3{,}66kN \quad , \qquad F_z' = 3{,}43kN \tag{6-17}, \ (6-18)$$

The actual axial and radial forces are, consequently:

$$F_a = F_z' = 3{,}43kN \quad , \quad F_r = \sqrt{F_y'^2 + F_x^{\ 2}} = 3{,}74kN \tag{6-19}, \ (6-20)$$

In this case, the following spherical roller bearing has been selected: 22205 EK by SKF (the specification sheet can be also found in the appendix). Self-aligning ball bearings are also suitable for this application, but the chosen type is able to support higher loads and is also stiffer. Having the bearing parameters clear, it is possible to calculate now the equivalent static load and the safety factor:

$$P_0 = F_r + Y_0 \cdot F_a = 3{,}74 + 1{,}8 \cdot 3{,}43 = 9{,}914kN \tag{6-21}$$

$$S_0 = \frac{C_0}{P_0} = \frac{44}{9{,}91} = 4{,}43 \tag{6-22}$$

The safety factor is also inside the desired range, what makes the selected bearing a viable solution.

- **Scenario 2: rider CoG height of 1200mm**

For this second scenario, a mock-up of a motorcycle with a high seat has been considered, like in the case of a KTM 690 Enduro, which has a seat height of 930mm. Following the same idea from the first scenario, what has been done is considering the rider's CoG at a height at the height of the waist, what would make 1200mm roughly.

The proceeding followed is the same as before, now considering that the maximum and minimum loads registered are the following ones:

Constraint loads (1200mm)	*Maximum*	*Minimum*
Revolute Fz (load-cell)	720N	-690N
Revolute Fx	1970N	-750N
Revolute Fy	3500N	-1300N
Revolute Mx	90Nm	-94Nm
Revolute My	54Nm	-52Nm
Spherical Fx	720N	-690N
Spherical Fy	750N	-1950N
Spherical Fz	1360N	-3400N

Table 6-3: Maximum and minimum loads registered on the joints for the scenario of a rider height of 1200mm

Following the same steps as before, the obtained loads on the roller thrust bearings are:

$$F_{r_A} = 2{,}99kN \quad , \quad F_{a_A} = 2{,}88kN \qquad \text{(6-23) , (6-24)}$$

$$F_{r_B} = 1{,}03kN \quad , \quad F_{a_B} = 3{,}60kN \qquad \text{(6-25) , (6-26)}$$

Next, the equivalent static loads and the safety factor:

$$P_{0_A} = 2{,}99 + 0{,}52 \cdot 2{,}88 = 4{,}49kN \qquad \text{(6-27)}$$

$$P_{0_B} = 1{,}03 + 0{,}52 \cdot 3{,}60 = 2{,}89kN \qquad \text{(6-28)}$$

$$S_0 = \frac{C_0}{P_0} = \frac{14}{4{,}49} = 3{,}12 \qquad \text{(6-29)}$$

Which means that for this opposite scenario, the selected bearing model also works.

To calculate the spherical bearing it is remarkable that the geometry has changed and that the angle α is 60º in this case. A part from that, the method used is the same.

$$F_y' = 3{,}92kN \quad , \quad F_z' = 3{,}38kN \qquad \text{(6-30) , (6-31)}$$

$$F_a = F_z' = 3{,}38kN \quad , \quad F_r = \sqrt{{F_y'}^2 + {F_x}^2} = 3{,}99kN \qquad \text{(6-32) , (6-33)}$$

$$P_0 = F_r + Y_0 \cdot F_a = 3{,}99 + 1{,}8 \cdot 3{,}38 = 10{,}07kN \qquad \text{(6-34)}$$

$$S_0 = \frac{C_0}{P_0} = \frac{44}{10{,}07} = 4{,}37 \qquad \text{(6-35)}$$

As it can be seen, the adequacy of the upper bearing is also verified for this scenario.

7 Conclusions and considerations

The main purpose of this thesis was to design a motorcycle mount with integrated roll-and-pitch-torques for the future FZD's motorcycle simulator. The current simulator located in the WIVW only considers the rolling rider-induced torque, and for the new one it was asked to consider also the torque generated around the pitch axis. Furthermore, it was also asked to provide an enhancement on the measuring precision, one of the biggest downfalls of the current system.

At the end of this thesis, it has been possible to provide a solution that answers to the above-mentioned requirements. However, as stated in the introduction, the design is not totally finished since the last stage has not been carried out for time reasons. The output of this thesis is a concept with tested behaviour and with a basic constructive design; what is left now is to detail the construction in order to be manufactured. Hence, this thesis should work as a blueprint for a future project regarding this last stage of the development.

From a performance point of view, the chosen solution presents clear advantages in comparison with the current simulator. It is true, though, that a direct measuring system that would not need to correct the data before sending it to the vehicle dynamics model has not been accomplished. By positioning the virtual rotation center at the same height as the system's CoG, the most part of the inertial forces generated by platform motion have been subtracted from the measurement. Still, as it has been shown, under certain scenarios (such as rotational accelerations or when there is a coupling between the motion of the platform and the rider position), inertial forces create a torque that is read on the measuring data, making necessary to make estimations of these effects in order to correct it. Furthermore, it has also been shown the problem that comes with not being able to distinguish the sources of the rider-induced torques, making unsuitable to correct the signal accordingly. These dynamic drawbacks are something that will have to be treated also during the last stage of the development, providing a valid way to correct the measurements.

Despite these considerations, taking a look at the request list it is visible that the work performed can be considered a success. All the requested requirements have been accomplished, and the majority of wishes listed there can be easily incorporated to the design; as a matter of fact, some of them represent the work of other fellow students developing other projects around the new FZD motorcycle simulator.

8 Appendix

8.1 MatLAB Simulink/Simscape model and geometry script

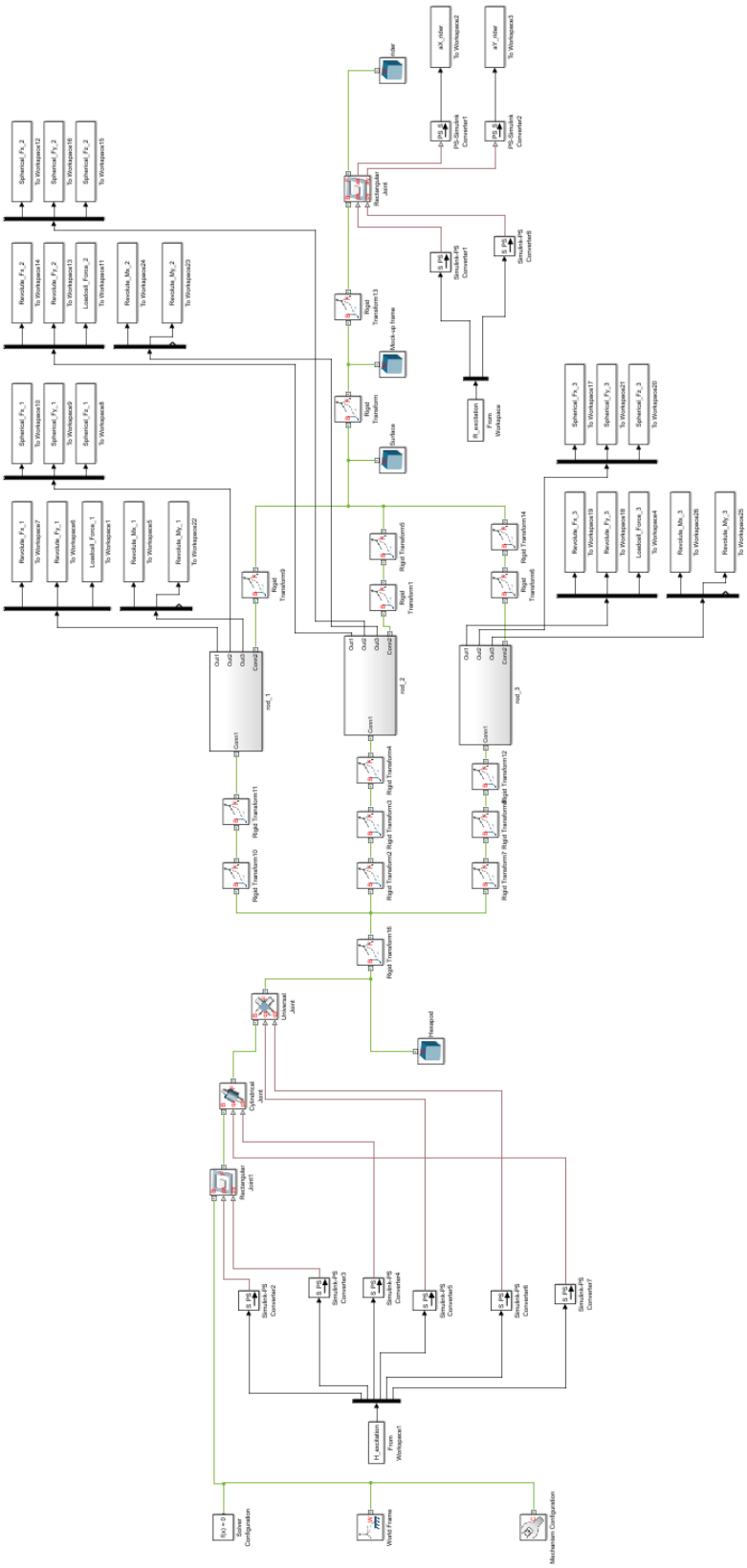

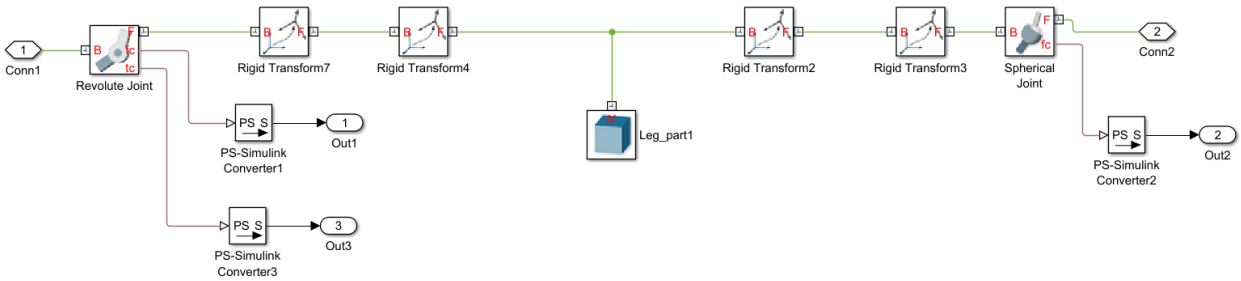
1
Conn1
Revolute Joint
Rigid Transform7
Rigid Transform4
Leg_part1
Rigid Transform2
Rigid Transform3
Spherical Joint
2
Conn2
PS-Simulink Converter1
1
Out1
PS-Simulink Converter2
2
Out2
PS-Simulink Converter3
3
Out3

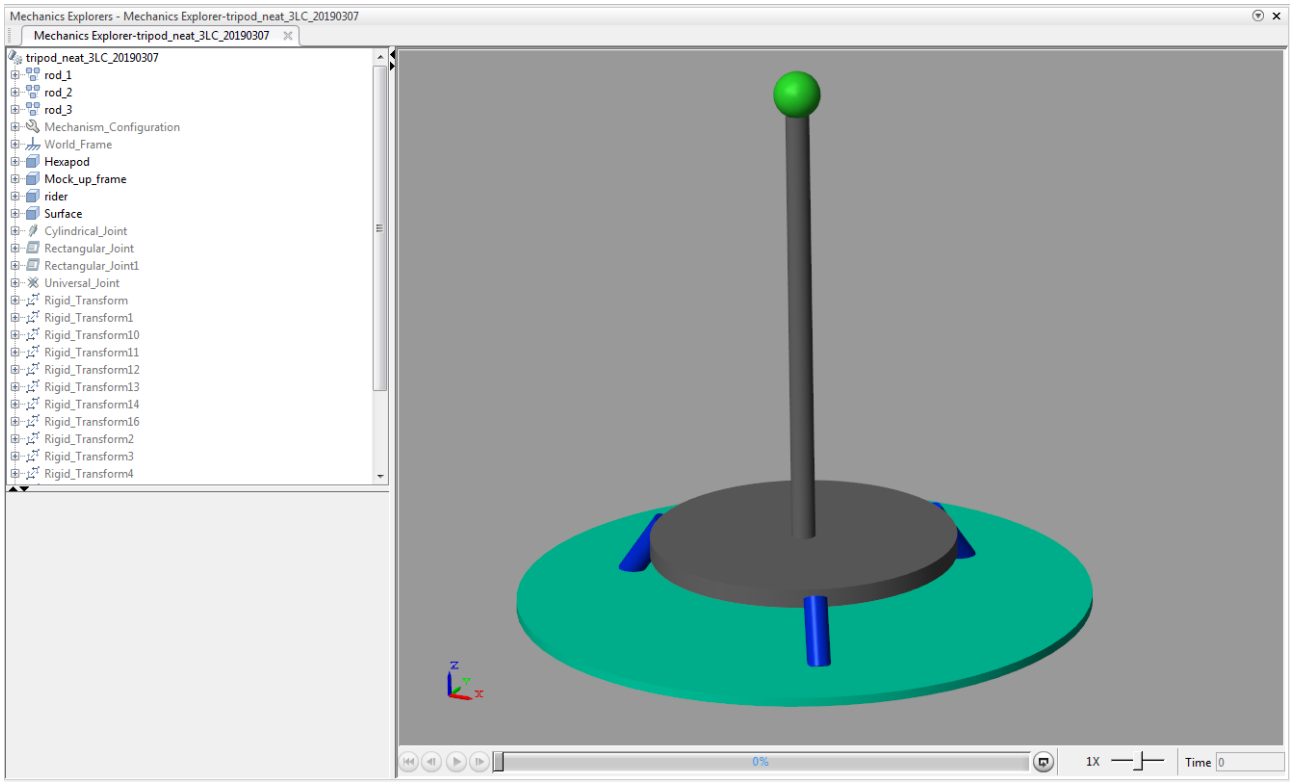
Mechanics Explorers - Mechanics Explorer-tripod_neat_3LC_20190307
Mechanics Explorer-tripod_neat_3LC_20190307
tripod_neat_3LC_20190307
rod_1
rod_2
rod_3
Mechanism_Configuration
World_Frame
Hexapod
Mock_up_frame
rider
Surface
Cylindrical_Joint
Rectangular_Joint
Rectangular_Joint1
Universal_Joint
Rigid_Transform
Rigid_Transform1
Rigid_Transform10
Rigid_Transform11
Rigid_Transform12
Rigid_Transform13
Rigid_Transform14
Rigid_Transform16
Rigid_Transform2
Rigid_Transform3
Rigid_Transform4
0%
1X
Time

```
clear all
close all
clc

%KINEMATIC PARAMETERS (all in mm)
%INPUT parameters
t_sim=10;
max_step=0.01;
noise_filter=0.05;
%Intrinsecal system parameters
rider_CoG_H=1000;
platform_R1=320;
platform_R2=platform_R1;
platform_R3=platform_R1;
rod_L1=150;

delta_12=(2*pi/3); %2pi/3 (symmetrical) to work propperly
delta_13=(2*pi/3);

%DYNAMIC PARAMETERS
rider_mass=80; %kg

hexapod_mass=50;
rod1_mass=10;
rod2_mass=10;
rod3_mass=10;
surface_mass=50;
mockup_mass=200;

%Calculation of the rest of parameters
syms platform_H;
syms base_R1;
syms base_R2;
syms base_R3;
syms alpha;
syms beta;
syms gamma;
syms rod_L2;
syms rod_L3;

% iterative method to find CoR
force_error=100;
CoR=500;
iter=0;
while abs(force_error)>1e-6
    S=fsolve(@(x)tripod_system(x,CoR, platform_R1, platform_R2, platform_R3,
rod_L1),[200,400,400,400,pi/10,pi/10,pi/10,150,150]);
    platform_H=S(1);
    base_R1=S(2);
    base_R2=S(3);
    base_R3=S(4);
    alpha=S(5);
    beta=S(6);
    gamma=S(7);
    rod_L2=S(8);
    rod_L3=S(9);
```

```
    H_excitation.time=[0:0.01:t_sim]';
    H_excitation.signals.values(:,1)=0*(cos(H_excitation.time*2*pi/5)-1);
    H_excitation.signals.values(:,2)=0*(cos(H_excitation.time*2*pi/5)-1);
    H_excitation.signals.values(:,3)=0*(cos(H_excitation.time*2*pi/5)-1);
    H_excitation.signals.values(:,4)=pi/2;
    H_excitation.signals.values(:,5)=0;
    H_excitation.signals.values(:,6)=0*(cos(H_excitation.time*2*pi/6));

    R_excitation.time=[0:0.01:t_sim]';
    R_excitation.signals.values(:,1)=0*(cos(R_excitation.time*2*pi/5)-1);
    R_excitation.signals.values(:,2)=0*(cos(R_excitation.time*2*pi/5)-1);

    sim('tripod_neat_3LC_20190307');

    Loadcell_pitch=Loadcell_Force_2.signals.values*sin(delta_12);
    Loadcell_roll=Loadcell_Force_1.signals.values+Loadcell_Force_2.signals.val-
ues*cos(delta_12);
    force_error=mean(Loadcell_roll);
    if force_error>CoR/2
        CoR=CoR-CoR/4;
    elseif force_error<CoR/2 && force_error>0
        CoR=CoR-force_error/10;
    elseif force_error>-CoR/2 && force_error<0
        CoR=CoR+force_error/4;
    elseif force_error<-CoR/10
        CoR=CoR+CoR/4;
    end

    iter=iter+1;
end

%% showing number of iterations
iter

%% save workspace
save('WS_parameters')

%%functions to find out kinematic parameters, (fsolve)
function F=tripod_system(x,CoR,platform_R1,platform_R2,platform_R3,rod_L1)
platform_H=x(1);
base_R1=x(2);
base_R2=x(3);
base_R3=x(4);
alpha=x(5);
beta=x(6);
gamma=x(7);
rod_L2=x(8);
rod_L3=x(9);
F(1)=rod_L1*sin(alpha)-platform_H;
F(2)=base_R1-(platform_R1+rod_L1*cos(alpha));
F(3)=tan(alpha)-(CoR/platform_R1);
F(4)=rod_L2*sin(beta)-platform_H;
F(5)=base_R2-(platform_R2+rod_L2*cos(beta));
F(6)=tan(beta)-(CoR/platform_R2);
F(7)=rod_L3*sin(gamma)-platform_H;
F(8)=base_R3-(platform_R3+rod_L3*cos(gamma));
F(9)=tan(gamma)-(CoR/platform_R3);
end
```

8.2 **Motion scenario 1:** rider motion in *X* direction, no platform motion

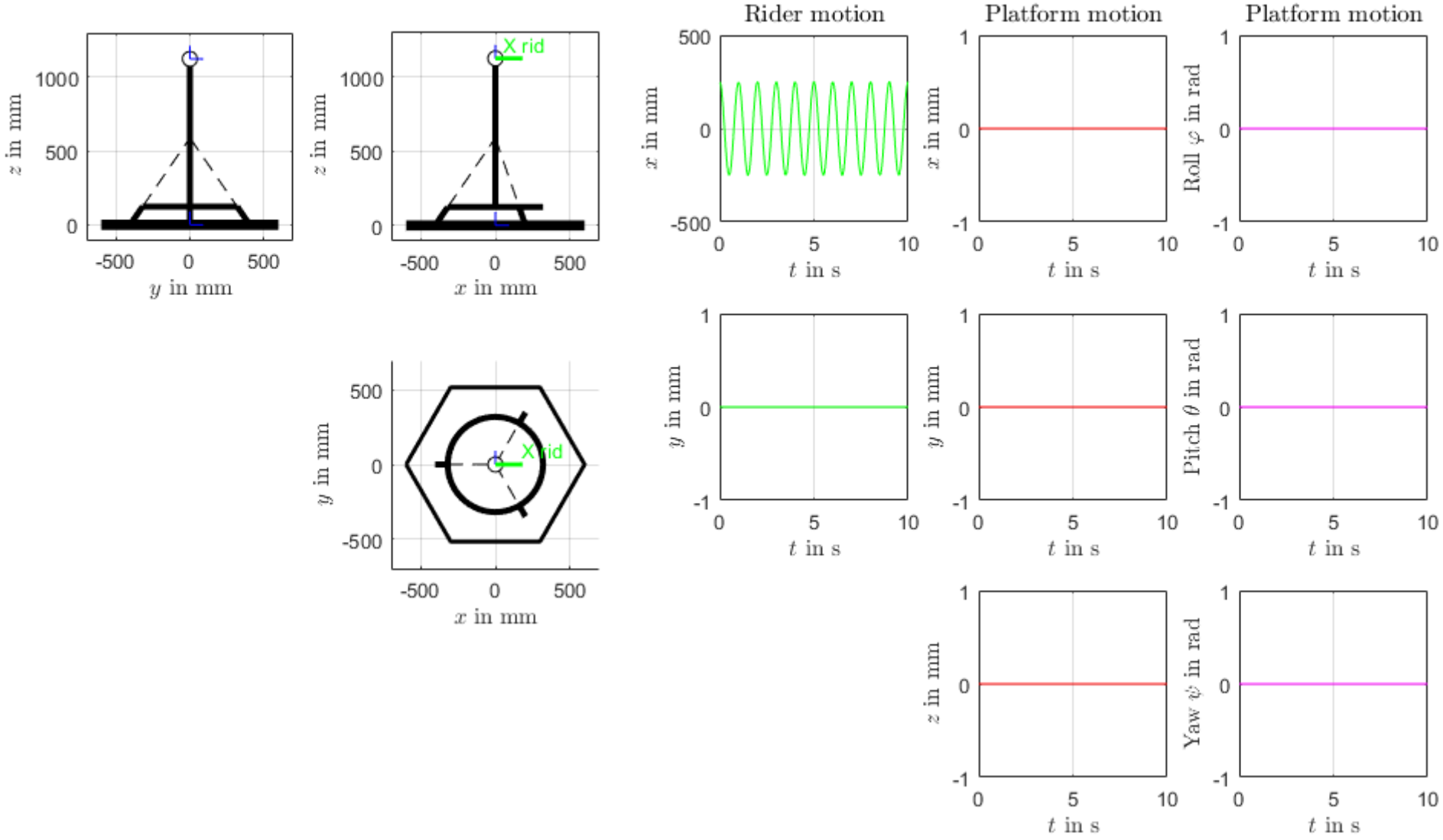

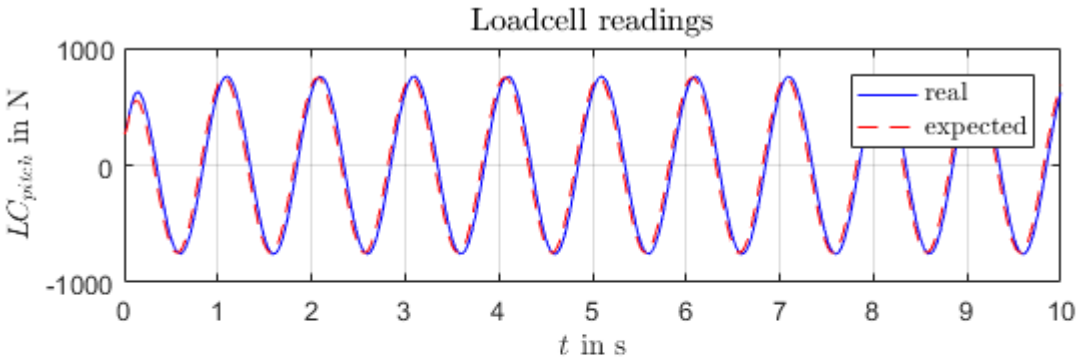
Loadcell readings
LC_{pitch} in N
real
expected
t in s

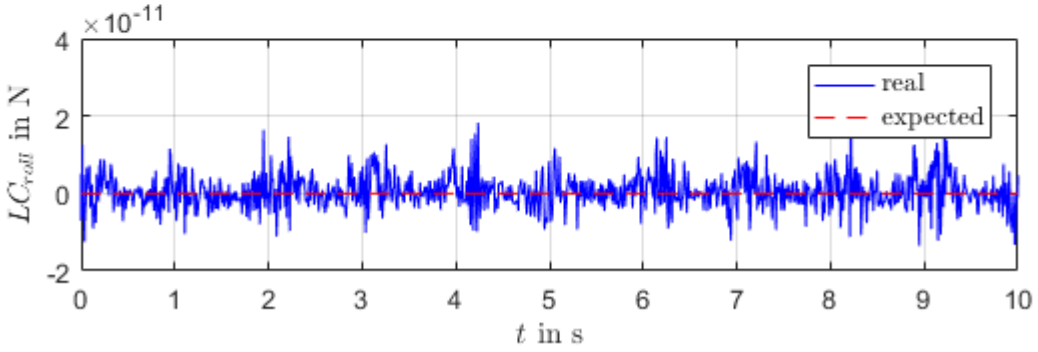
$\times 10^{-11}$
LC_{roll} in N
real
expected
t in s

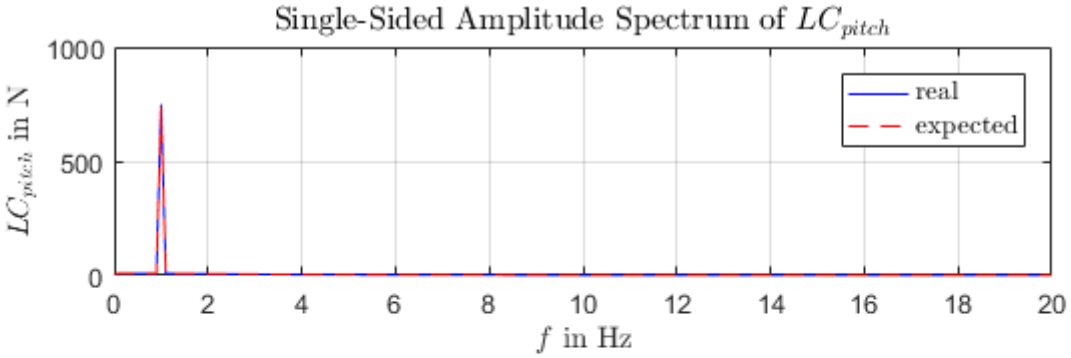
Single-Sided Amplitude Spectrum of LC_{pitch}
LC_{pitch} in N
real
expected
f in Hz

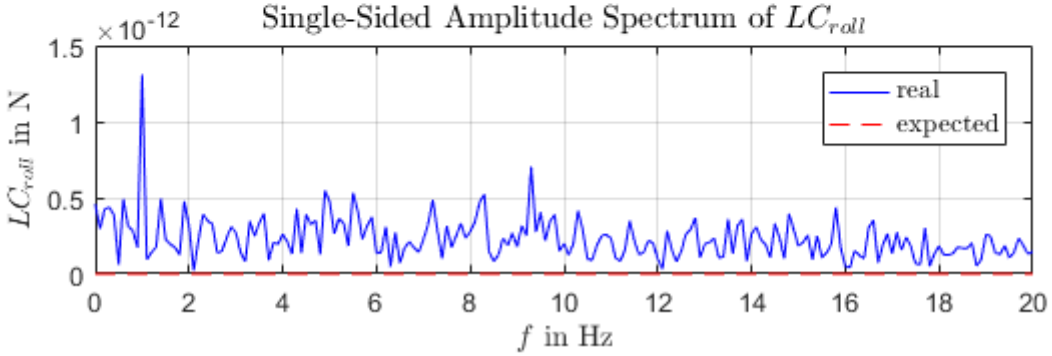
$\times 10^{-12}$
Single-Sided Amplitude Spectrum of LC_{roll}
LC_{roll} in N
real
expected
f in Hz

8.3 **Motion scenario 2:** rider motion in *Y* direction, no platform motion

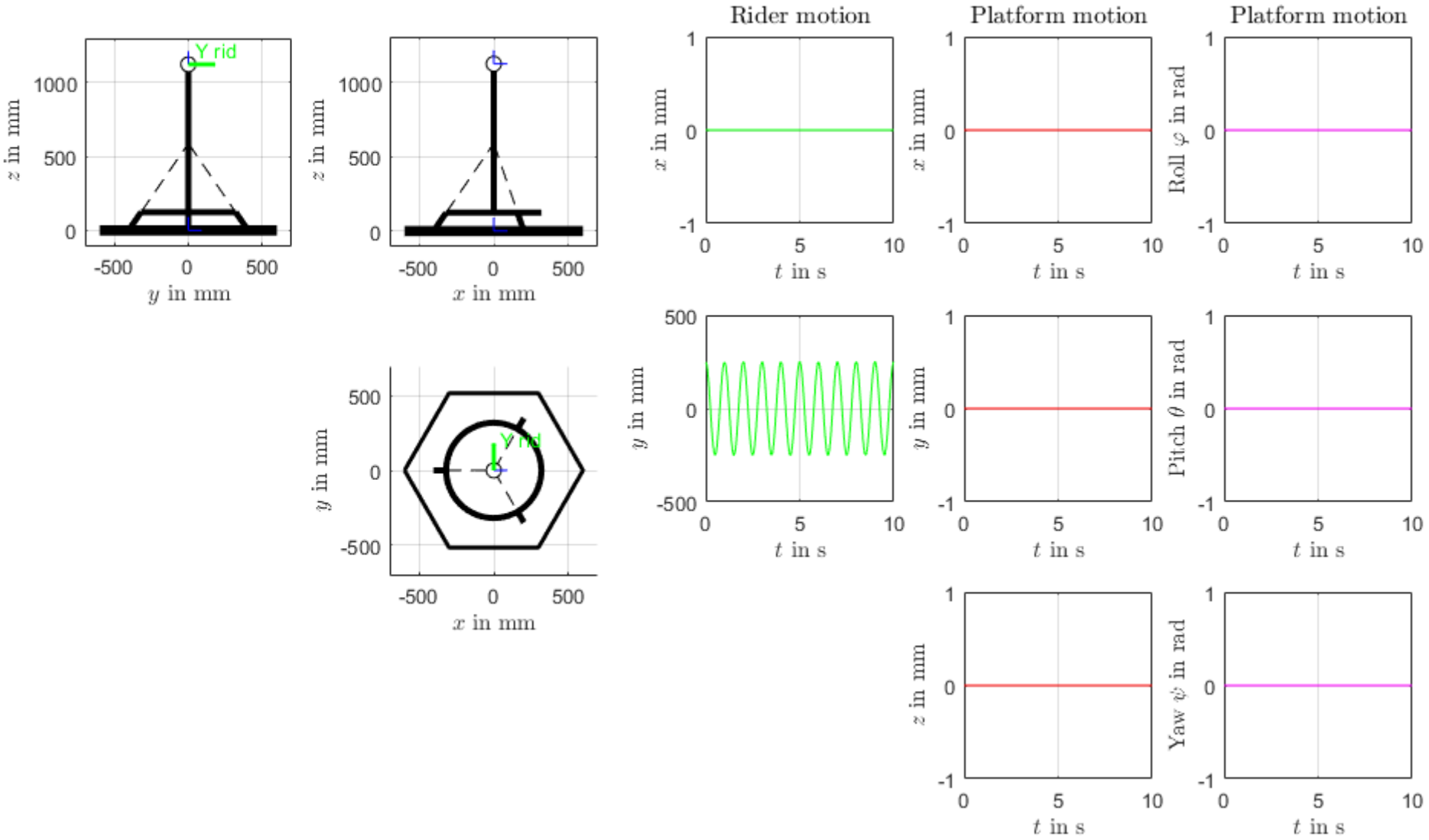

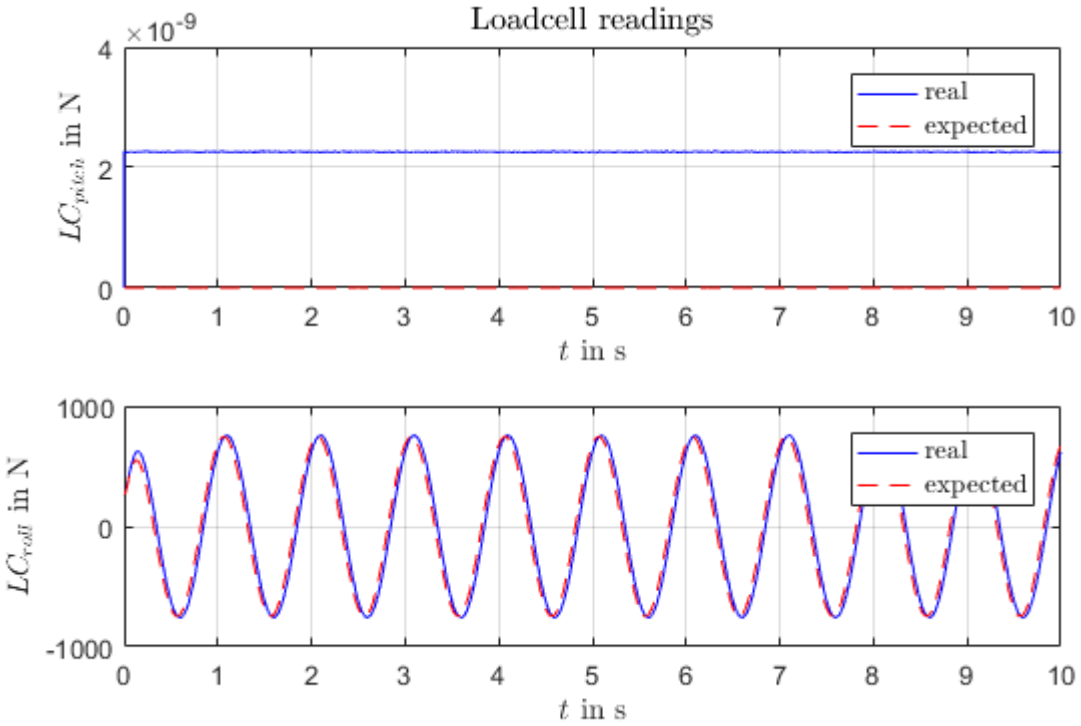
Loadcell readings
×10-9
4
2
0
LC_{pitch} in N
real
expected
0 1 2 3 4 5 6 7 8 9 10
t in s
1000
0
-1000
LC_{roll} in N
real
expected
0 1 2 3 4 5 6 7 8 9 10
t in s

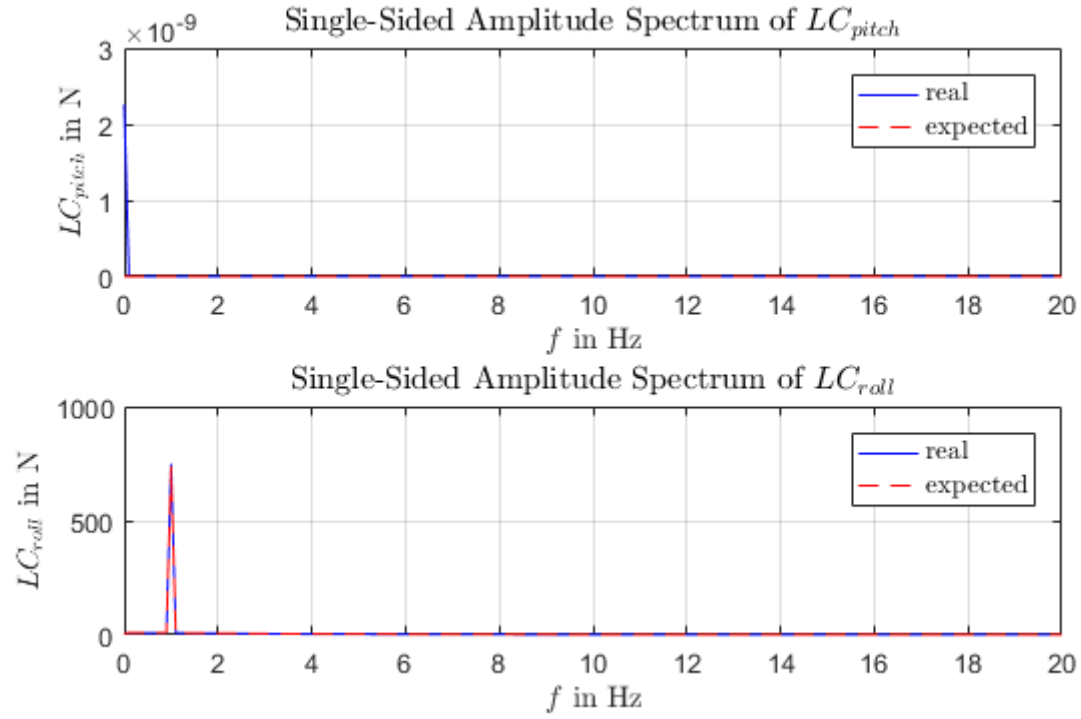
Single-Sided Amplitude Spectrum of LC_{pitch}
×10-9
3
2
1
0
LC_{pitch} in N
real
expected
0 2 4 6 8 10 12 14 16 18 20
f in Hz
Single-Sided Amplitude Spectrum of LC_{roll}
1000
500
0
LC_{roll} in N
real
expected
0 2 4 6 8 10 12 14 16 18 20
f in Hz

8.4 **Motion scenario 3:** no rider motion, platform motion in *X* direction

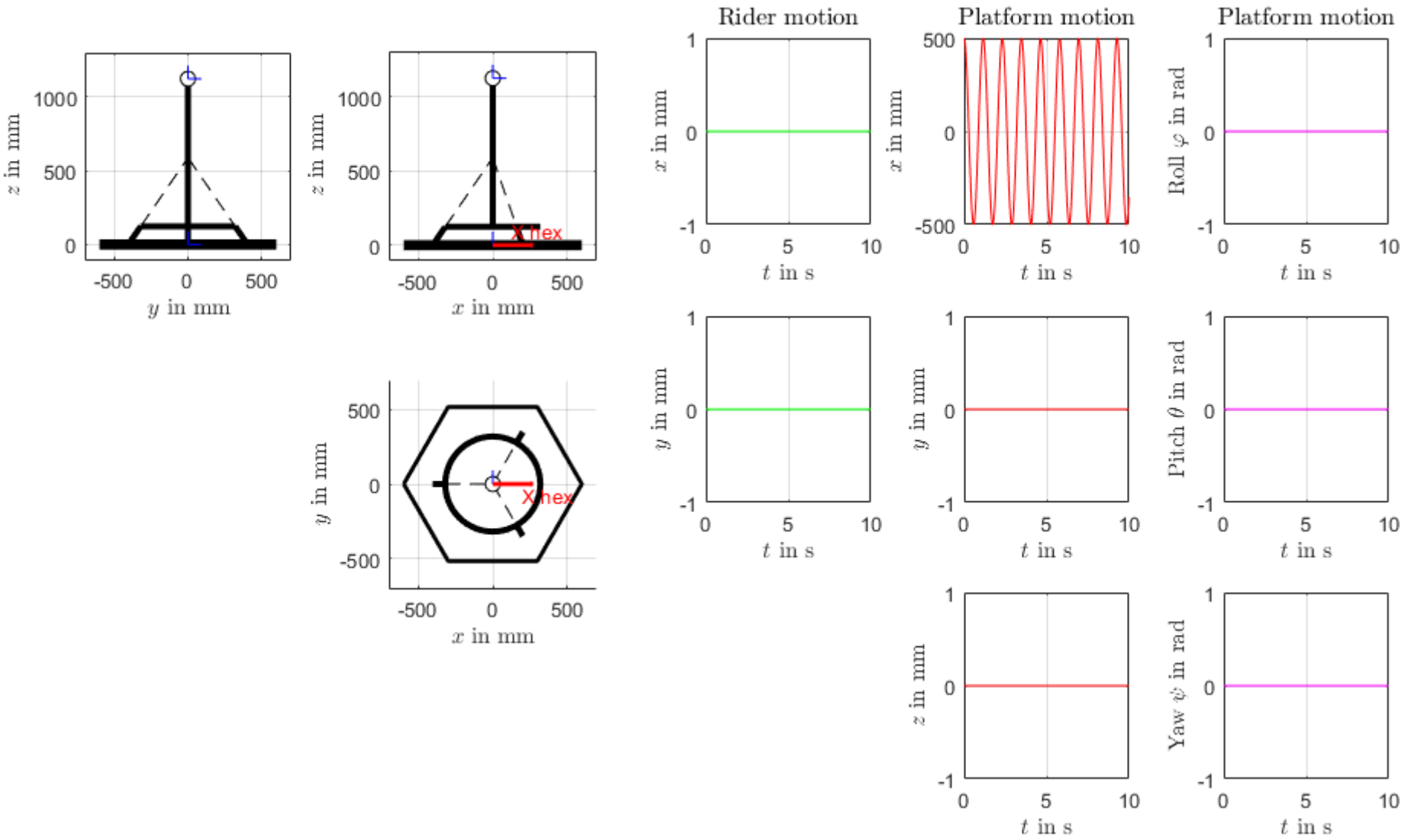

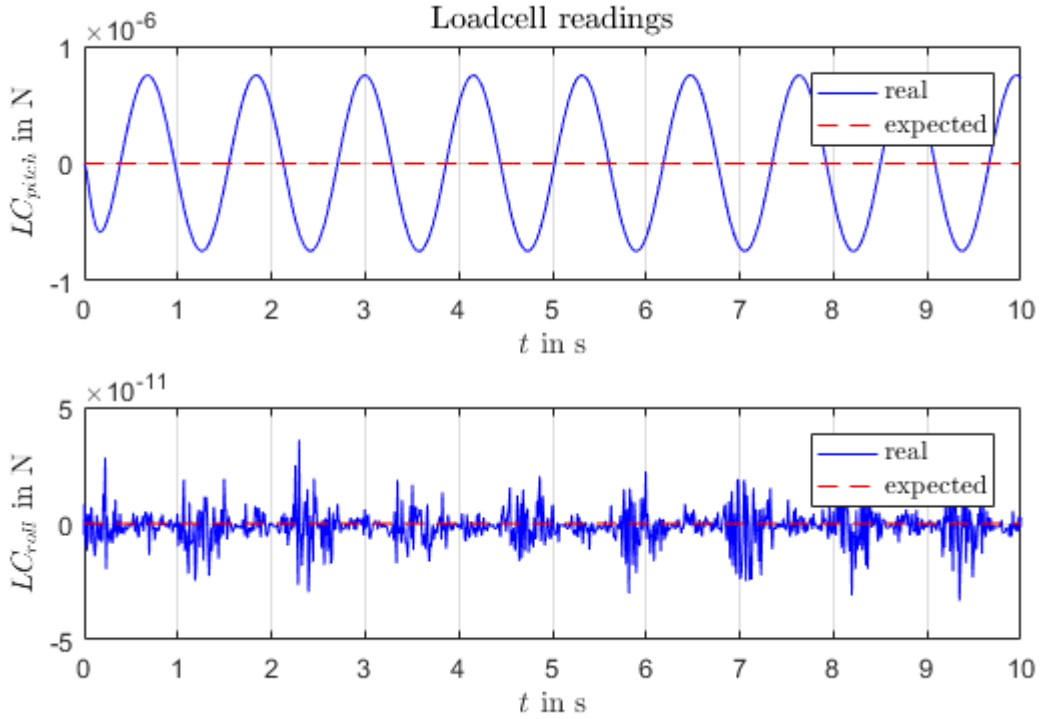
Loadcell readings
×10^-6
1
0
-1
LC_{pitch} in N
real
expected
0 1 2 3 4 5 6 7 8 9 10
t in s
×10^-11
5
0
-5
LC_{roll} in N
real
expected
0 1 2 3 4 5 6 7 8 9 10
t in s

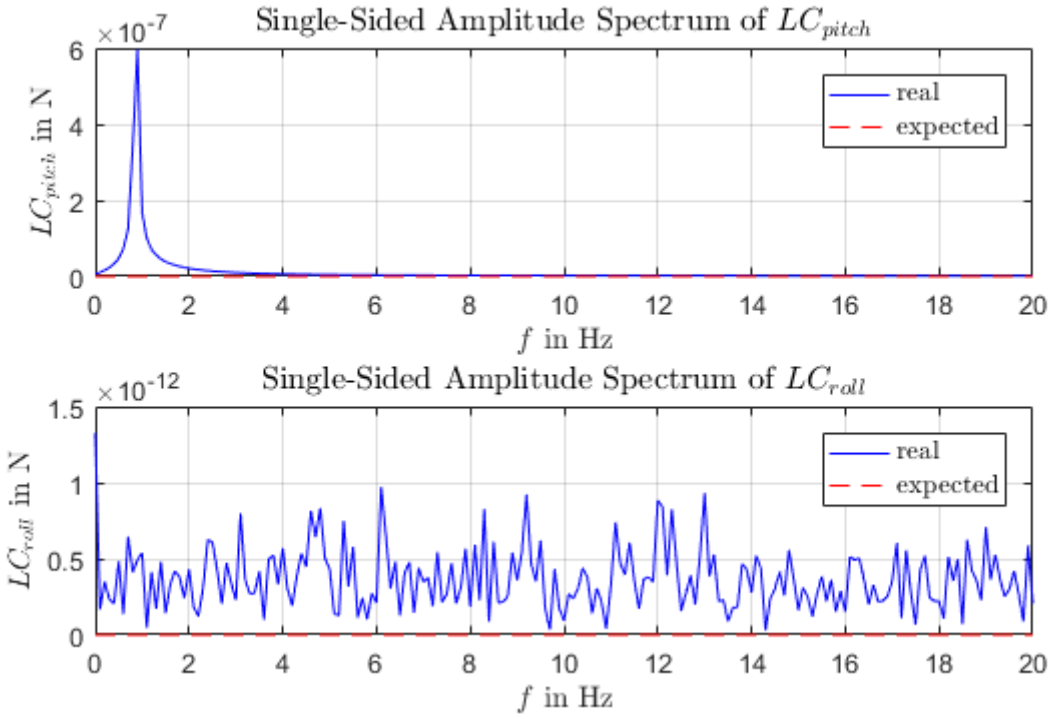
Single-Sided Amplitude Spectrum of LC_{pitch}
×10^-7
6
4
2
0
LC_{pitch} in N
real
expected
0 2 4 6 8 10 12 14 16 18 20
f in Hz
Single-Sided Amplitude Spectrum of LC_{roll}
×10^-12
1.5
1
0.5
0
LC_{roll} in N
real
expected
0 2 4 6 8 10 12 14 16 18 20
f in Hz

8.5 **Motion scenario 4:** no rider motion, platform motion in Y direction

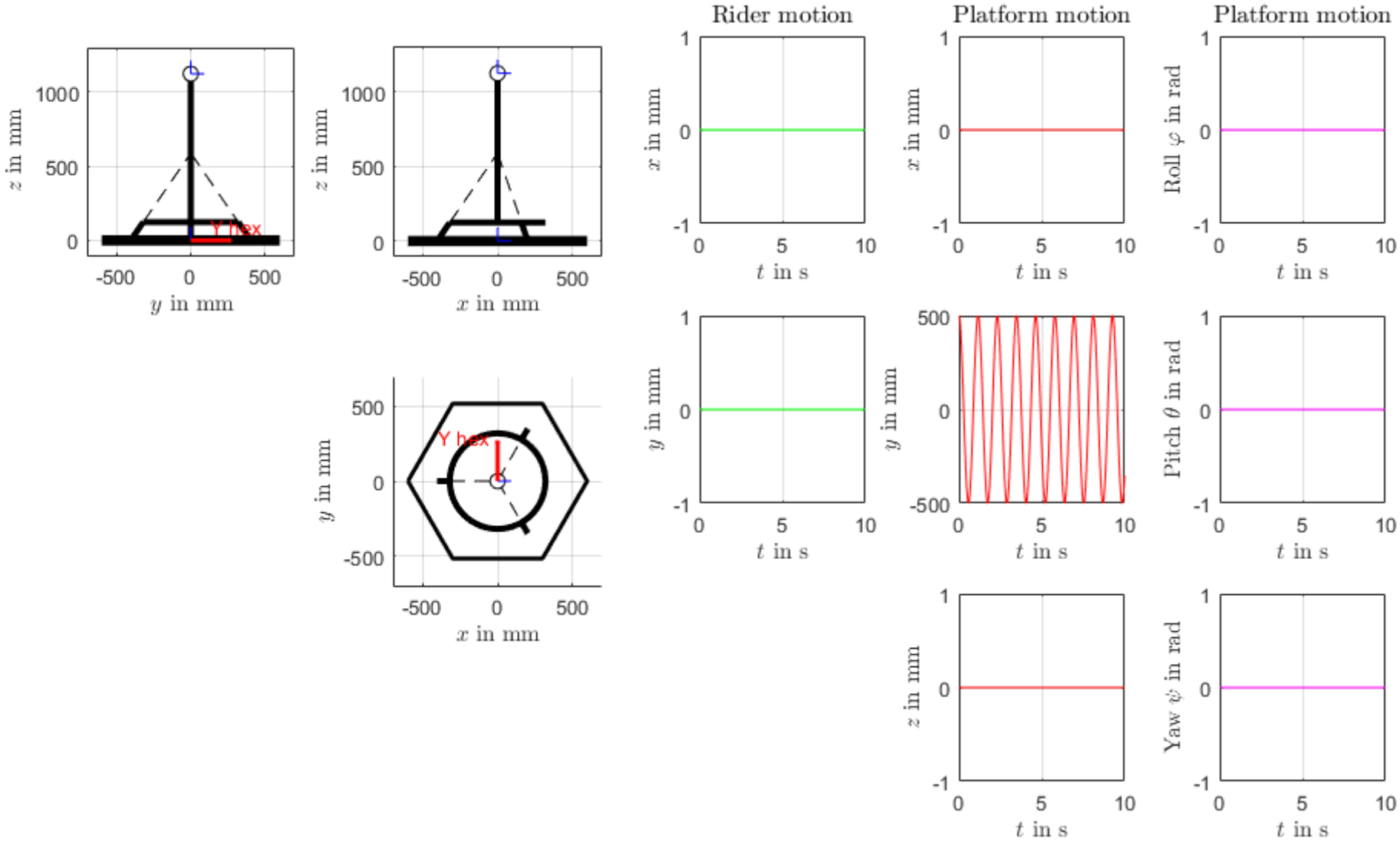

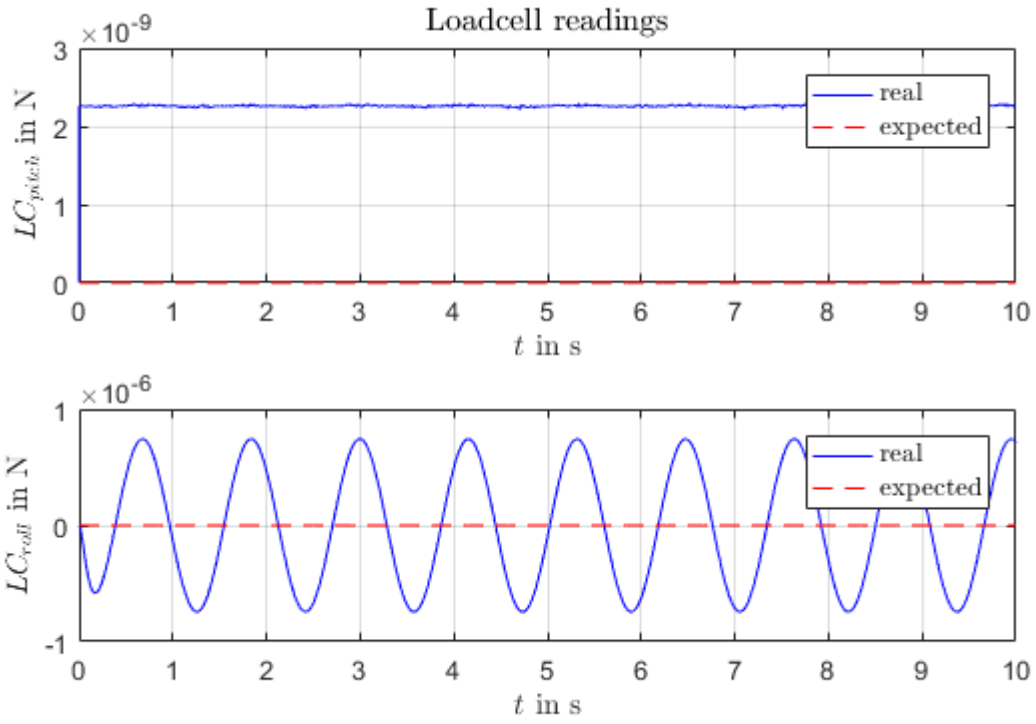
Loadcell readings
×10-9
3
2
1
0
LC_{pitch} in N
real
expected
0 1 2 3 4 5 6 7 8 9 10
t in s
×10-6
1
0
-1
LC_{roll} in N
real
expected
0 1 2 3 4 5 6 7 8 9 10
t in s

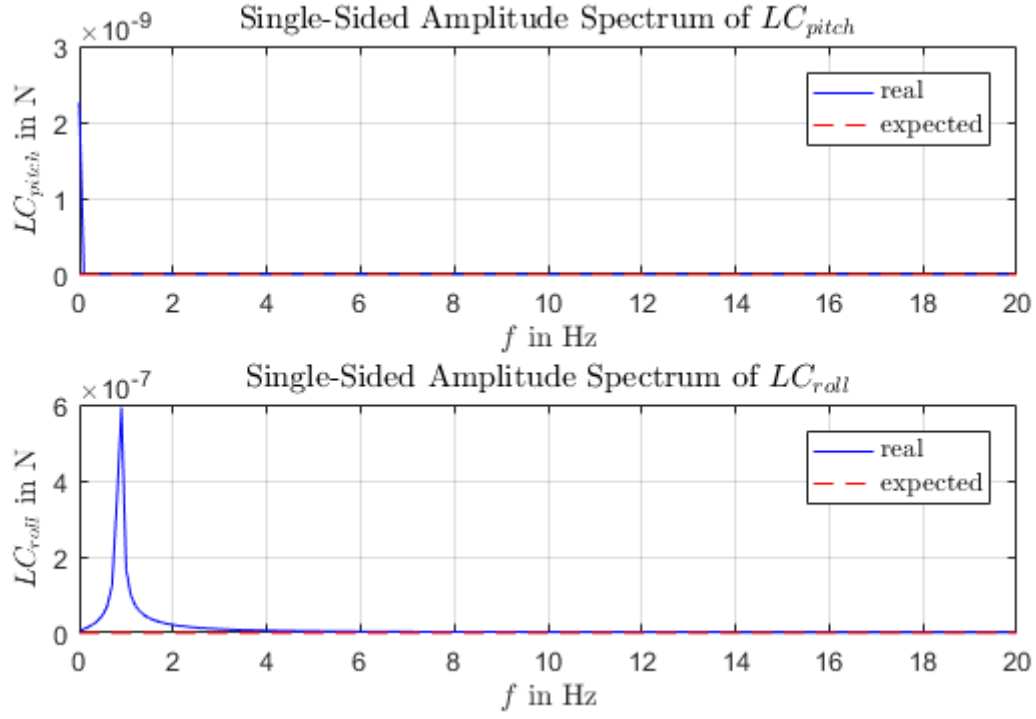
Single-Sided Amplitude Spectrum of LC_{pitch}
×10-9
3
2
1
0
LC_{pitch} in N
real
expected
0 2 4 6 8 10 12 14 16 18 20
f in Hz
Single-Sided Amplitude Spectrum of LC_{roll}
×10-7
6
4
2
0
LC_{roll} in N
real
expected
0 2 4 6 8 10 12 14 16 18 20
f in Hz

8.6 **Motion scenario 5:** no rider motion, platform motion in *Z* direction

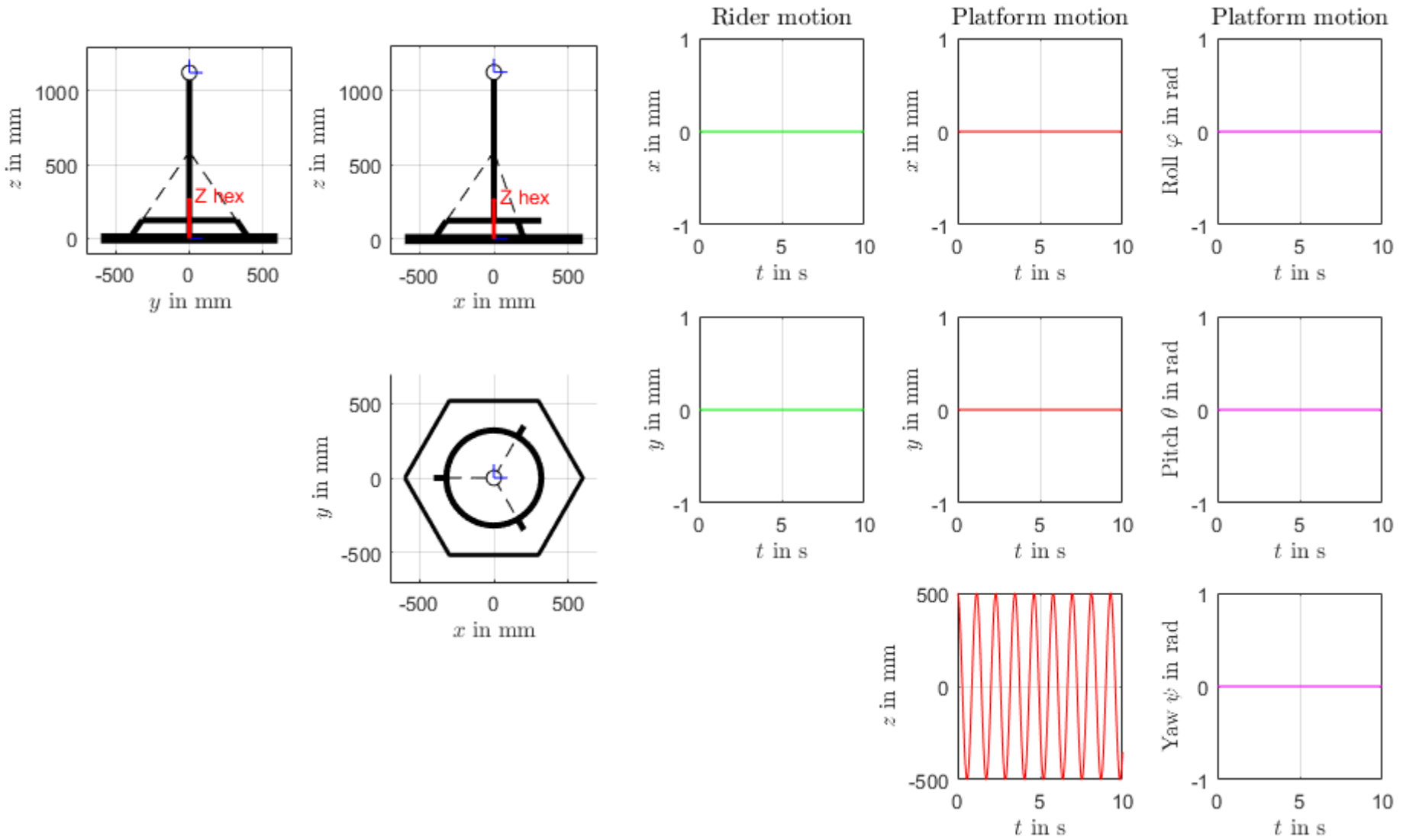

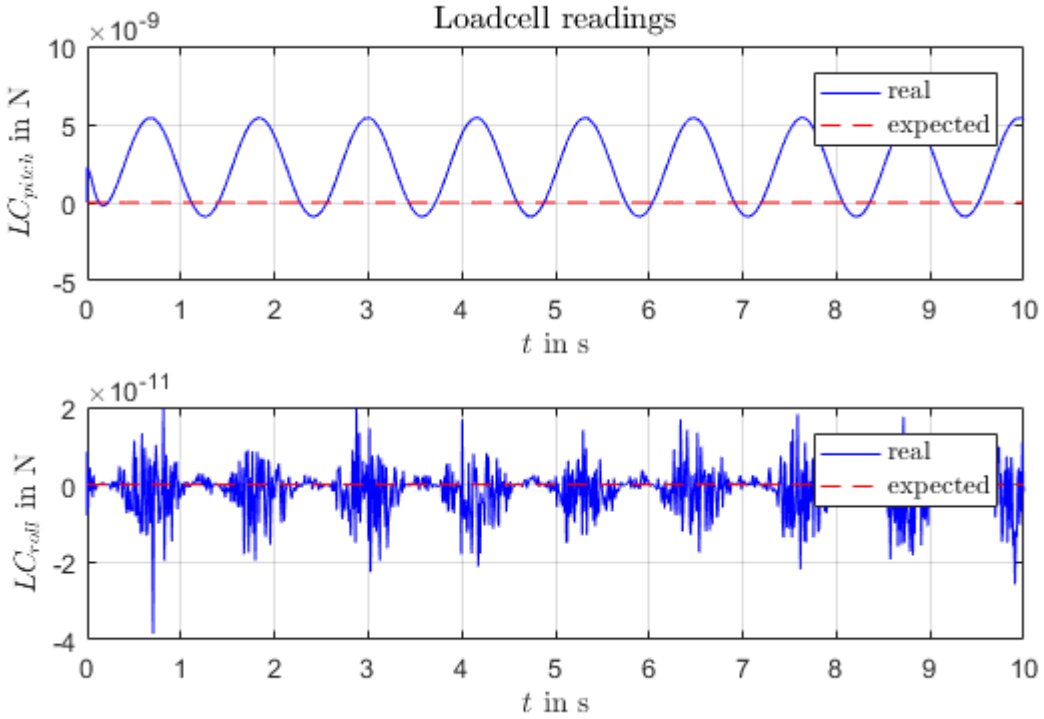
Loadcell readings
×10^-9
10
5
0
-5
LC_{pitch} in N
real
expected
0 1 2 3 4 5 6 7 8 9 10
t in s
×10^-11
2
0
-2
-4
LC_{roll} in N
real
expected
0 1 2 3 4 5 6 7 8 9 10
t in s

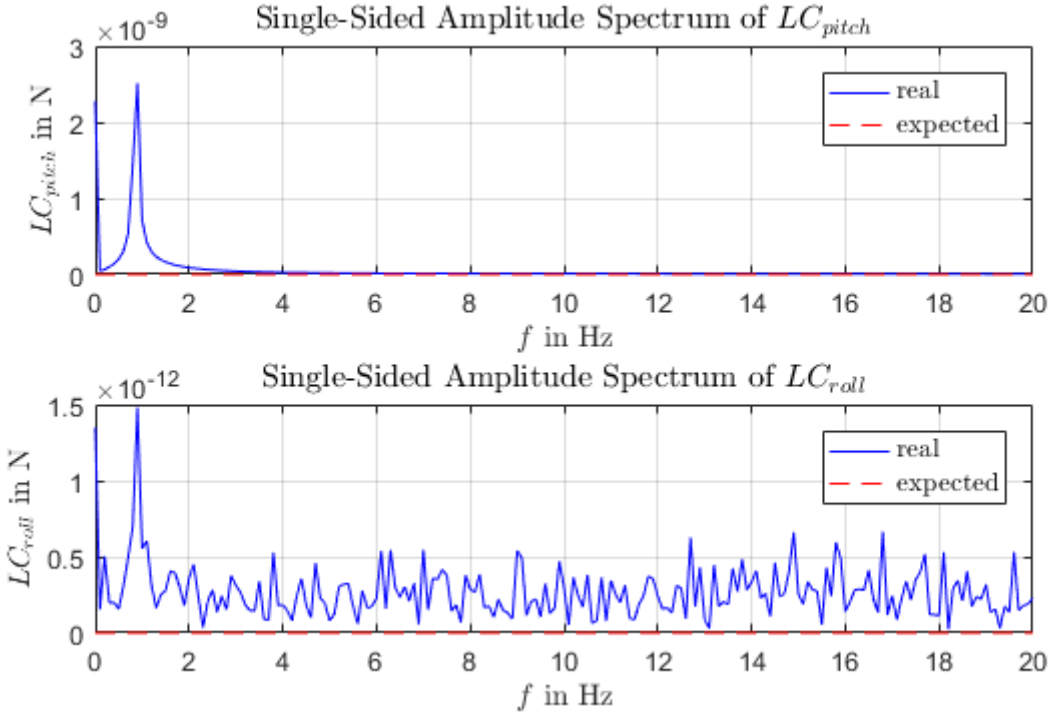
Single-Sided Amplitude Spectrum of LC_{pitch}
×10^-9
3
2
1
0
LC_{pitch} in N
real
expected
0 2 4 6 8 10 12 14 16 18 20
f in Hz
Single-Sided Amplitude Spectrum of LC_{roll}
×10^-12
1.5
1
0.5
0
LC_{roll} in N
real
expected
0 2 4 6 8 10 12 14 16 18 20
f in Hz

8.7 **Motion scenario 6:** no rider motion, rolling platform motion

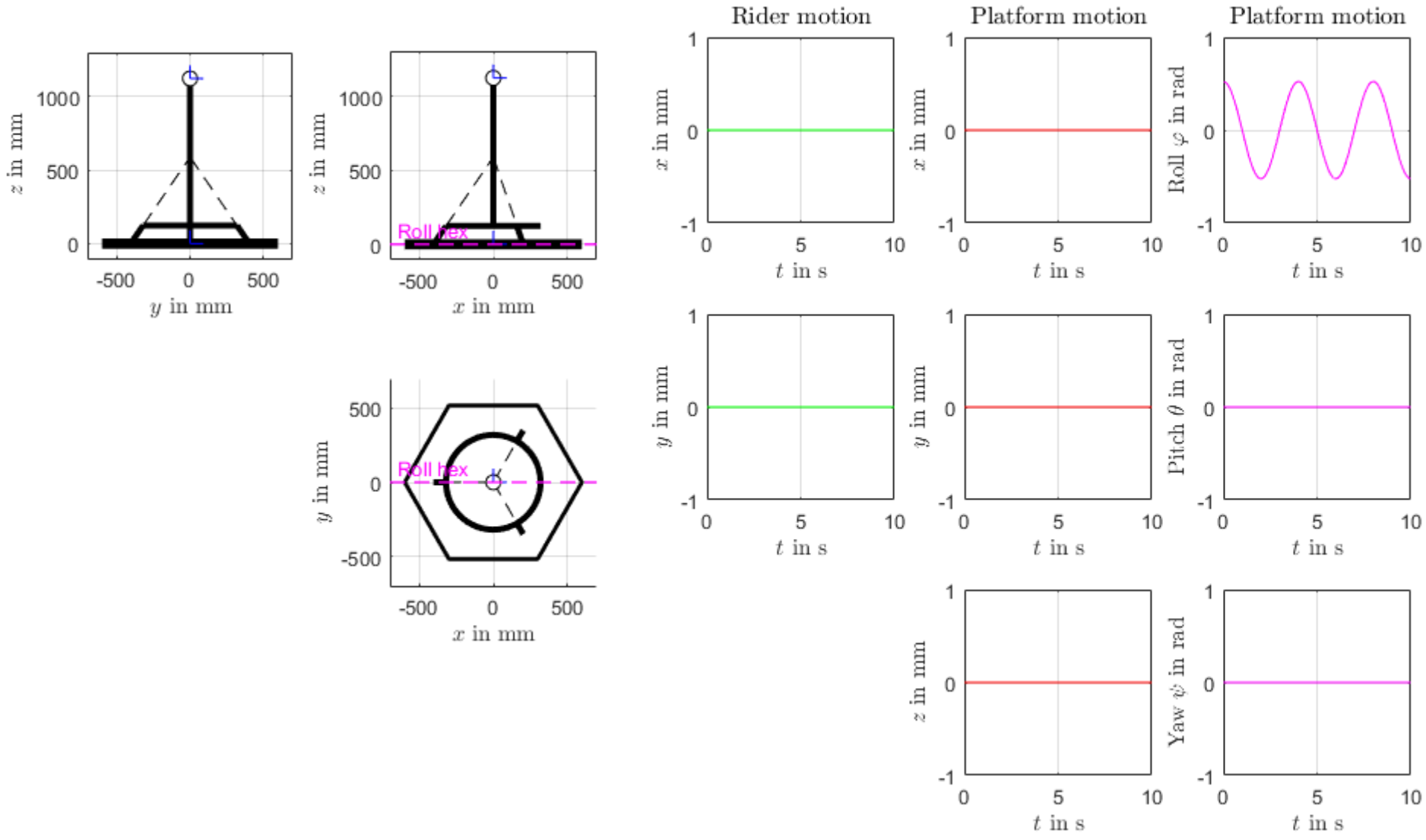

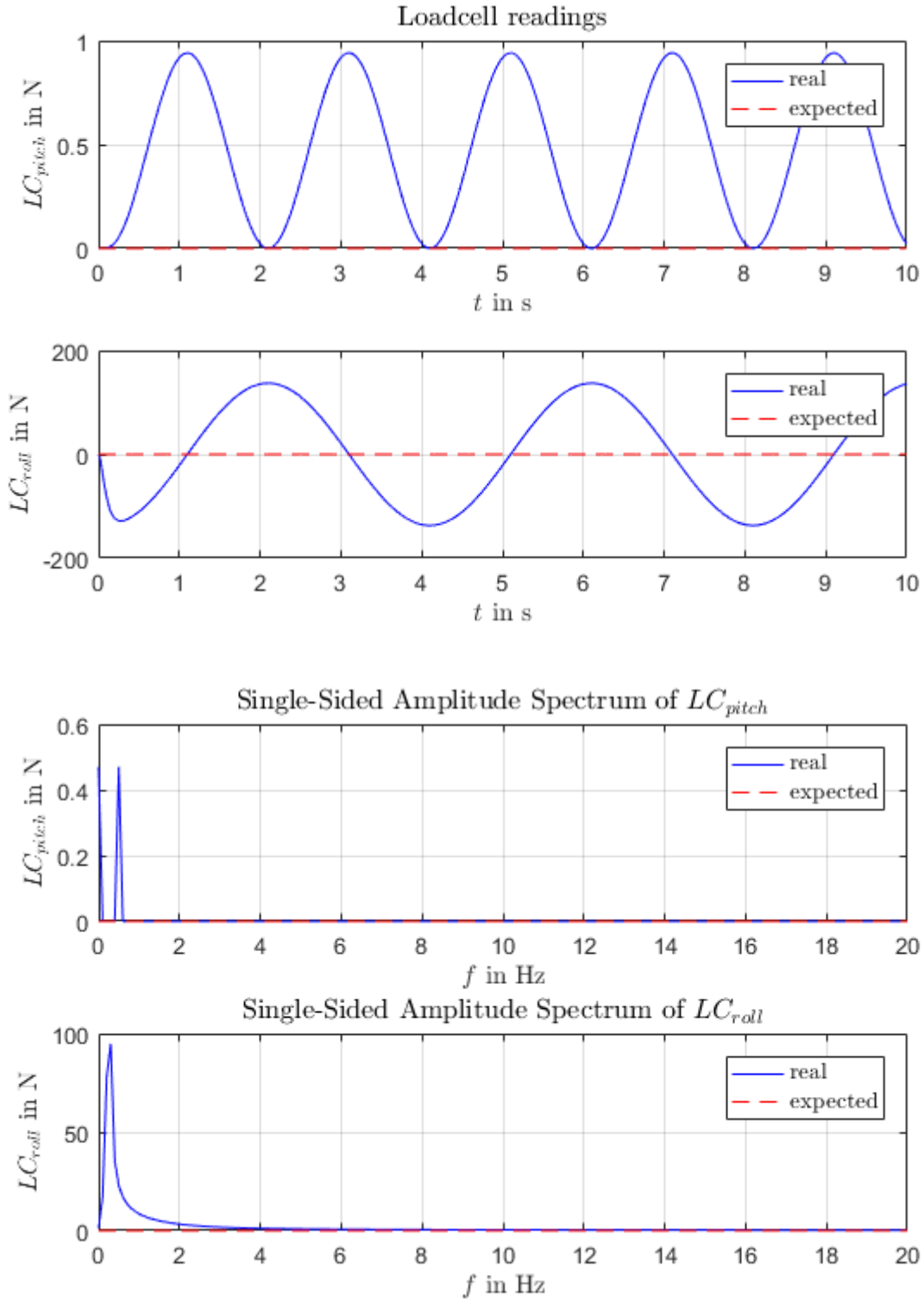
Loadcell readings
LC_{pitch} in N
real
expected
t in s
LC_{roll} in N
real
expected
t in s
Single-Sided Amplitude Spectrum of LC_{pitch}
LC_{pitch} in N
real
expected
f in Hz
Single-Sided Amplitude Spectrum of LC_{roll}
LC_{roll} in N
real
expected
f in Hz

8.8 **Motion scenario 7:** no rider motion, pitching platform motion

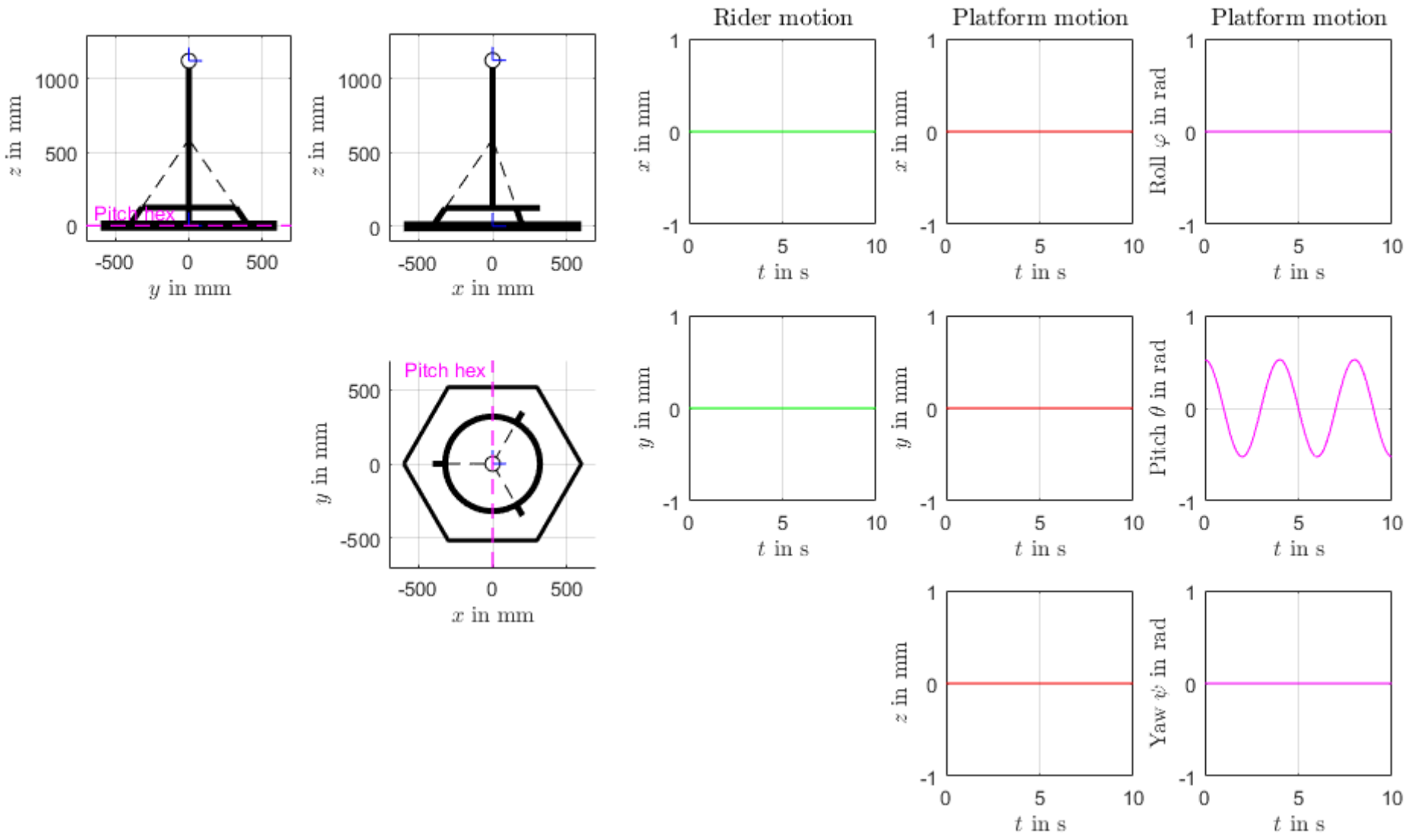

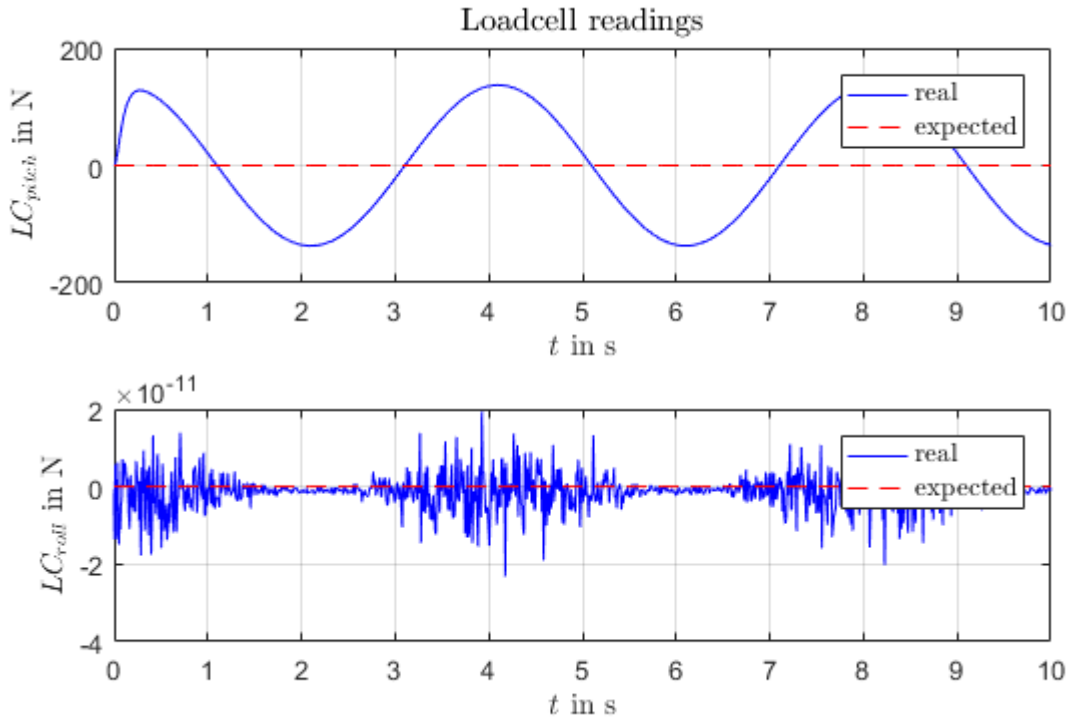
Loadcell readings
200
0
-200
LC_{pitch} in N
real
expected
0 1 2 3 4 5 6 7 8 9 10
t in s
$\times 10^{-11}$
2
0
-2
-4
LC_{roll} in N
real
expected
0 1 2 3 4 5 6 7 8 9 10
t in s

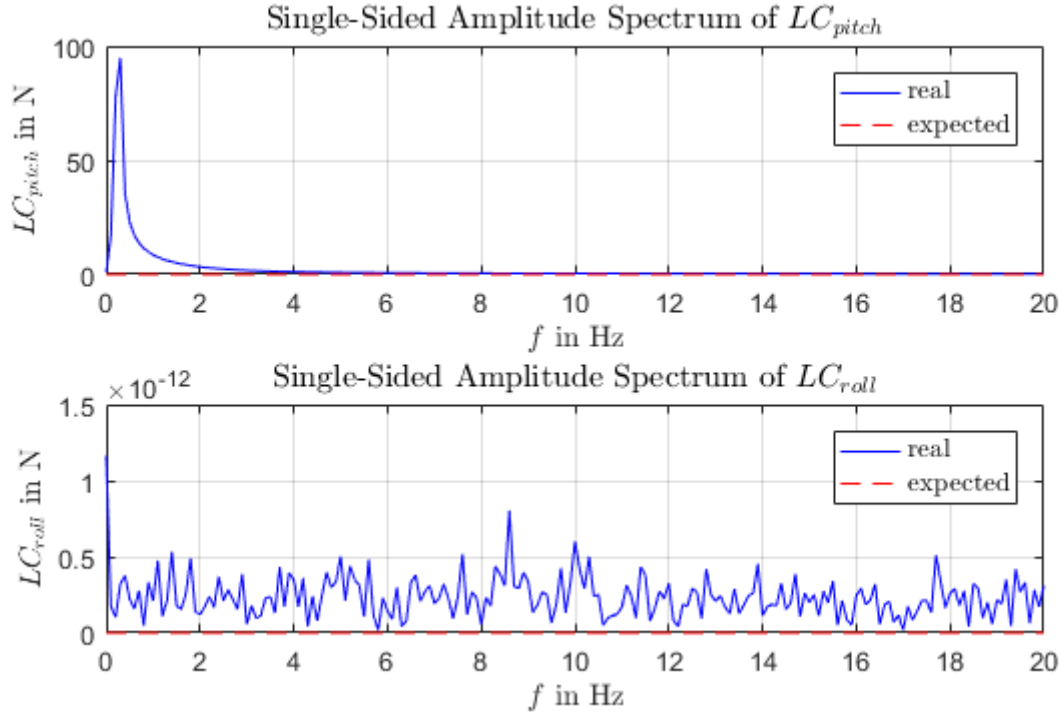
Single-Sided Amplitude Spectrum of LC_{pitch}
100
50
0
LC_{pitch} in N
real
expected
0 2 4 6 8 10 12 14 16 18 20
f in Hz
$\times 10^{-12}$
Single-Sided Amplitude Spectrum of LC_{roll}
1.5
1
0.5
0
LC_{roll} in N
real
expected
0 2 4 6 8 10 12 14 16 18 20
f in Hz

8.9 **Motion scenario 8:** no rider motion, yawing platform motion

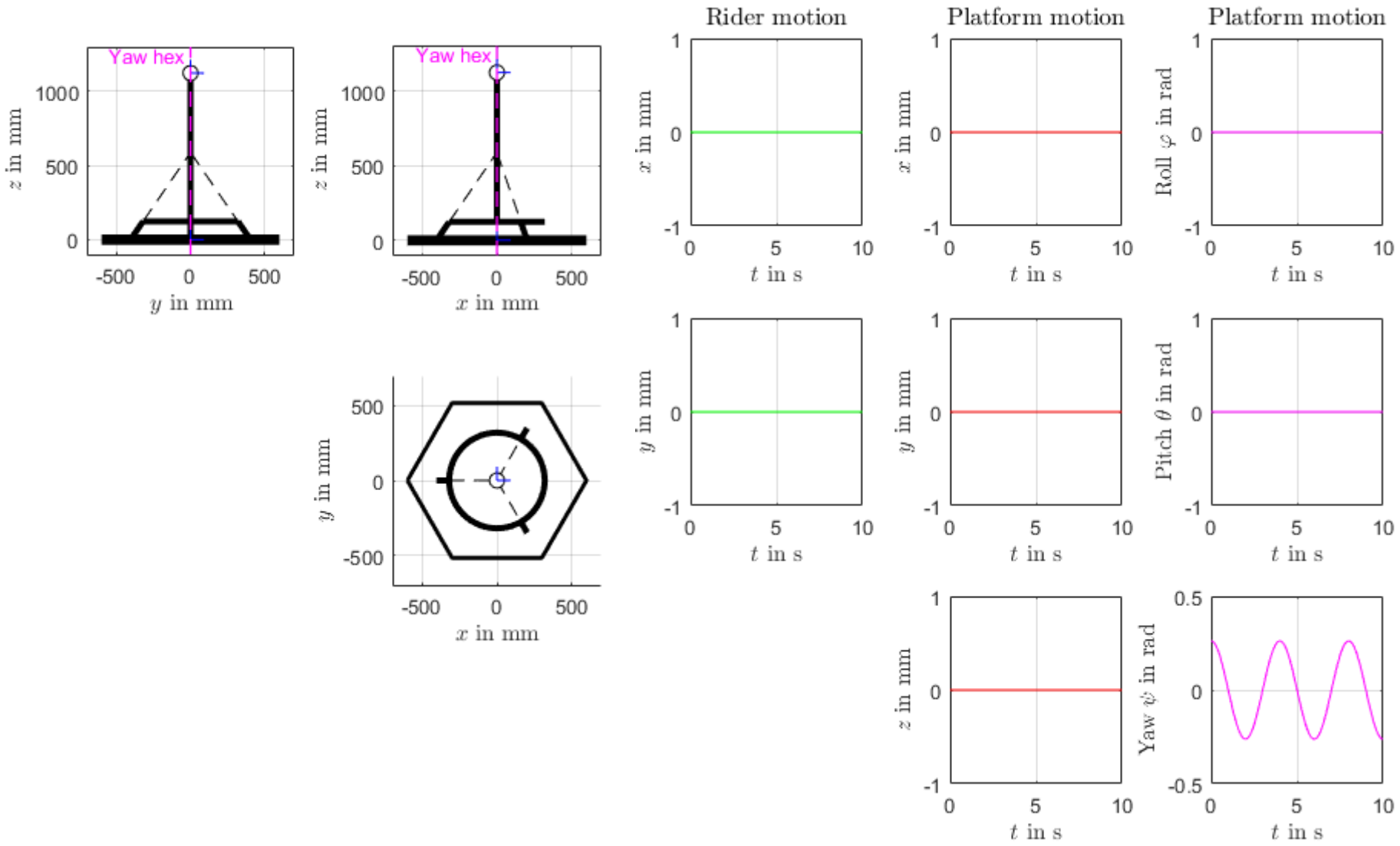

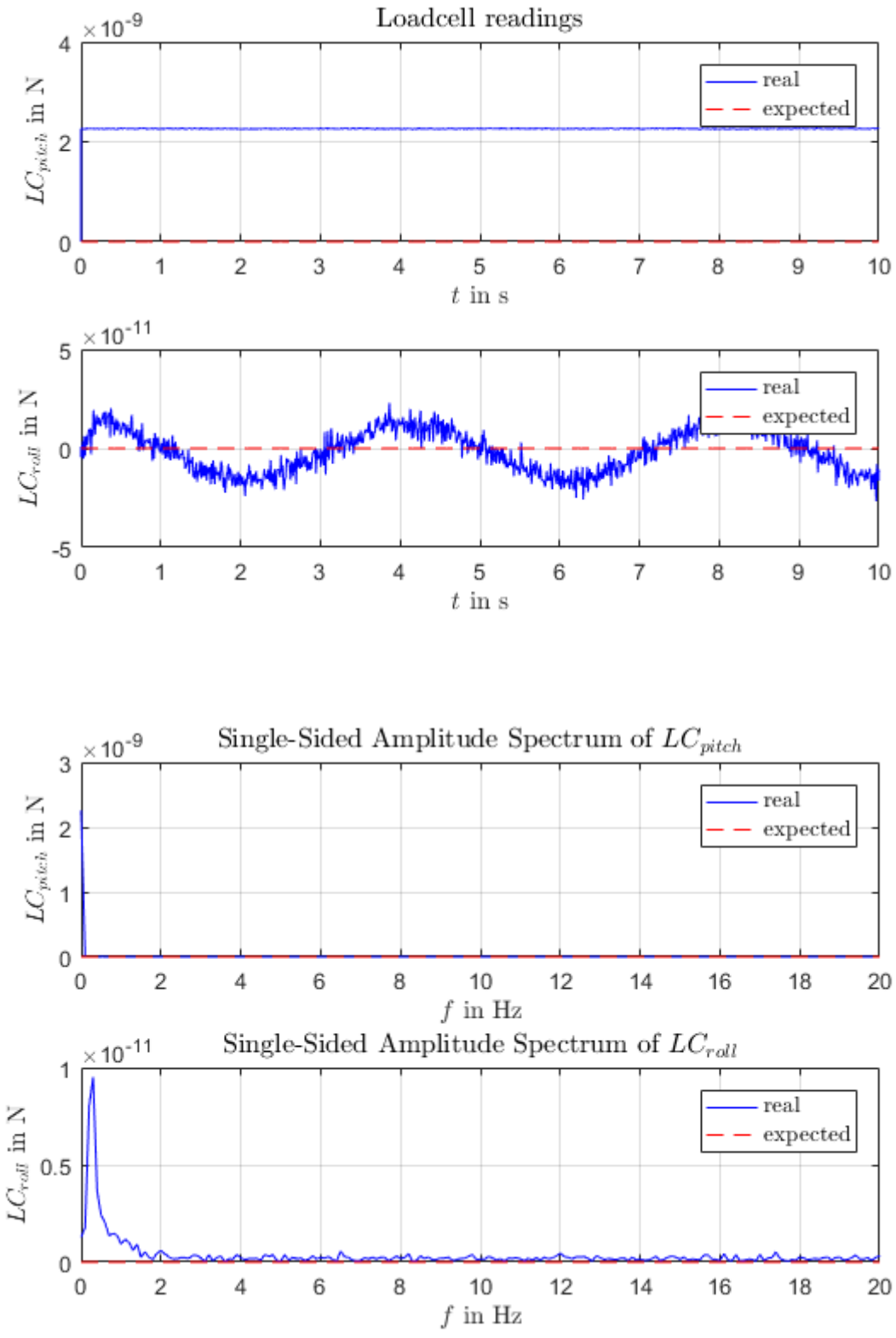
Loadcell readings
×10^-9
LC_{pitch} in N
real
expected
t in s
×10^-11
LC_{roll} in N
real
expected
t in s
Single-Sided Amplitude Spectrum of LC_{pitch}
×10^-9
LC_{pitch} in N
real
expected
f in Hz
Single-Sided Amplitude Spectrum of LC_{roll}
×10^-11
LC_{roll} in N
real
expected
f in Hz

8.10 **Motion scenario 9:** rider motion in *XY* directions, platform motion in *X* direction

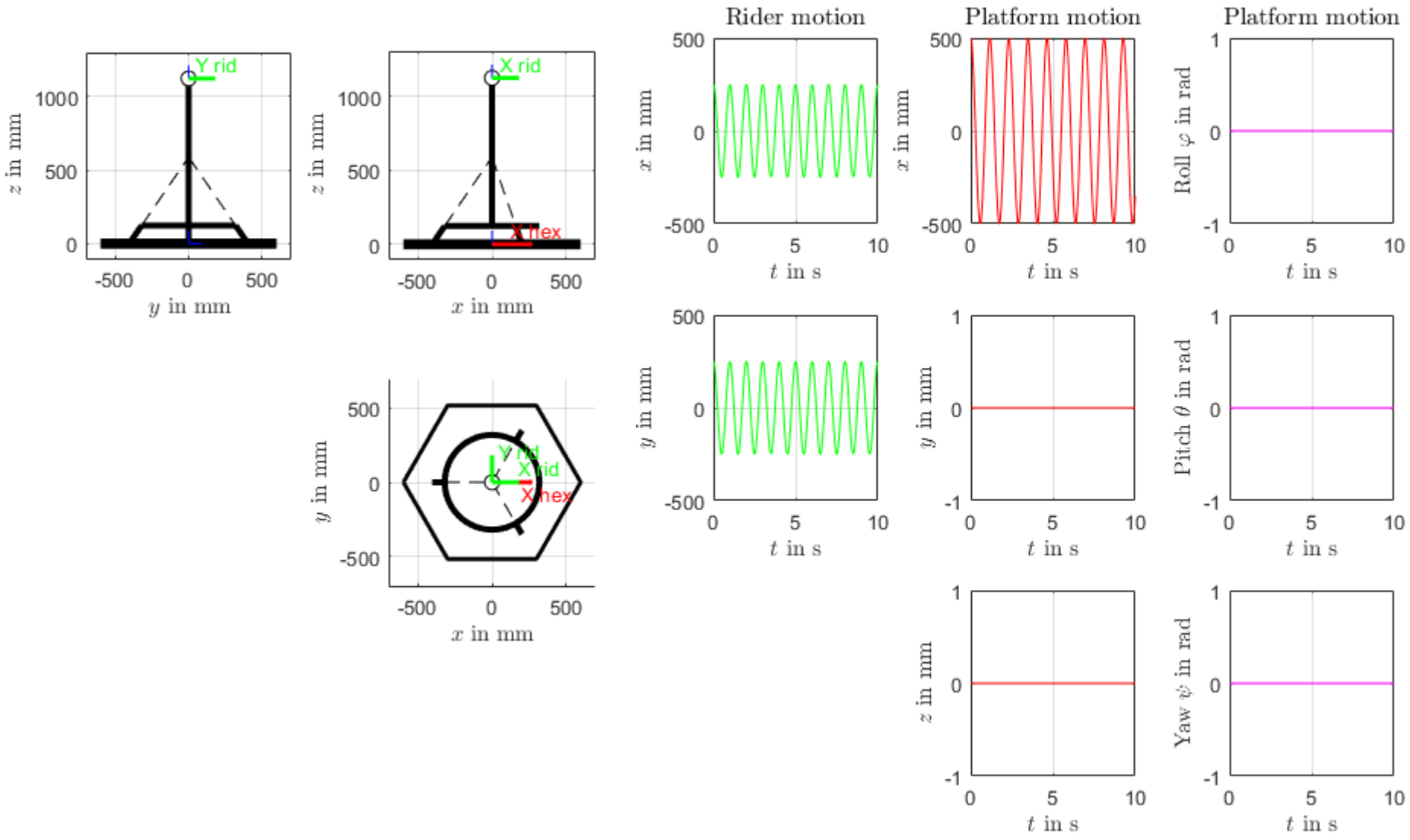

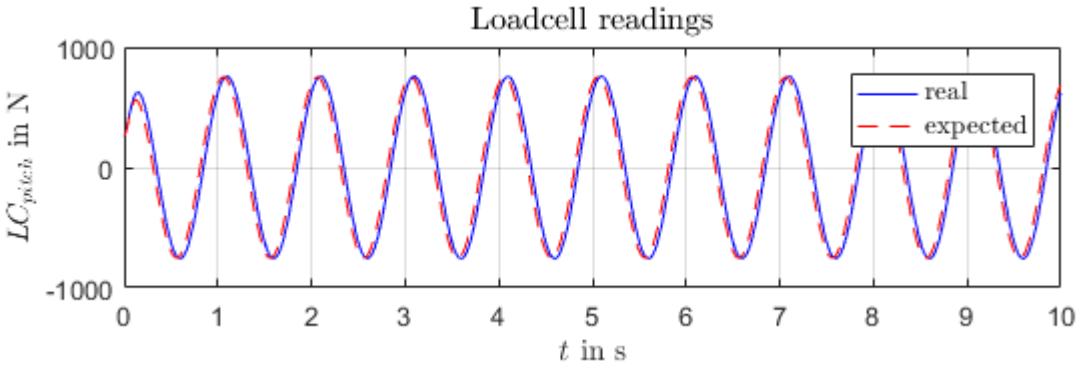
Loadcell readings
1000
0
-1000
LC_{pitch} in N
real
expected
0 1 2 3 4 5 6 7 8 9 10
t in s

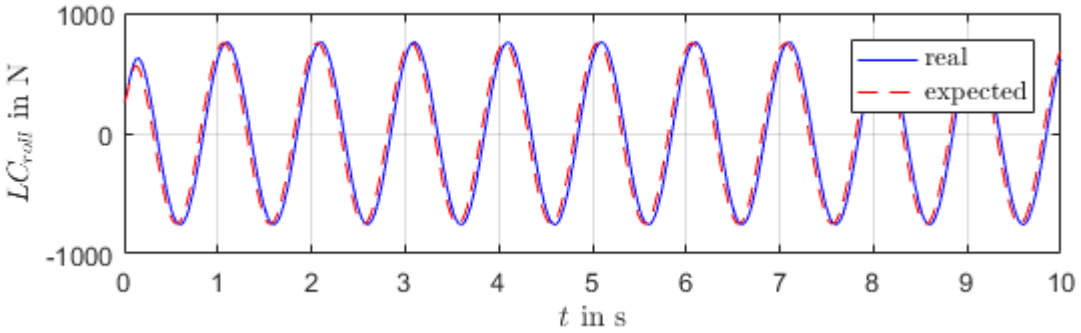
1000
0
-1000
LC_{roll} in N
real
expected
0 1 2 3 4 5 6 7 8 9 10
t in s

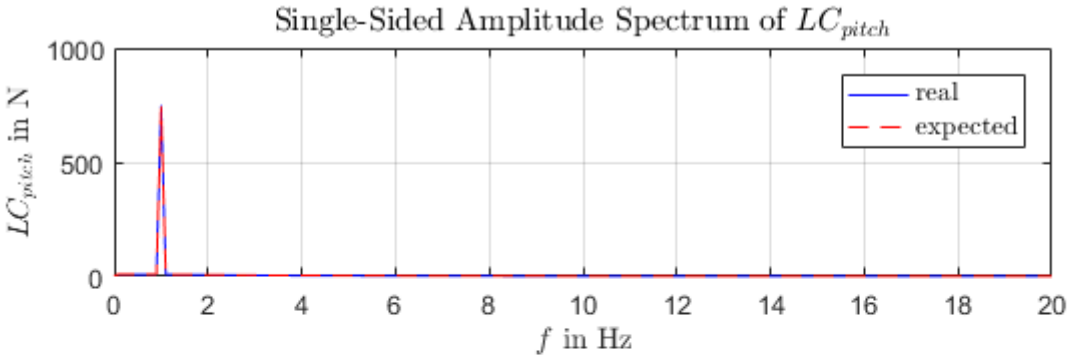
Single-Sided Amplitude Spectrum of LC_{pitch}
1000
500
0
LC_{pitch} in N
real
expected
0 2 4 6 8 10 12 14 16 18 20
f in Hz

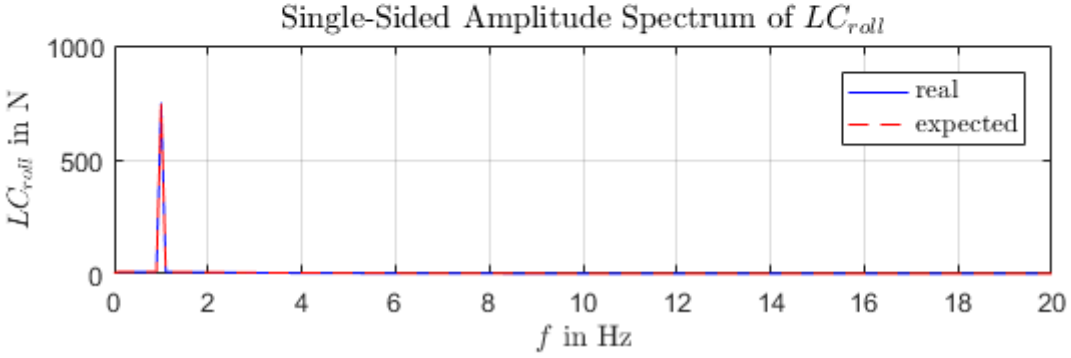
Single-Sided Amplitude Spectrum of LC_{roll}
1000
500
0
LC_{roll} in N
real
expected
0 2 4 6 8 10 12 14 16 18 20
f in Hz

8.11 **Motion scenario 10:** rider motion in *XY* directions, platform motion in *Y* direction

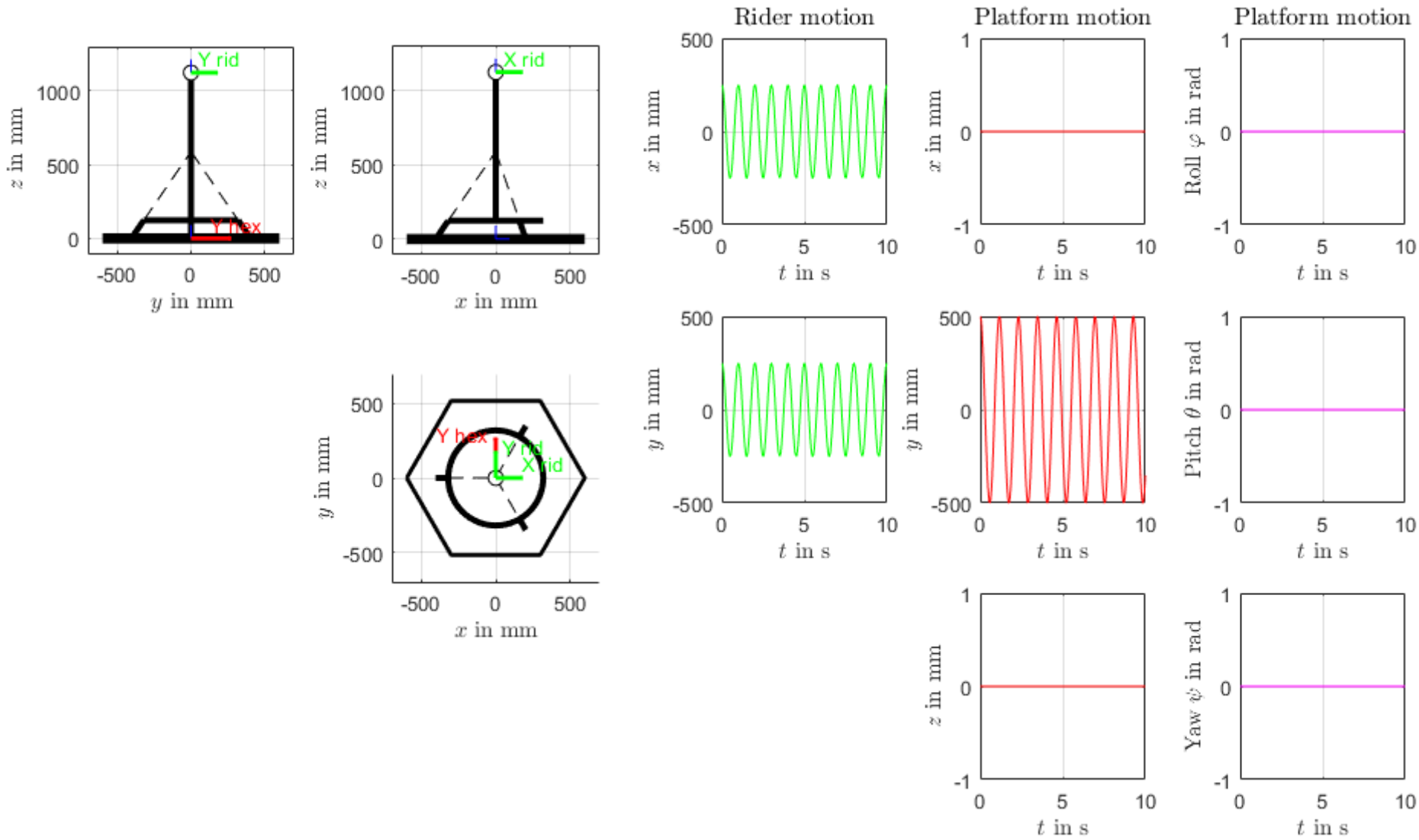

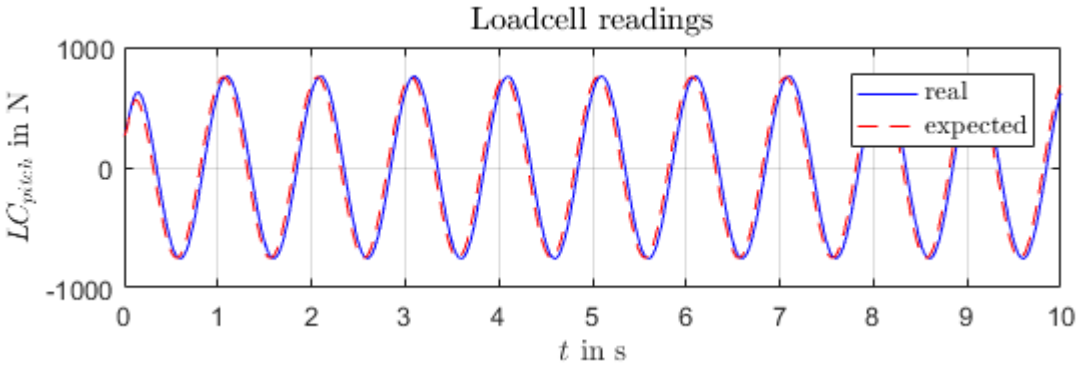
Loadcell readings
1000
0
-1000
LC_{pitch} in N
real
expected
0 1 2 3 4 5 6 7 8 9 10
t in s

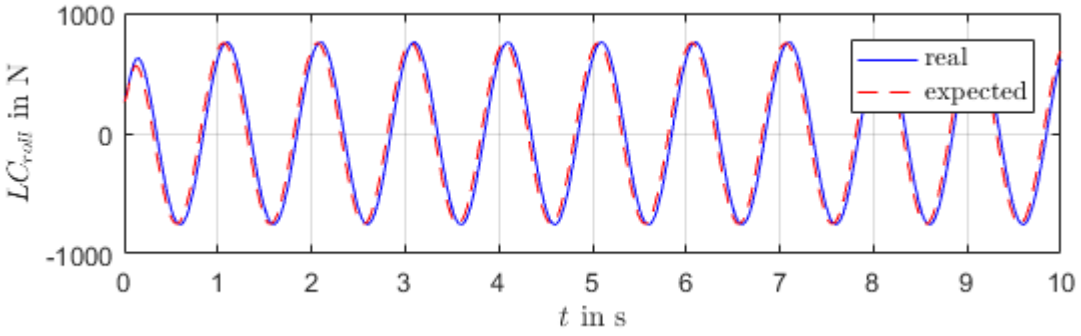
1000
0
-1000
LC_{roll} in N
real
expected
0 1 2 3 4 5 6 7 8 9 10
t in s

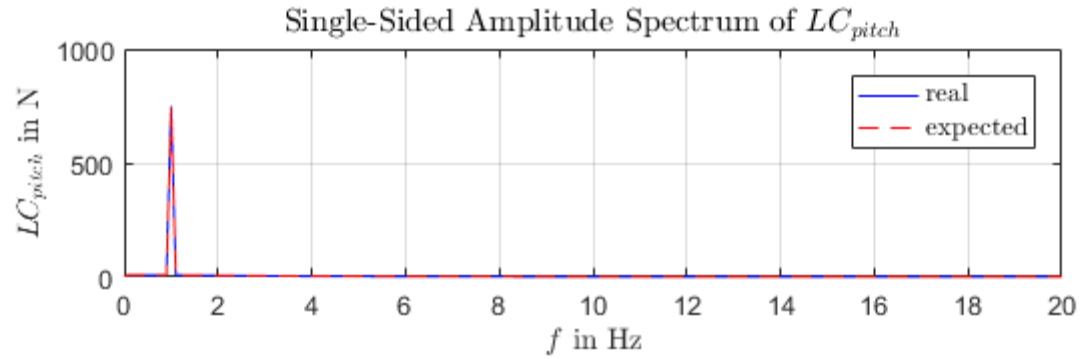
Single-Sided Amplitude Spectrum of LC_{pitch}
1000
500
0
LC_{pitch} in N
real
expected
0 2 4 6 8 10 12 14 16 18 20
f in Hz

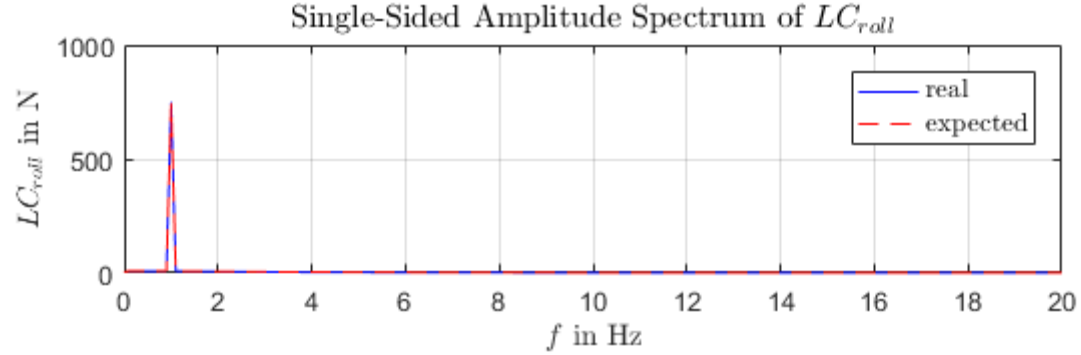
Single-Sided Amplitude Spectrum of LC_{roll}
1000
500
0
LC_{roll} in N
real
expected
0 2 4 6 8 10 12 14 16 18 20
f in Hz

8.12 **Motion scenario 11:** rider motion in *XY* directions, platform motion in *Z* direction

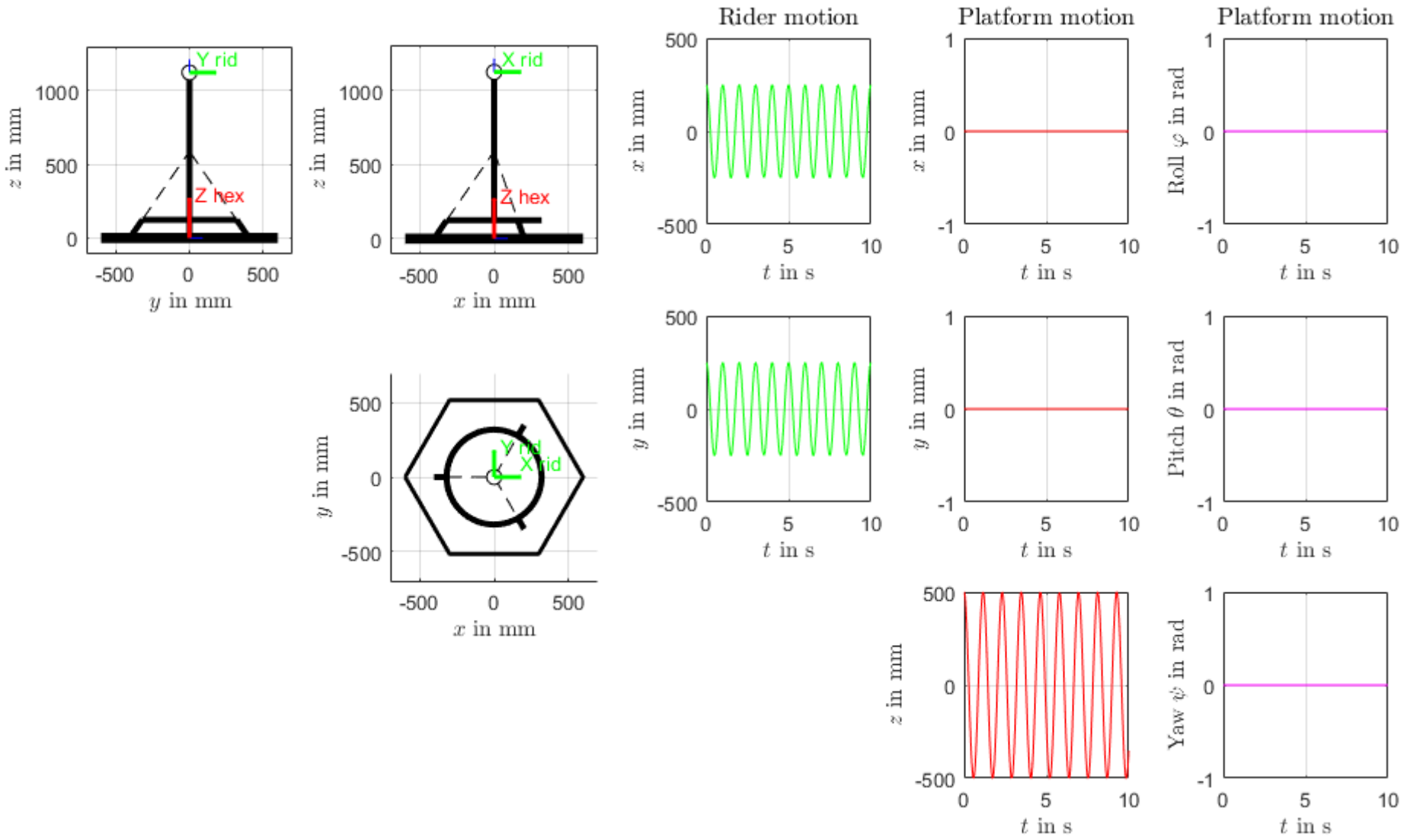

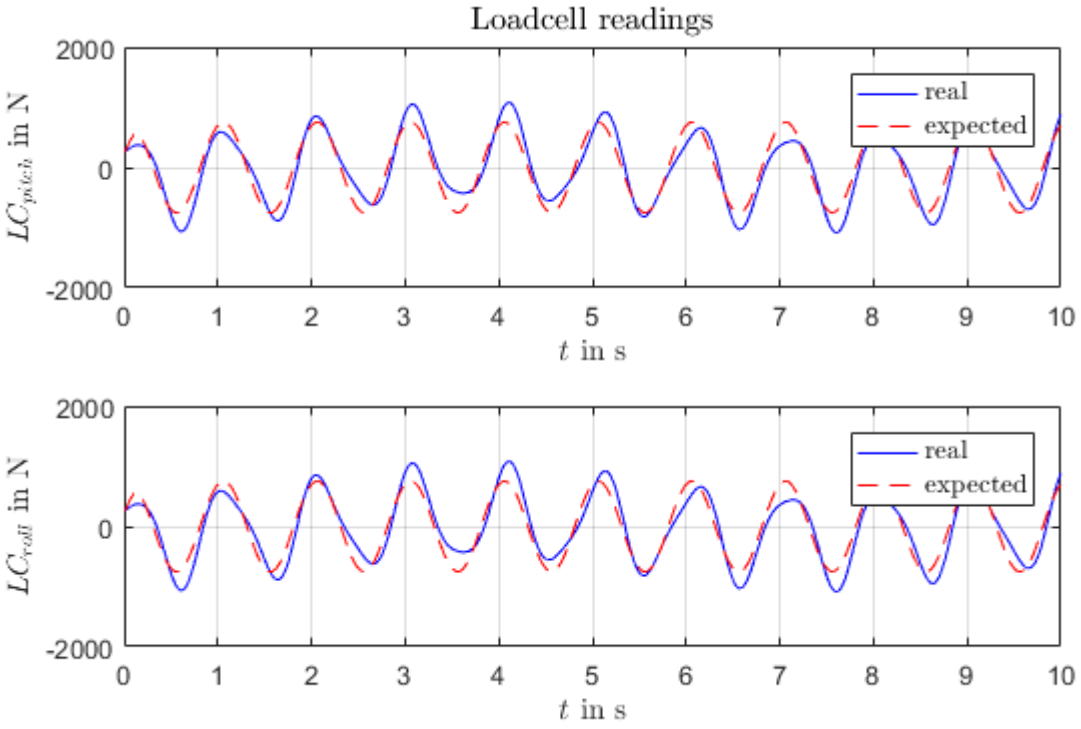
Loadcell readings
2000
0
-2000
LC_{pitch} in N
real
expected
0 1 2 3 4 5 6 7 8 9 10
t in s
2000
0
-2000
LC_{roll} in N
real
expected
0 1 2 3 4 5 6 7 8 9 10
t in s

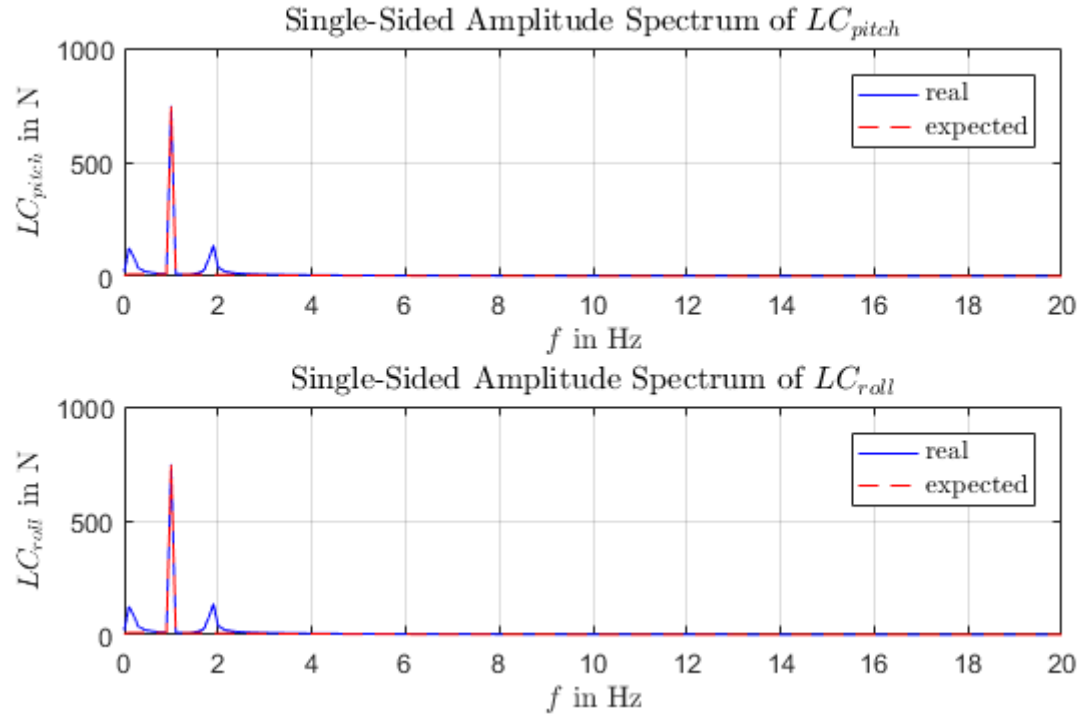
Single-Sided Amplitude Spectrum of LC_{pitch}
1000
500
0
LC_{pitch} in N
real
expected
0 2 4 6 8 10 12 14 16 18 20
f in Hz
Single-Sided Amplitude Spectrum of LC_{roll}
1000
500
0
LC_{roll} in N
real
expected
0 2 4 6 8 10 12 14 16 18 20
f in Hz

8.13 **Motion scenario 12:** rider motion in *XY* directions, rolling platform motion

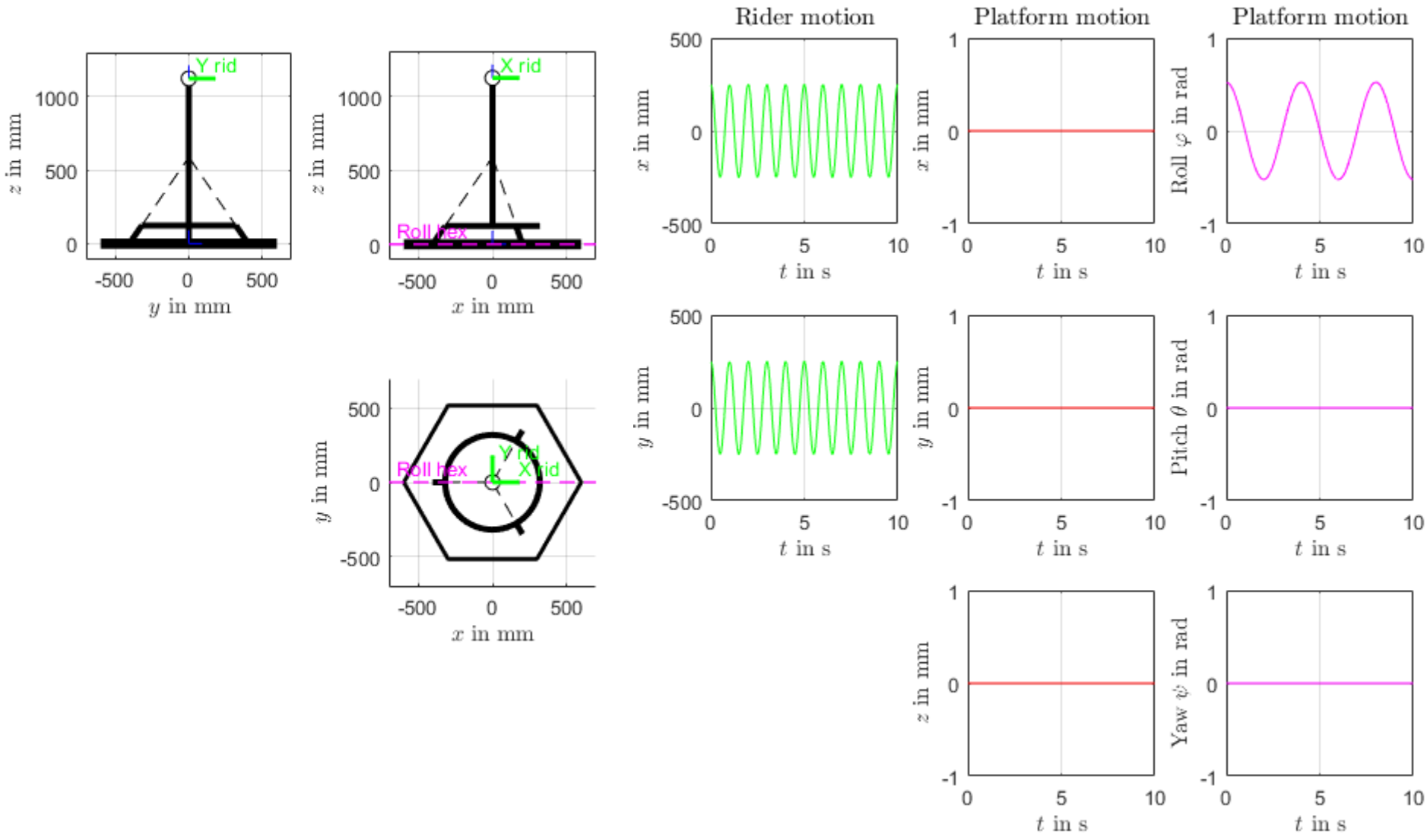

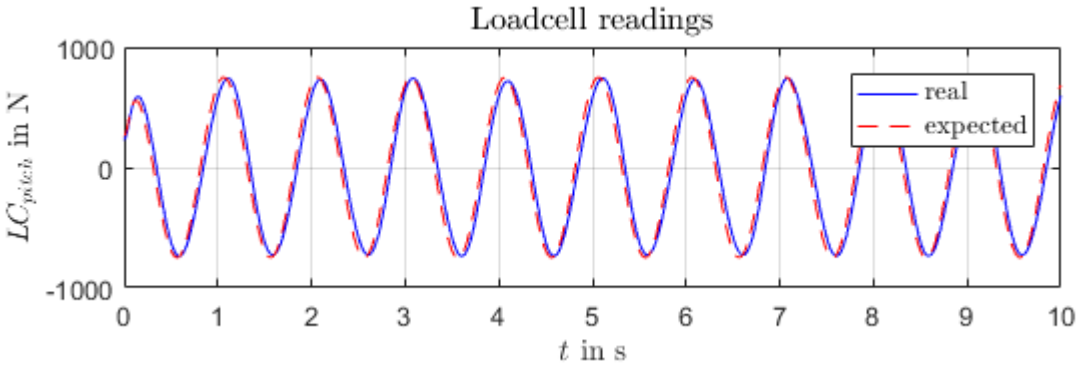
Loadcell readings
1000
0
-1000
LC_{pitch} in N
real
expected
0 1 2 3 4 5 6 7 8 9 10
t in s

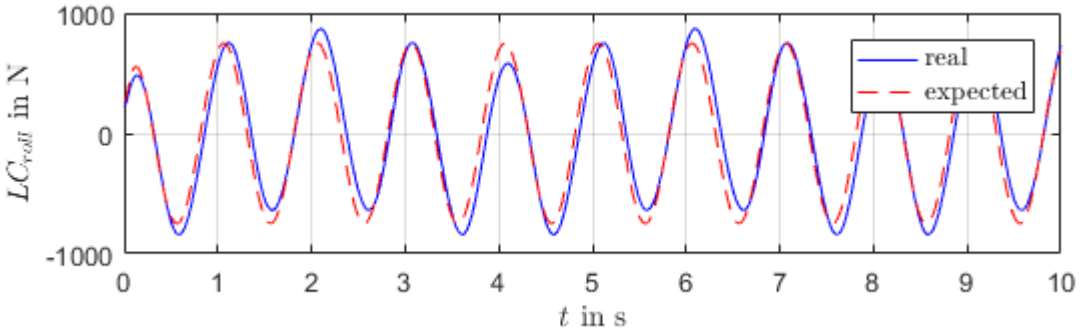
1000
0
-1000
LC_{roll} in N
real
expected
0 1 2 3 4 5 6 7 8 9 10
t in s

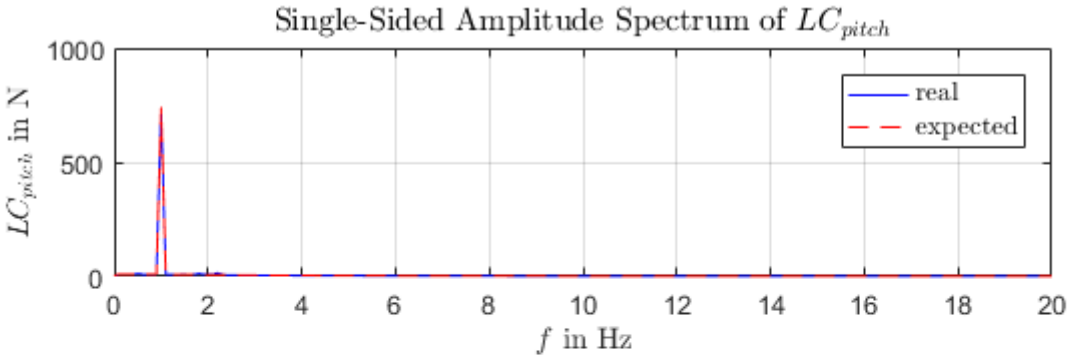
Single-Sided Amplitude Spectrum of LC_{pitch}
1000
500
0
LC_{pitch} in N
real
expected
0 2 4 6 8 10 12 14 16 18 20
f in Hz

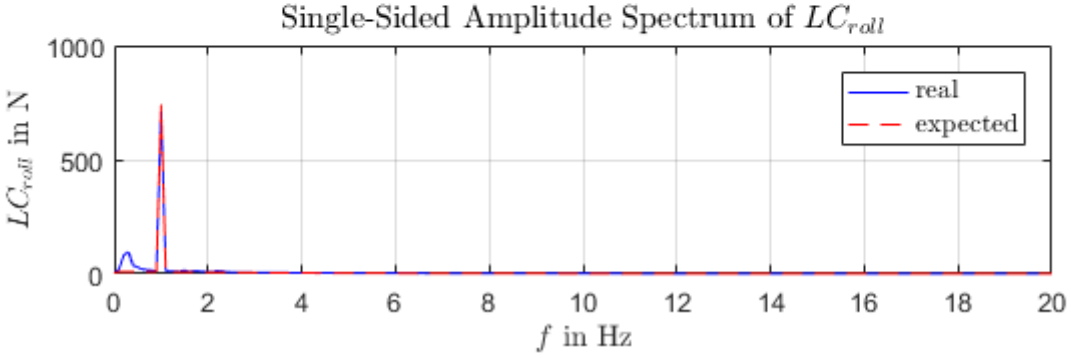
Single-Sided Amplitude Spectrum of LC_{roll}
1000
500
0
LC_{roll} in N
real
expected
0 2 4 6 8 10 12 14 16 18 20
f in Hz

8.14 **Motion scenario 13:** rider motion in *XY* directions, pitching platform motion

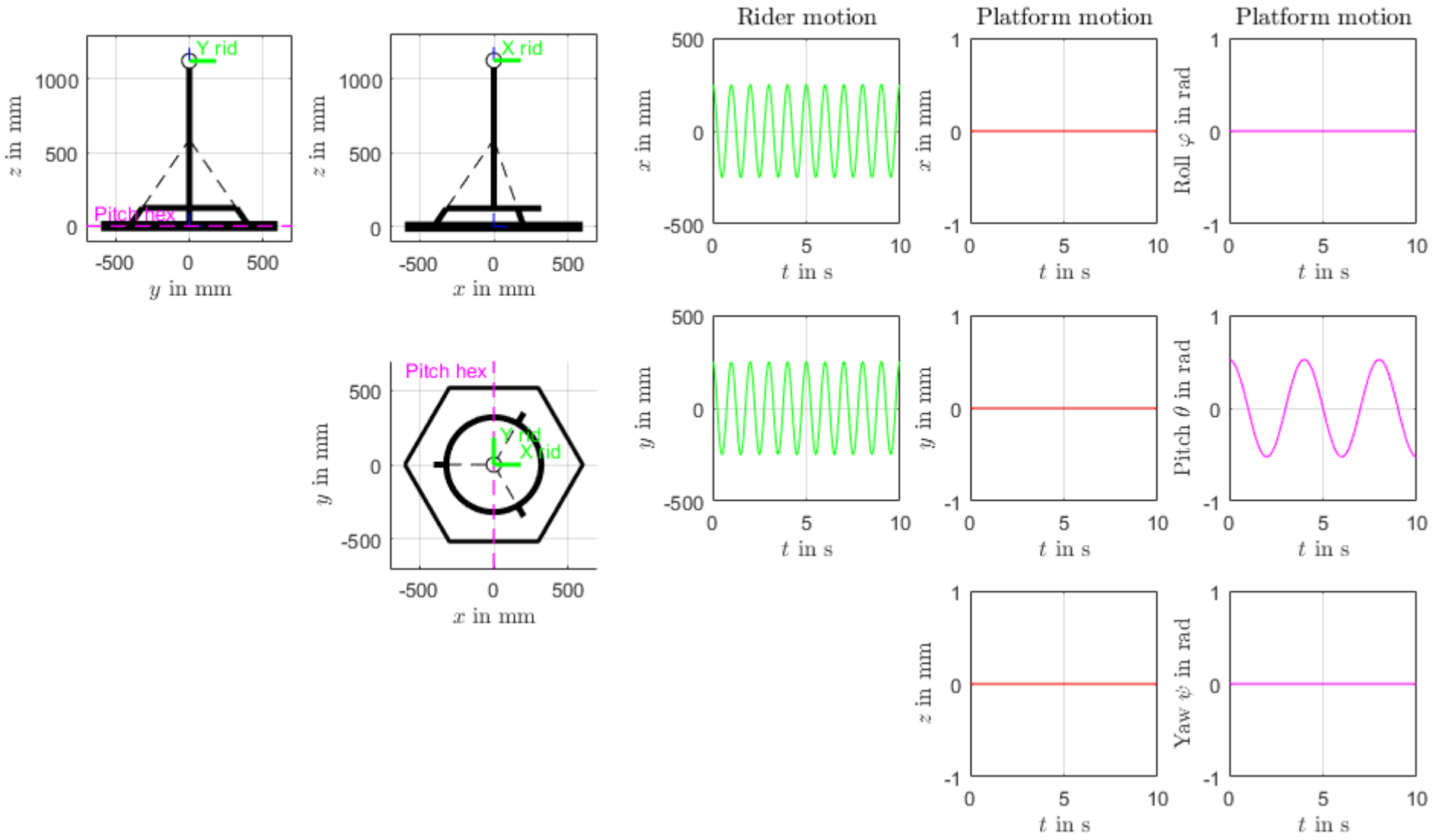

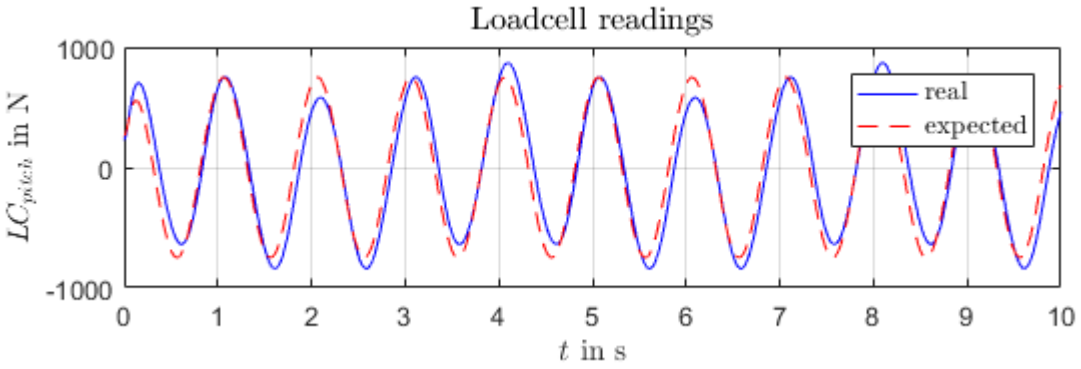
Loadcell readings
LC_{pitch} in N
1000
0
-1000
0 1 2 3 4 5 6 7 8 9 10
t in s
real
expected

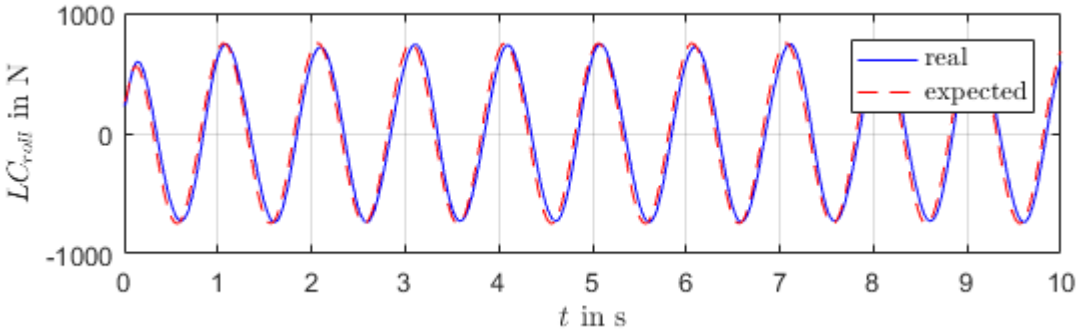
LC_{roll} in N
1000
0
-1000
0 1 2 3 4 5 6 7 8 9 10
t in s
real
expected

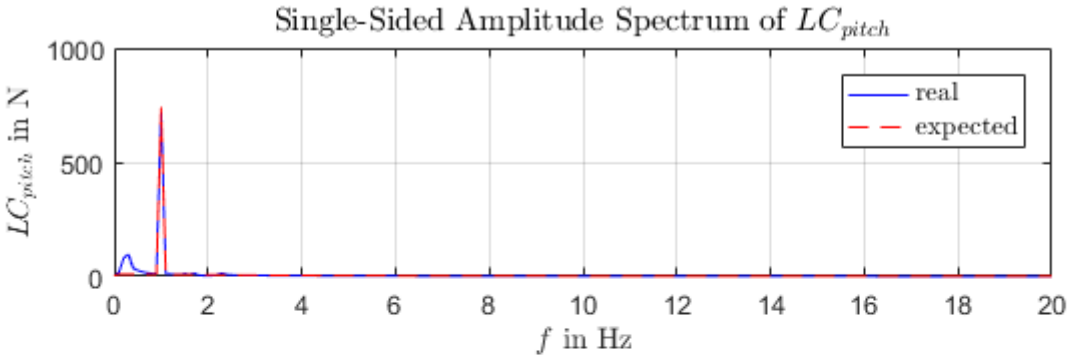
Single-Sided Amplitude Spectrum of LC_{pitch}
LC_{pitch} in N
1000
500
0
0 2 4 6 8 10 12 14 16 18 20
f in Hz
real
expected

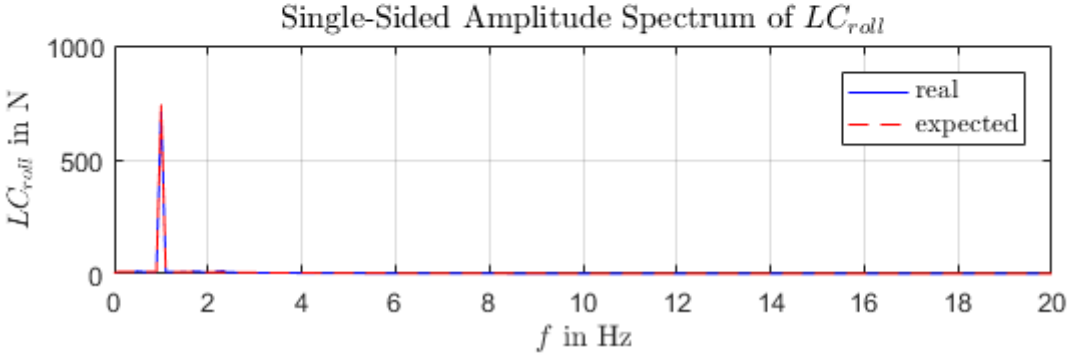
Single-Sided Amplitude Spectrum of LC_{roll}
LC_{roll} in N
1000
500
0
0 2 4 6 8 10 12 14 16 18 20
f in Hz
real
expected

8.15 **Motion scenario 14:** rider motion in *XY* directions, yawing platform motion

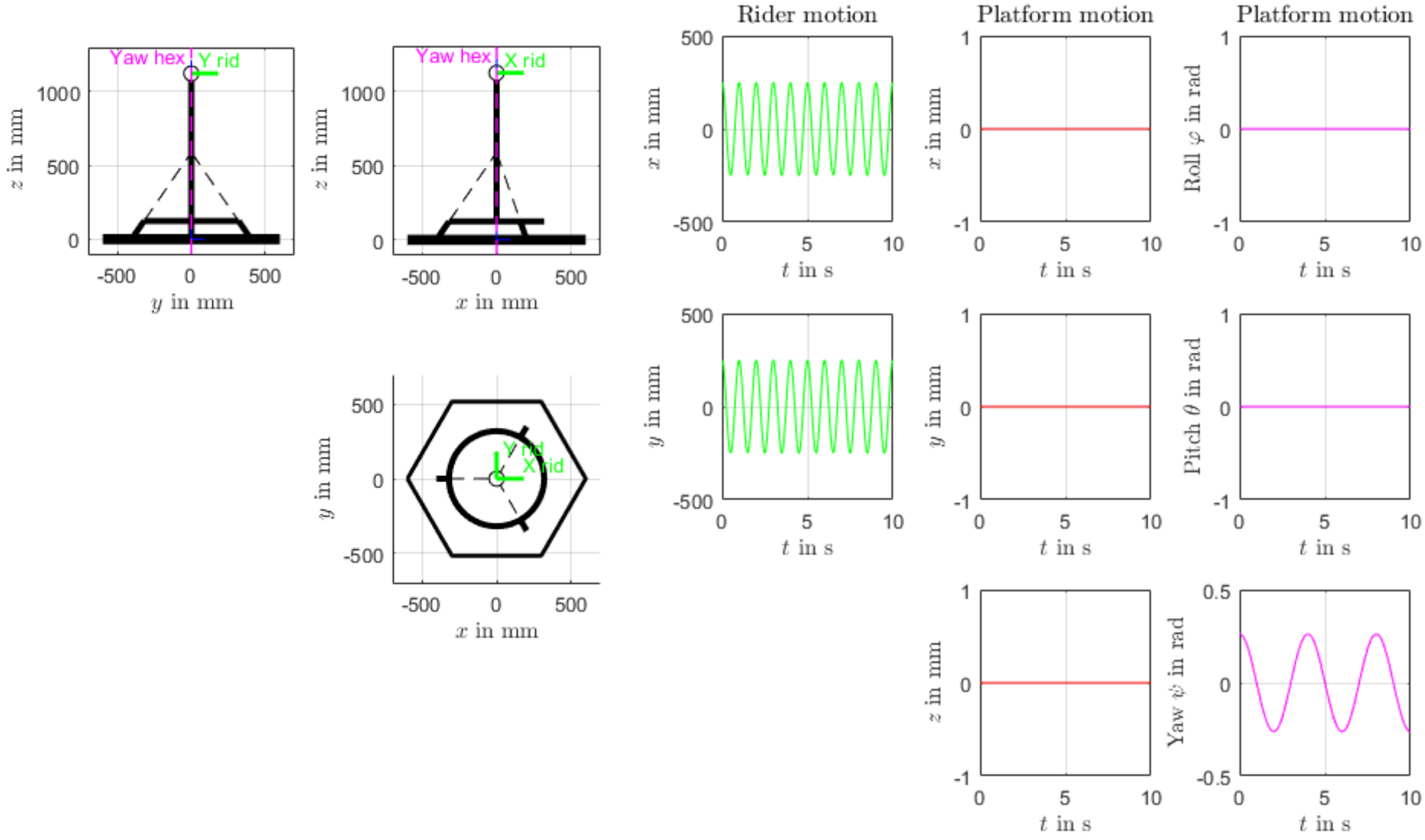

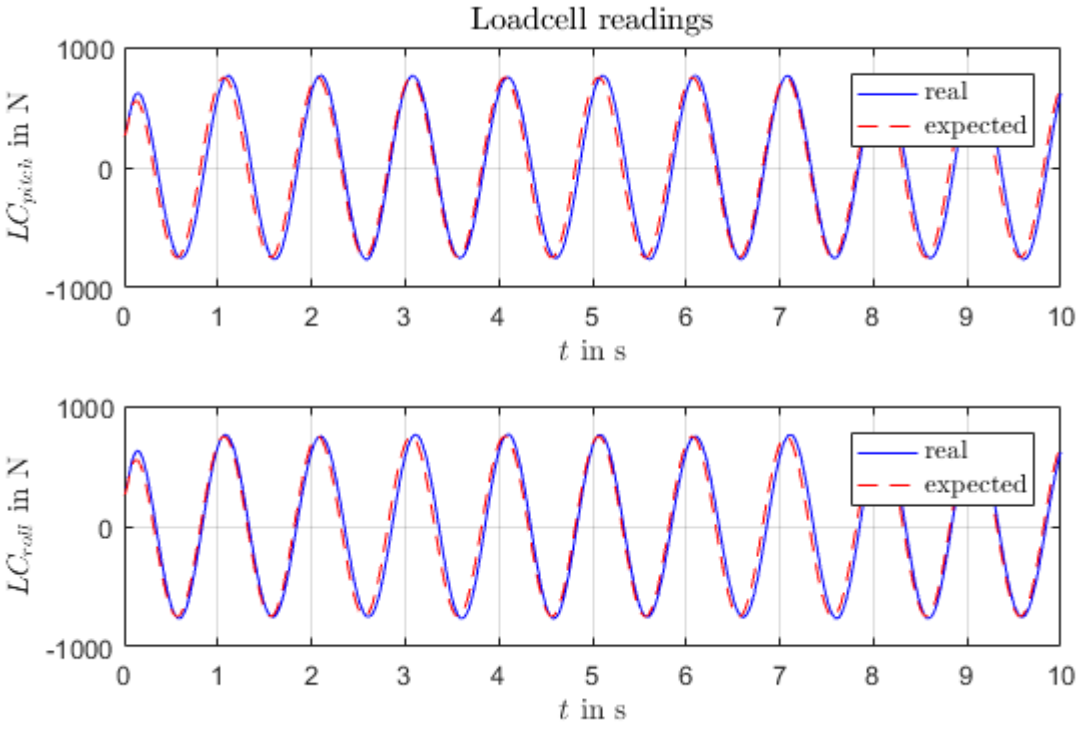
Loadcell readings
LC_{pitch} in N
1000
0
-1000
real
expected
0 1 2 3 4 5 6 7 8 9 10
t in s
LC_{roll} in N
1000
0
-1000
real
expected
0 1 2 3 4 5 6 7 8 9 10
t in s

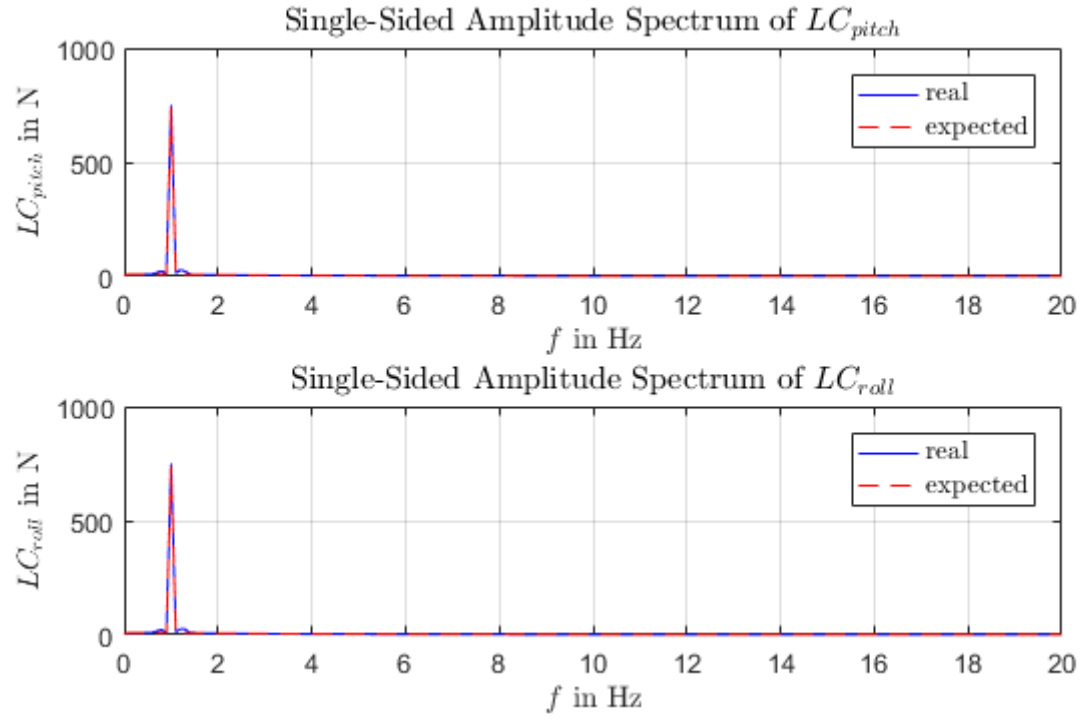
Single-Sided Amplitude Spectrum of LC_{pitch}
LC_{pitch} in N
1000
500
0
real
expected
0 2 4 6 8 10 12 14 16 18 20
f in Hz
Single-Sided Amplitude Spectrum of LC_{roll}
LC_{roll} in N
1000
500
0
real
expected
0 2 4 6 8 10 12 14 16 18 20
f in Hz

8.16 Specification sheet: angular contact ball bearing 7305BEP

►7305 BEP

Popular item

Dimensions

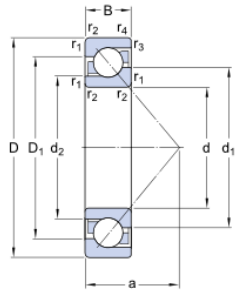

d		25	mm
D		62	mm
B		17	mm
d_1	≈	39.75	mm
d_2	≈	32.38	mm
D_1	≈	48.25	mm
a		26.8	mm
$r_{1,2}$	min.	1.1	mm
$r_{3,4}$	min.	0.6	mm

Abutment dimensions

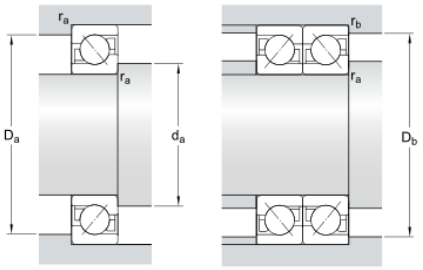

d_a	min.	32	mm
D_a	max.	55	mm
D_b	max.	57.8	mm
r_a	max.	1	mm
r_b	max.	0.6	mm

Calculation data

Basic dynamic load rating	C	24.2	kN
Basic static load rating	C_0	14	kN
Fatigue load limit	P_u	0.6	kN
Reference speed		14000	r/min
Limiting speed		14000	r/min
Calculation factor	A	0.00391	
Calculation factor	k_r	0.1	
Calculation factor	e	1.14	
Single bearing or bearing pair arranged in tandem			
Calculation factor	X	0.35	
Calculation factor	Y_0	0.26	
Calculation factor	Y_2	0.57	
Bearing pair arranged back-to-back or face-to-face			
Calculation factor	X	0.57	
Calculation factor	Y_0	0.52	
Calculation factor	Y_1	0.55	
Calculation factor	Y_2	0.93	

Mass

Mass bearing		0.23	kg

8.17 Specification sheet: spherical roller bearing 22205 EK

►22205 EK

Popular item
SKF Explorer

Dimensions

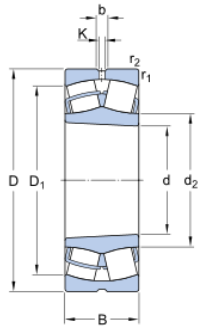

d		25	mm
D		52	mm
B		18	mm
	≈	31.3	mm
D_1	≈	44.2	mm
b		3.7	mm
K		2	mm
$r_{1,2}$	min.	1	mm

Tapered bore, taper 1:12

Abutment dimensions

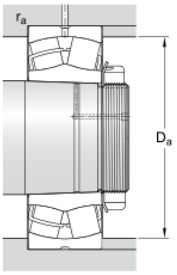

D_a	max.	46.4	mm
r_a	max.	1	mm

Calculation data

Basic dynamic load rating	C	49.9	kN
Basic static load rating	C_0	44	kN
Fatigue load limit	P_u	4.75	kN
Reference speed		13000	r/min
Limiting speed		17000	r/min
Calculation factor	e	0.35	
Calculation factor	Y_1	1.9	
Calculation factor	Y_2	2.9	
Calculation factor	Y_0	1.8	

Mass

Mass bearing		0.26	kg

Mounting information

Recommended lock nut tightening angle	α	100	°

8.18 Gantt diagram of the project

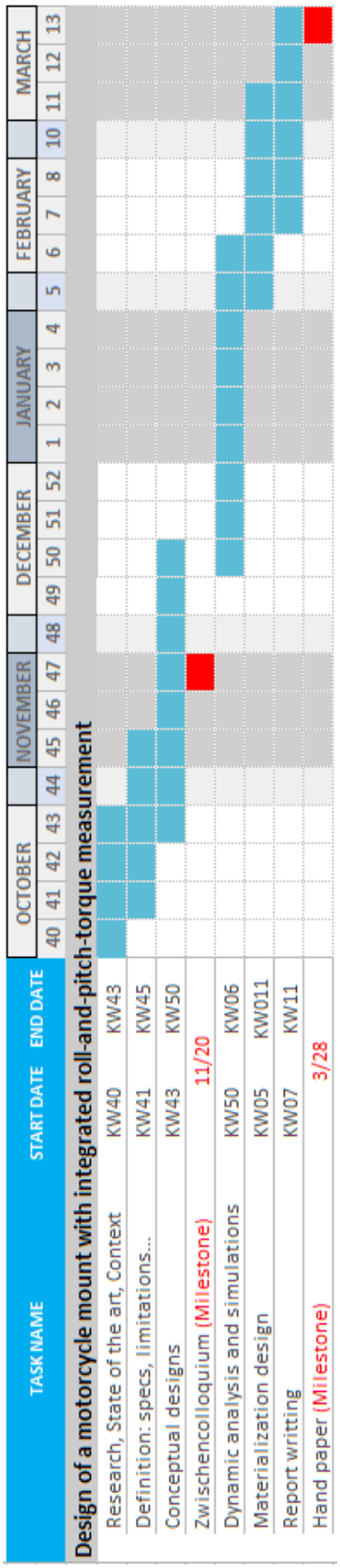

List of References

Cossalter, V.: Motorcycle dynamics
Cossalter, Vittore: Motorcycle dynamics

Foale, T.: Motorcycle handling and chassis design
Foale, Tony: Motorcycle handling and chassis design

Massaro, M. et al.: Using Simulators for the Assessment of Handling of Motorcycles
Massaro, M.; Cossalter, V.; Sadauckas, J.; Lot, R.: Using Simulators for the Assessment of Handling of Motorcycles, in:

Nehaoua, L. et al.: Motorcycle riding simulator: How to estimate robustly the rider's action?
Nehaoua, Lamri; Arioui, Hichem; Mammar, Said: Motorcycle riding simulator: How to estimate robustly the rider's action?, in:

Pleß, R. et al.: Approach to a holistic rider input determination for a dynamic motorcycle riding simulator
Pleß, R.; Will, S.; Hofmann, M.; Winner, H.: Approach to a holistic rider input determination for a dynamic motorcycle riding simulator, in:

Riba Romeva, C.: Disseny de màquines V
Riba Romeva, Carles: Disseny de màquines V

Shin, J.-C.; Lee, C.-W.: Rider's net moment estimation using control force of motion system for bicycle simulator (2004)
Shin, Jae-Cheol; Lee, Chong-Won: Rider's net moment estimation using control force of motion system for bicycle simulator, in: Journal of Robotic Systems (11), Issues 21, pp. 597–607, 2004

Stedmon, A. W. et al.: 'MotorcycleSim': An Evaluation of Rider Interaction with an Innovative Motorcycle Simulator (2011)
Stedmon, A. W.; Hasseldine, B.; Rice, D.; Young, M.; Markham, S.; Hancox, M.; Brickell, E.; Noble, J.: 'MotorcycleSim': An Evaluation of Rider Interaction with an Innovative Motorcycle Simulator, in: The Computer Journal (7), Issues 54, pp. 1010–1025, 2011

Weidele, A.; Klonecki, K.: VGU+FZD: Motorcycles 2015
Weidele, Alois; Klonecki, Kamil (Eds.) VGU+FZD: Motorcycles 2015

Westerhof, B. E.: Evaluation of the Cruden Motorcycle Simulator
Westerhof, Bernhard E.: Evaluation of the Cruden Motorcycle Simulator, in: